High-Rate Space-Time Block Codes in Frequency-Selective Fading Channels

A thesis submitted in partial fulfilment
of the requirements for the degree of
Master of Engineering
in
Electrical and Electronic Engineering
at the
University of Canterbury,
Christchurch, New Zealand

by

Alice P. Chu
B.E.(Hons)
May 17, 2012

Acknowledgements

First and foremost, I would like to express my deepest gratitude to my supervisor, Dr. Philippa Martin for her generous guidance and encouragement. Her unwavering enthusiasm and good humour have been a source of great motivation throughout this entire journey. I truly could not have asked for a better supervisor. I would also like to thank Associate Professor Peter Smith for accepting the role of co-supervisor and being readily available to share his expertise when needed.

To the Communications Research Group, I would like to thank them for the friendship and companionship they provided on a daily basis. It is a privilege to have shared the same office with all of them and I have greatly valued the experiences and wisdom they shared with me. They have taught me so much, research related or otherwise.

A great big thanks must be given to all my friends. They have been my strength and support, much needed during the long arduous hours of writing. In no particular order, I would like to mention the Old Elec crew; their sustaining friendships have proven the rooted comradeship planted at university cannot be broken over distance and time.

Also, to all the strong and amazing women in electrical engineering, thank you for bringing your individuality to the group. Their support and compassion have been absolutely invaluable and shall continue to be greatly appreciated.

To my fellow postgraduate students, their mutual understanding have provided a source of great comfort and I thank them for that.

In Youthline CSI, I have met the most amazing and inspiring people who have provided plentiful laughter and fun, and the perfect place to go to when I needed a breather from writing.

To my friends from Bishop Julius, who had been with me since the first day at UC and whose friendships I shall always cherish.

To my parents, I thank them for their unconditional love and support, and giving me the upbringing that has made me the person that I am today. Also to Lisa and Amy, they are the best kind of friends I could ever wish for.

Lastly, I would like to acknowledge Tait Electronics for offering me their scholarship which is greatly appreciated.

Alice Chu

Abstract

The growing popularity of wireless communications networks has resulted in greater bandwidth contention and therefore spectrally efficient transmission schemes are highly sought after by designers.

Space-time block codes (STBCs) in multiple-input, multiple-output (MIMO) systems are able to increase channel capacity as well as reduce error rate. A general linear space-time structure known as linear dispersion codes (LDCs) can be designed to achieve high-data rates and has been researched extensively for flat fading channels. However, very little research has been done on frequency-selective fading channels. The combination of ISI, signal interference from other transmitters and noise at the receiver mean that maximum likelihood sequence estimation (MLSE) requires high computational complexity. Detection schemes that can mitigate the signal interference can significantly reduce the complexity and allow intersymbol interference (ISI) equalization to be performed by a Viterbi decoder.

In this thesis, detection of LDCs on frequency-selective channels is investigated. Two predominant detection schemes are investigated, namely linear processing and zero forcing (ZF). Linear processing depends on code orthogonality and is only suited for short channels and small modulation schemes. ZF cancels interfering signals when a sufficient number of receive antennas is deployed. However, this number increases with the channel length. Channel decay profiles are investigated for high-rate LDCs to ameliorate this limitation. Performance improves when the equalizer assumes a shorter channel than the actual length provided the truncated taps carry only a small portion of the total channel power.

The LDC is also extended to a multiuser scenario where two independent users cooperate over half-duplex frequency-selective channels to achieve cooperative gain. The cooperative scheme transmits over three successive block intervals. Linear and zero-forcing detection are considered.

Contents

List of Figures

LIST OF FIGURES

Chapter 1

Introduction

"You must do the thing you think you cannot do."

Eleanor Roosevelt

1.1 General Introduction

Wireless communications pre-dates modern mankind when horns and drums were used to signal warnings and messages to the tribe. A more sophisticated exchange involved smoke signals to communicate over longer distances provided a line-of-sight (LOS) existed between the link. The modern wireless communications industry did not begin until 1901 when Guglielmo Marconi succeeded in sending the first long distance wireless telegraph across the Atlantic Ocean from Cornwall to Signal Hill [**?**]. Driven by military applications in the Second World War, the field saw further research and development. This included Shannon's [**?**] ground breaking work on channel capacity and the birth of mobile telephony in 1946 [**?**]. Further improvements and miniaturisa-

tion of solid-state radio frequency hardware in the 1970s fuelled the explosive growth of the wireless industry. Today, wireless is ubiquitous, replacing cables for short and mid-range control devices, long distance communications for fixed, mobile and portable cellular telephones as well as wireless networks in homes and enterprises.

The convergence of mobile and internet in smart phones has extended data traffic beyond the limits of voice calls. The continuous growth of subscribers in addition to the popularity of cloud based applications have resulted in greater bandwidth contention. Networks must be able to cope with the growing traffic in face of the equally growing competition for spectrum. Therefore, the desire for spectral efficiency is prevalent in network designs. Multiple-input, multiple-output (MIMO) communication systems deploy multiple antennas at both ends of the communication links and have been proven to achieve higher spectral efficiency [**?**] and better reliability [**?**] in fading environments without consuming more bandwidth or power.

In this chapter, the physical modelling to characterise the wireless channel is discussed, primarily focusing on two different types of channels: frequency-flat and frequency-selective fading channels. MIMO systems are introduced outlining the performance attained by spatial multiplexing and diversity through the design of space-time codes (STCs) in frequency-flat channels. The challenge of STCs in frequency-selective channels is discussed and leads to the motivation for the thesis. The chapter concludes with the thesis contributions and an outline of the thesis structure.

1.2 The Wireless Channel

Signals are transmitted in the form of electromagnetic waves which propagate from the source in multiple directions. As a consequence, signal strengths decay exponentially with distance. Furthermore, there is typically no direct LOS between the source and destination for long distance channels. When the signal strikes an object in its path, it undergoes reflection, refraction or scattering [**?** **?**]. As a result, multiple copies of the signal attenuated by different paths reach the receiver separately. The signals combine constructively, boosting the signal power or destructively, creating further signal degradation. Figure **??** depicts multipath propagation in a wireless environment.

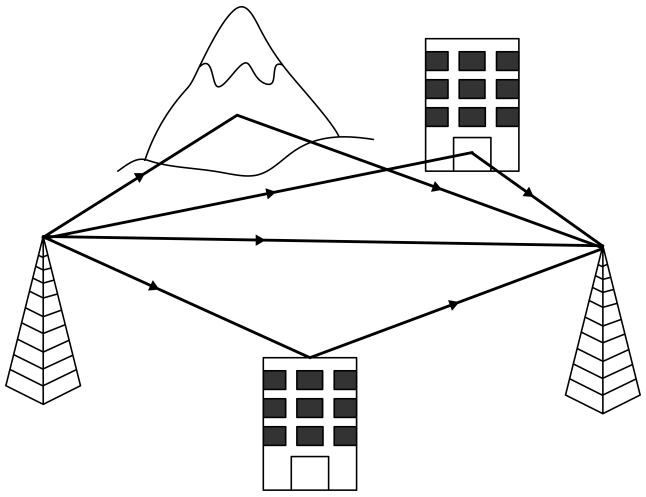

Figure 1.1: Multipath in a wireless environment.

Various propagation models can be used to characterise the wireless fading channel [**?**]. This thesis, in particular, is interested in small-scale models which simulate the statistical property of the received signals over short distances or short time intervals. Large-scale path loss is ignored. Thus, the channel is modelled by rapid fluctuations of power over time, maintained by

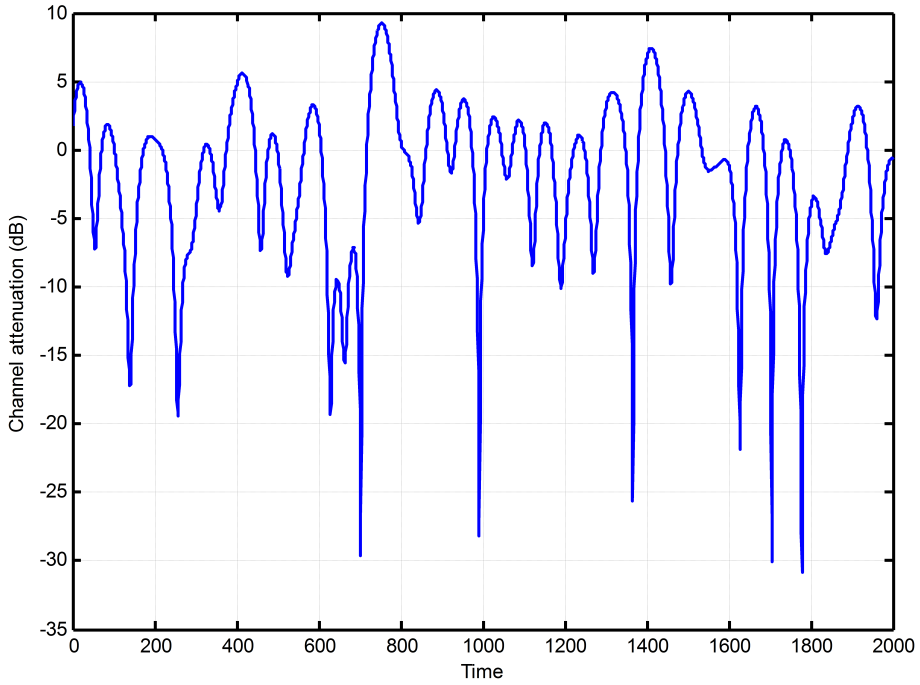

Figure 1.2: Random wireless fading channel.

a constant average. Variation in the wireless channel induced from multipath is known as random fading [**?**]. A sample of channel attenuation for small-scale random fading is shown in Figure **??**. Random fading is classified into frequency-flat and frequency-selective fading channels and is described in the next section. The fading channels are modelled by Rayleigh distributed Gaussian random variables [**?** **?**] which assume no LOS component and zero mean.

1.2.1 Flat Fading Channels

The wireless channel has a coherence bandwidth in which the signal will experience a response of constant gain and linear phase [**?**]. When the bandwidth

of the transmitted signal falls within the channel coherence bandwidth, all frequency components of the signal experience the same fading and the channel is said to be frequency-flat or frequency-nonselective. The mathematical model for a flat fading channel can be represented by a filter with a single tap, h, which is an independent and identically distributed (iid) complex-valued Gaussian random variable with a Rayleigh distributed amplitude. A single-input, single-output (SISO) flat fading system is shown in Figure **??**.

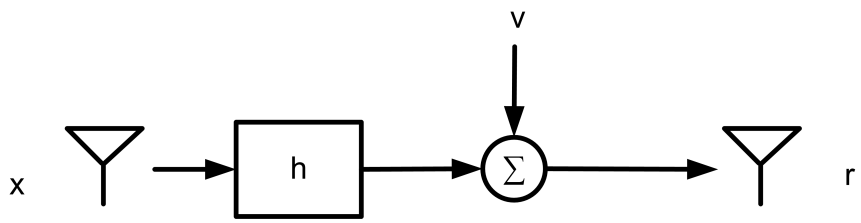

Figure 1.3: Model for a flat fading SISO system.

At the receive antenna, a single symbol r is received, which is the product of the channel tap, h, and the transmitted symbol, x, chosen from an arbitrary modulation plus additive white Gaussian noise (AWGN), v, with zero mean and variance σ^2 at the receiver. The received signal can be written as

$$r(t) = h(t)x(t) + v(t). \tag{1.1}$$

1.2.2 Frequency-selective Fading Channels

When the signal bandwidth exceeds the channel coherence bandwidth, the broadband signal experiences different attenuations and phase delays at different frequencies [**?**]. The channel is said to be frequency-selective and is usually modelled by a finite impulse response filter with $L_h + 1$ taps. A frequency-

selective channel model is shown in Figure **??**, where L_h is the delay in symbols caused by the channel in the time-domain. The dispersion of symbols by the frequency-selective channel is shown in Figure **??**.

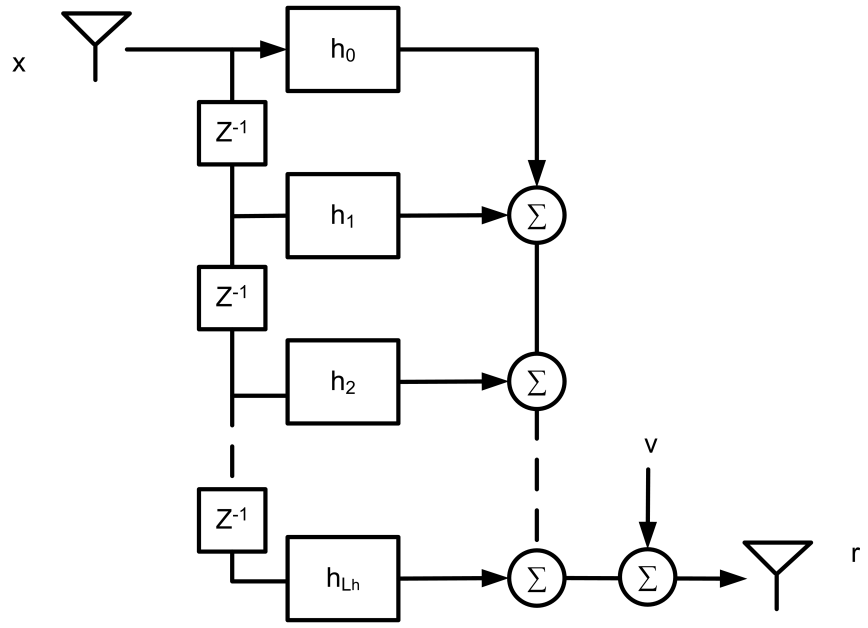

Figure 1.4: A frequency-selective channel.

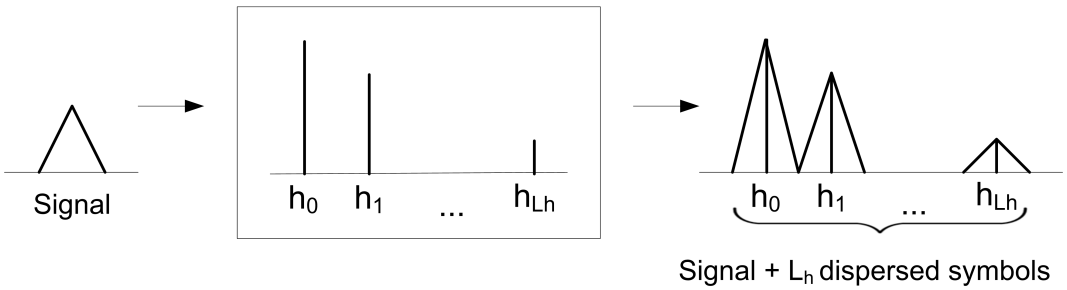

Figure 1.5: Signal dispersion through a frequency-selective channel.

The consequence of channel dispersion, unfortunately, is the presence of intersymbol interference (ISI) which is depicted in Figure **??** when three successive symbols are passed through a three tap frequency-selective fading channel. The effects of dispersive channels on STCs can only be observed

over a stream of successive symbols. Thus, block modelling is used to emulate systems in dispersive environments.

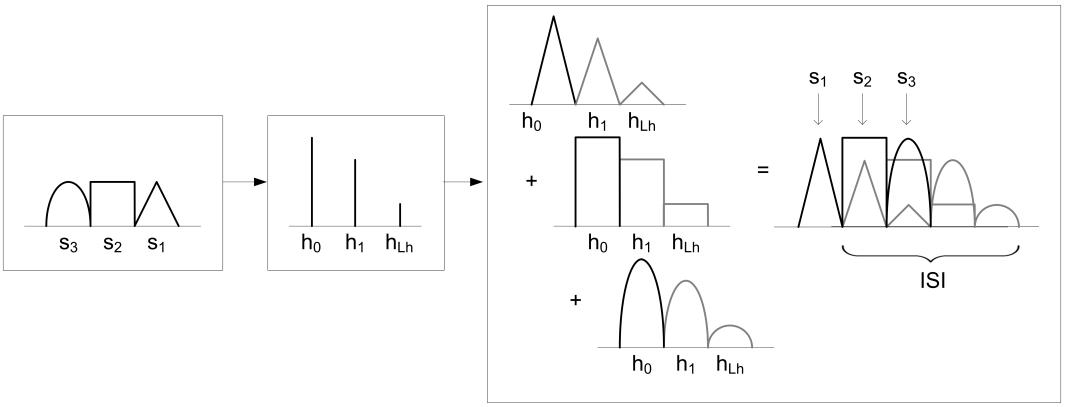

Figure 1.6: ISI in a frequency-selective channel.

In MIMO systems, the antennas at the transmitter and receiver are located in similar environments separated by small distances. Therefore, throughout the thesis, frequency-selective channels in the same system are assumed to be uncorrelated but have the same delay spread. In addition, perfect sampling and synchronisation are assumed which also applies to flat fading systems.

1.3 The MIMO System

The purpose of using multiple transmit and receive antennas is to exploit multipath propagation in wireless fading channels and therefore, deliver better performances. This technology has the ability to increase channel capacity [**? ?**] and lower the probability of error, enhancing the quality of service in the system. A single user MIMO system is shown in Figure **??** with N_t transmit antennas and N_r receive antennas. The channel tap, h_{nm}, denotes the complex gain between the m-th transmit antenna and n-th receive antenna.

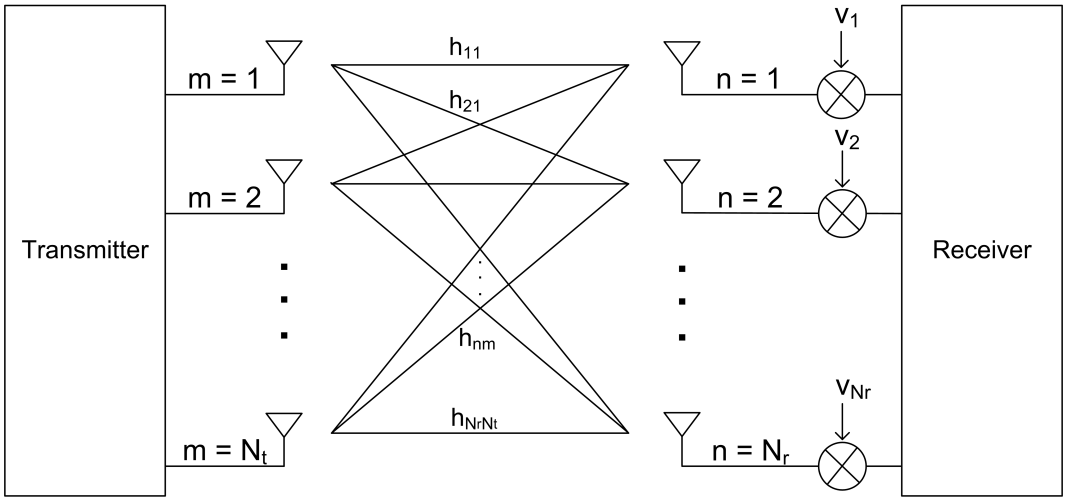

Figure 1.7: A MIMO system with N_t transmit antennas and N_r receive antennas.

MIMO systems can also be extended to multiple users when there are multiple concurrent MIMO systems sharing the same channel [**?**]. A different design strategy is required to handle multiuser interference and exploit the advantages offered by multiuser systems.

There are two classes of STCs [**?**]: space-time block codes (STBCs) and space-time trellis codes (STTCs). STTCs distribute convolutional codes over space and time and attain both coding and diversity performance gains [**?** **?**]. On the other hand, STBCs are simple with no temporal interference in flat fading channels [**?**]. In this thesis, the goal is to design high-rate STBCs in frequency-selective channels which suffer from ISI. The design of STBCs dictates the performance and rate of the system.

1.4 Literature Reviews

The growing traffic volume in wireless broadband networks demands high-rate transmission schemes in frequency-selective channels. Frequency-selectivity introduces time dispersion of symbols across the channel generating unwanted ISI. Literature reviews of high-rate coding schemes in flat fading channels and existing coding schemes in frequency-selective channels are summarised in this section.

In flat fading channels quasi-orthogonal STBCs (QOSTBCs) [**?**] are able to achieve full transmission rate and exploit the embedded partial orthogonal structure. The spatial multiplexing Vertical Bell Laboratories Layered Space-Time (VBLAST) [**?**] architecture pushes the boundary even further and achieves rate N_t where N_t is the number of transmit antennas. However, it does not take advantage of diversity and does not support any coding gain. Linear dispersion codes (LDCs) [**?**], on the other hand, have been demonstrated to achieve rates greater than one as well as coding gain. Extensions and variants of these schemes have been developed to achieve high-rate codes in flat fading systems.

Multiple design techniques have been used to combat wideband systems undergoing frequency-selectivity. Orthogonal frequency division multiplexing (OFDM) [**?** **?**] is one such scheme that aims to eliminate interference by converting the frequency-selective channel into multiple flat fading channels. OFDM is a multi-carrier modulation technique that is not suitable for narrowband channels and requires costly amplifiers. Another scheme is the single-carrier frequency-domain-equalized (SC-FDE) STBC [**?**] which maintains a

low level of peak to average power ratio. Both of these schemes achieve good performance in long dispersive channels, but equalisation is in the frequency domain and thus, require Fourier transforms. In this thesis, frequency-selective channels with a small number of taps are examined.

1.5 Thesis Contributions and Outline

The LDC has the ability to achieve high throughputs in flat flading systems. A general framework of LDCs in frequency-selective channels is proposed in this thesis with time-domain detection and equalisation at the receiver. Block processing models the frequency-selective system through the use of partitioned matrices. Linear and zero-forcing (ZF) receivers are investigated and reveals ZF is the better scheme for high-rate STBCs in frequency-selective channels.

The structure of the partitioned LDC system is extended to a multiuser co-operative dispersive environment. Through the assistance of another user in close proximity, two source nodes use the exchanged information to improve the reception of the signals at a distant destination. Linear and ZF detection are investigated for the multiuser system. The thesis is organised as outlined below.

Chapter 2 of the thesis describes two special cases of STBCs that have been developed in both frequency-flat and frequency-selective channels. The chapter begins with the classic Alamouti STBC offering diversity gain and simple linear maximum likelihood (ML) detection. Time reversal STBC shows the extension of the orthogonal code to dispersive environments. Maximum likelihood sequence estimation (MLSE) is introduced using the Viterbi algo-

rithm. On the other end of the STBC performance spectrum is the maximum rate achieving V-BLAST scheme described in both flat and frequency-selective environments. The chapter concludes with the general LDC structure that encompasses Alamouti STBC and V-BLAST as special cases.

Chapter 3 develops a general LDC structure for frequency-selective channels. Two detection schemes with moderate complexity are investigated, namely linear processing and ZF. ZF is shown to be a good detection scheme, but performance is limited by the system load. Exponential delay channel profiles are investigated where low power taps are excised to reduce load.

Chapter 4 describes a new multiuser cooperation system in frequency-selective environments. The transmission scheme employs the structure of the partitioned LDC system proposed in Chapter 2 in a half-duplex channel. The cooperative system requires the transmission of LDCs over three successive block intervals. Detection at the end of the cooperative frame is investigated for linear processing and ZF.

Chapter 5 concludes the thesis and presents suggestions for future work.

Chapter 2

Space-Time Block Codes

"It is not the mountain we conquer but ourselves."

Edmund Hillary

2.1 Introduction

The effects of multipath propagation in wireless channels give rise to random fluctuations of signal power at the receiver [**?**]. This is known as random fading and has the potential to severely degrade transmission reliability. However, multiple antennas can be used to create uncorrelated sub-channels in a multiple-input, multiple-output (MIMO) link assuming sufficient antenna spacing. The uncorrelated channels can be exploited to achieve diversity gain by sending replicas of the same signal across spatially separated antennas and thus increase the probability of correct signal detection. Additionally, uncorrelated channels can be exploited to send more data through the link, by sending different information from each antenna. The availability of both spatial and

temporal dimensions in multiple antenna systems can be explored to improve reliability and increase channel throughput [**?**]. The design of space-time block codes (STBCs) govern how the available dimensions are used and determine the system performance.

In this chapter, three design schemes are investigated, namely the Alamouti STBC, the Vertical Bell Laboratories Layered Space-Time (V-BLAST) code and a general class of STBCs called linear dispersion codes (LDCs) that subsumes the first two schemes as special cases.

The Alamouti STBC [**?**] achieves diversity gains by transmitting two data symbols using two transmit antennas and two time slots. A distinguishable property of the Alamouti STBC is its inherent orthogonality. It belongs to the group of codes called orthogonal STBCs (OSTBCs) [**?**]. There is considerable interest in OSTBCs due to their linear detection complexity. The OSTBC scheme has be studied in both frequency-flat and frequency-selective channels [**?** **?**]. The presence of ISI in frequency-selective channels increases receiver complexity, therefore, reinforcing the importance of simple linear detection as offered by OSTBCs.

The second space-time structure considered in this chapter is the multiplexing V-BLAST architecture [**?**]. This scheme realises the maximum achievable rate for a MIMO system by sacrificing system reliability. V-BLAST is also investigated in both flat and frequency-selective fading environments. The two contrasting systems depict the motivational advantages for using MIMO technology and lay out the challenges that will be encountered by broadband transmissions.

Lastly, LDC is the general class of STBCs that encompasses all linear

designs including the Alamouti STBC and the V-BLAST transmission scheme [**?**]. The general framework of LDCs offers designers the flexibility to attain a variety of code rates up to the maximum multiplexed rate, where each transmit antenna is used to send a different symbol during each time slot. In this chapter, the structure of LDCs at the encoder and decoder is described followed by an examination of a high-rate LDC by Hassibi and Hochwald [**?**].

2.2 Orthogonal STBCs

The desire for high-rate STBCs is often limited by the receiver processing power. Many factors including the modulation level, system size and code rate influence the processing complexity. STBCs with both full [**?**] and partial orthogonal designs [**?** **?** **?**] can significantly reduce detection complexity. In this section, the simplest OSTBC, named after its inventor, Alamouti [**?**] will be examined in flat fading channels. Larsson [**?**] extended the Alamouti STBC to frequency-selective channels and called it a time-reversal space-time block code (TR-STBC).

2.2.1 OSTBCs in Flat Fading Channels

The transmit diversity system designed by Alamouti [**?**] is shown in Figure **??** with $N_t = 2$ transmit antennas sending symbols across two independent wireless channels to a receive antenna denoted n. The diagram shows only one receive antenna, however, the same processing can be extended to any number of receive antennas, $n = 1, ..., N_r$ for $N_r > 1$. The scheme transmits $Q = 2$ data symbols over $T = 2$ symbol intervals and achieves a full rate of

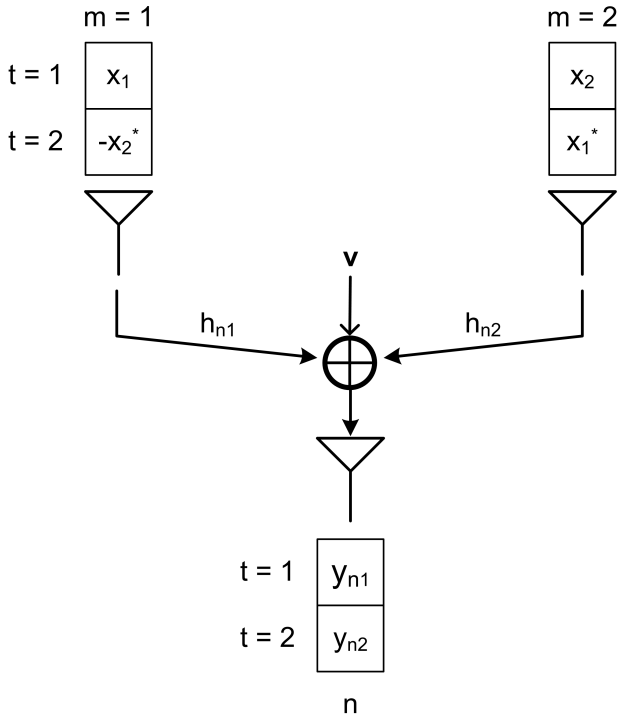

Figure 2.1: Two transmit antennas sending an Alamouti code to receive antenna n, $n = 1, ..., N_r$.

one. The rate of the STBC is defined as

$$R = \frac{\text{number of data symbols, Q}}{\text{number of time slots used, T}}. \tag{2.1}$$

Data is firstly mapped onto symbols x_q, for $q = 1, ..., Q$, chosen from an arbitrary M-ary symbol constellation. The symbols are encoded across space and time according to the STBC

$$\mathbf{S} = \begin{bmatrix} s_{11} & s_{12} \\ s_{21} & s_{22} \end{bmatrix} = \begin{bmatrix} x_1 & -x_2^* \\ x_2 & x_1^* \end{bmatrix}, \tag{2.2}$$

where $(\cdot)^*$ denotes complex symbol conjugation, $\mathbf{S} \in \mathbb{C}^{N_t \times T}$ is the notation for the Alamouti STBC with matrix dimensions of N_t rows and T columns and corresponding index s_{mt} denoting the data symbol sent from the m-th transmit antenna over the t-th symbol interval. Equation (**??**) shows symbols x_1 and x_2 are transmitted by antenna one and two, respectively, in the first symbol slot which is followed by the transmission of $-x_2^*$ and x_1^* from antenna one and two, respectively, in the second time slot. Assuming perfect synchronisation of symbols, the receiver observes signals from both transmit antennas at the same time. The resulting signal is a combination of transmitted signals multiplied by their respective channel taps and degraded by noise at the receiver. The noise is assumed to be additive white Gaussian noise (AWGN) with constant power over the entire bandwidth. This is the assumed noise for all the systems discussed in this thesis and is modelled by random Gaussian variables with zero mean and variance σ^2. The system is linear and represented in matrix

form as

$$\begin{bmatrix} y_{n1} & y_{n2} \end{bmatrix} = \begin{bmatrix} h_{n1} & h_{n2} \end{bmatrix} \begin{bmatrix} x_1 & -x_2^* \\ x_2 & x_1^* \end{bmatrix} + \begin{bmatrix} v_{n1} & v_{n2} \end{bmatrix}, \tag{2.3a}$$

$$\mathbf{Y} = \mathbf{HS} + \mathbf{V}, \tag{2.3b}$$

where $\mathbf{Y} \in \mathbb{C}^{N_r \times T}$ is the received matrix with y_{nt} denoting the symbol received at time t by receive antenna n, $\mathbf{H} \in \mathbb{C}^{N_r \times N_t}$ is the channel matrix with h_{nm} denoting the flat fading channel from the m-th transmit antenna to the n-th receive antenna and $\mathbf{V} \in \mathbb{C}^{N_r \times T}$ is the AWGN at the receiver, with v_{nt} denoting a random noise variable seen by the n-th receive antenna at time t. The received signal can also be represented by the equivalent matrix system

$$\begin{bmatrix} y_{n1} \\ y_{n2}^* \end{bmatrix} = \begin{bmatrix} h_{n1} & h_{n2} \\ h_{n2}^* & -h_{n1}^* \end{bmatrix} \begin{bmatrix} x_1 \\ x_2 \end{bmatrix} + \begin{bmatrix} v_{n1} \\ v_{n2}^* \end{bmatrix}, \tag{2.4a}$$

$$\mathbf{y}'_n = \mathcal{H}_n \mathbf{x} + \mathbf{v}'_n, \tag{2.4b}$$

for $n = 1, ...N_r$ where $\mathbf{y}_n$ and $\mathbf{v}_n \in \mathbb{C}^{1 \times T}$ are the n-th row of $\mathbf{Y}$ and $\mathbf{V}$, respectively, with symbol conjugation at $t = 2$, $\mathcal{H}_n \in \mathbb{C}^{T \times N_t}$ is an orthogonal channel matrix formed from the channel taps h_{n1} and h_{n2} and $\mathbf{x} \in \mathbb{C}^{N_t \times 1}$ is a vector of the modulated symbols. The orthogonal channel matrix has the property

$$\mathcal{H}_n^H \mathcal{H}_n = \begin{bmatrix} h_{n1}^* & h_{n2} \\ h_{n2}^* & -h_{n1} \end{bmatrix} \begin{bmatrix} h_{n1} & h_{n2} \\ h_{n2}^* & -h_{n1}^* \end{bmatrix} = \left(\|h_{n1}|^2 + |h_{n2}\|^2 \right) \mathbf{I}_2, \tag{2.5}$$

where $(\cdot)^H$ denotes the Hermitian transpose, $\|\cdot\|^2$ denotes the Euclidean norm and $\mathbf{I}_L$ denotes an identity matrix of size $L \times L$. This property makes it possible for the received symbols to be linearly combined in such a way that the transmit symbols are decoupled,

$$\hat{y}_1 = \sum_{n=1}^{N_r} (h_{n1}^* y_{n1} + h_{n2} y_{n2}^*) = \mathcal{H} x_1 + \underbrace{\sum_{n=1}^{N_r} (h_{11}^* v_{11} + h_{12} v_{12}^*)}_{\text{noise}}, \tag{2.6a}$$

$$\hat{y}_2 = \sum_{n=1}^{N_r} (h_{n2}^* y_{n1} - h_{n1} y_{n2}^*) = \mathcal{H} x_2 + \underbrace{\sum_{n=1}^{N_r} (h_{n2}^* v_{n1} - h_{n1} v_{n2}^*)}_{\text{noise}}, \tag{2.6b}$$

where $\mathcal{H}$ is the sum of the channel taps

$$\mathcal{H} = \sum_{n=1}^{N_r} \left(\|h_{n1}\|^2 + \|h_{n2}\|^2 \right). \tag{2.7}$$

Assuming full channel state information is available at the receiver, maximum likelihood (ML) decoding can be performed on the processed symbols $\hat{y}_1$ and $\hat{y}_2$ to estimate the most likely transmitted symbols $\hat{x}_1$ and $\hat{x}_2$. The ML algorithm searches over all constellation symbols and selects the symbol with the highest probability density function which equates to the symbol with the minimum Euclidean distance from the received signal as defined by

$$\hat{x}_1 = \arg \min_{m \in M} \|\hat{y}_1 - \mathcal{H} a_m\|^2, \tag{2.8a}$$

$$\hat{x}_2 = \arg \min_{m \in M} \|\hat{y}_2 - \mathcal{H} a_m\|^2, \tag{2.8b}$$

where a_m for $m = 1, ..., M$ is the set of symbols in the M-ary constellation. The structure of OSTBCs enables symbol decoupling which reduces the number of ML searches from M^Q to MQ as demonstrated by the Alamouti STBC.

The Alamouti OSTBC was generalised to $N_t > 2$ transmit antennas by Tarokh *et al* [**?**]. Tarokh showed that for complex-constellations, full rate OSTBCs exist only for $N_t = 2$ transmit antennas, $N_t = 3$ and 4 transmit antenna systems are able to achieve a rate of 3/4 and for other $N_t > 4$ systems, the rate achieved is only 1/2.

The bit-error rate (BER) performance of the Alamouti STBC in flat fading channels is shown in Figure **??** for different numbers of receive antennas. The BER is plotted against the signal-to-noise ratio (SNR), which is defined as the ratio of bit energy, E_b to noise spectral density with noise variance normalised to

$$\sigma^2 = \frac{N_t N_r E_s}{2R \cdot log_2(M) SNR_{dB}}, \tag{2.9}$$

where E_s is the energy per symbol. The order of diversity in the Alamouti system is increased by using more receive antennas.

2.2.2 OSTBC in Frequency-Selective Fading Channels

When a signal falls outside the channel coherence bandwidth, the wideband signal experiences frequency-selectivity [**?**] and channel dispersion in the time domain. The effects of dispersive channels on STBCs is observed over a stream of successive symbols and therefore, block modelling is used for frequency-selective systems.

The OSTBC in frequency-selective channels [**?**] for two transmit an-

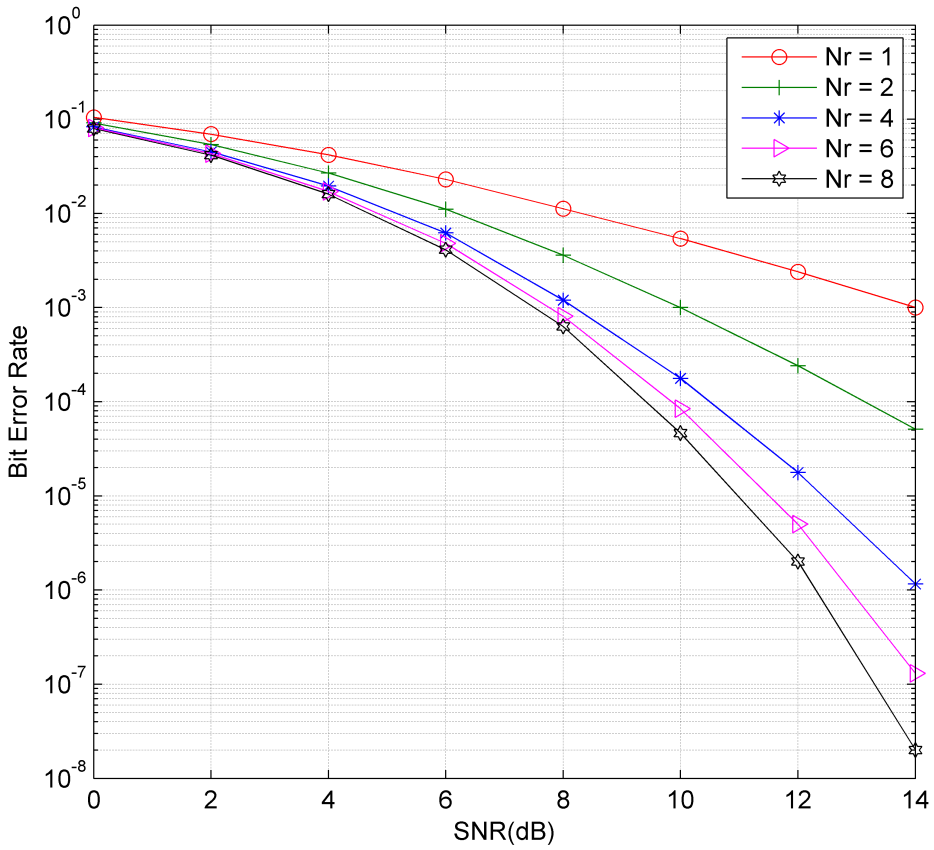

Figure 2.2: BER performance of Alamouti STBC versus number of receive antennas in flat fading channels using QPSK modulation.

tennas is depicted by the Alamouti scheme in Figure **??**, however, each symbol interval is replaced by a signalling interval capable of transmitting L_s symbols. Matrices in frequency-selective systems operate at a block level which will be defined explicitly using partitioned matrices [**?**]. For the Alamouti STBC in frequency-selective channels, $Q = 2$ symbol streams, consisting of L_x modulated symbols and a preamble and postamble composed of L_p known symbols appended to each end of the data sequences are sent using two transmit antennas over two signalling intervals. A stream of $L_s = L_x + 2L_p$ symbols is given as

$$\mathbf{x}_q = x_q[k] = \begin{bmatrix} x_q[1] & \dots & x_q[L_s] \end{bmatrix}, \quad q = 1, ..., Q, \tag{2.10}$$

where $x_q[l]$ for $l = 1, ..., L_s$ denotes the l-th symbol in the q-th symbol stream. The preamble and postamble act as guard intervals to prevent interference from successive symbol streams which can also be used to estimate the channel.

The Alamouti STBC in frequency-selective channels is denoted by the partitioned matrix

$$\underset{\sim}{\mathbf{S}} = \begin{bmatrix} \mathbf{S}_{11} & \mathbf{S}_{12} \\ \mathbf{S}_{21} & \mathbf{S}_{22} \end{bmatrix}, \tag{2.11}$$

which represents the symbol streams sent by $N_t = 2$ transmit antennas over

$T = 2$ signalling intervals. The partitioned matrix is denoted by

$$\underset{\sim}{\mathbf{S}} = \left[\underset{\sim}{\mathbf{s}}_{mt}\right]_{m=1,...N_t,t=1,...T}, \tag{2.12a}$$

$$\underset{\sim}{\mathbf{s}}_{mt} : p_m \times q_t = 1 \times L_s, \tag{2.12b}$$

indicating $\underset{\sim}{\mathbf{S}}$ is a partitioned matrix composed of $N_t = 2$ rows and $T = 2$ columns of the block entry, $\underset{\sim}{\mathbf{s}}_{mt}$ which has $p_m = 1$ rows and $q_t = L_s$ columns. These block elements are vectors of length $1 \times L_s$ denoting the symbol streams transmitted by antenna m during time slot t.

The total number of rows and columns in the matrix are computed by summing the rows and columns, respectively, of the submatrices and subvectors in the partitioned matrix. Therefore, the dimensions of the equivalent unpartitioned transmit matrix are

$$\text{total number of rows} = \sum_{m=1}^{N_t} p_m = N_t, \tag{2.13a}$$

$$\text{total number of columns} = \sum_{t=1}^{T} q_t = TL_s, \tag{2.13b}$$

and is denoted by the standard notation, $\mathbf{S} \in \mathbb{C}^{N_t \times TL_s}$. The m'-th row of the unpartitioned matrix $\mathbf{S}$ is the same as the d-th row in the c-th block entry, $\underset{\sim}{\mathbf{s}}_{c:} = [\underset{\sim}{\mathbf{s}}_{c1}, ..., \underset{\sim}{\mathbf{s}}_{cT}]$, where : denotes all entries from $t = 1, ...T$, as shown in Figure **??** and is equivalent to

$$m' = d + \sum_{m=1}^{c-1} p_m. \tag{2.14}$$

The t'-th column of $\mathbf{S}$ is depicted by the f-th column in the e-th block entry,

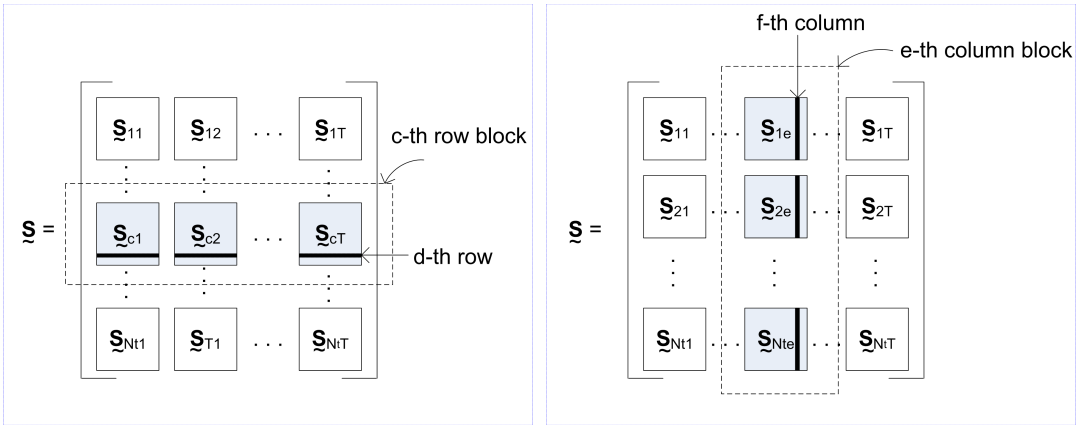

(a) Indexing a row **(b)** Indexing a column

Figure 2.3: Indexing a row and a column of a partitioned matrix.

$\underset{\sim}{\mathbf{S}}_{:e}[\underset{\sim}{\mathbf{S}}_{1e}, ..., \underset{\sim}{\mathbf{S}}_{N_t e}]^T$, where $[\cdot]^T$ denotes block transpose and : denotes all entries from $m = 1, ..., N_t$. This as shown in Figure **??** and is equivalent to

$$t' = f + \sum_{t=1}^{e-1} q_t. \tag{2.15}$$

Therefore, an element in the partitioned block is denoted as

$$\underset{\sim}{S}_{(c,d)(e,f)} = s_{m't'} \tag{2.16}$$

where $s_{m't'}$ denotes the single element in the m'-th row and t'-th column of the unpartitioned matrix $\mathbf{S}$.

Similar to the flat fading Alamouti STBC, $\mathbf{x}_1$ and $\mathbf{x}_2$ are transmitted from the corresponding transmit antennas in the first signalling interval. In the second signalling slot, transmit antenna one transmits a time reversed, symbol conjugated and negated stream of $\mathbf{x}_2$ while transmit antenna two sends a time

reversed and symbol conjugated stream of $\mathbf{x}_1$. This is written as

$$\underset{\sim}{\mathbf{s}}_{11} = \mathbf{x}_1, \tag{2.17a}$$

$$\underset{\sim}{\mathbf{s}}_{21} = \mathbf{x}_2, \tag{2.17b}$$

$$\underset{\sim}{\mathbf{s}}_{12} = -\mathbf{x}_2^* \mathbf{P}_{L_s}^{(0)}, \tag{2.17c}$$

$$\underset{\sim}{\mathbf{s}}_{22} = \mathbf{x}_1^* \mathbf{P}_{L_s}^{(0)}, \tag{2.17d}$$

where $\mathbf{P}_L^{(z)}$ is a $L \times L$ permutation matrix drawn from a set of permutation matrices $\left\{\mathbf{P}_L^{(z)}\right\}_{z=0}^{L-1}$ that performs a reverse cyclic shift depending on z [**?**]. The special case of z = 0 performs a time reversal of a vector of length L. The OSTBC in frequency-selective channel is shown pictorially in Figure **??**.

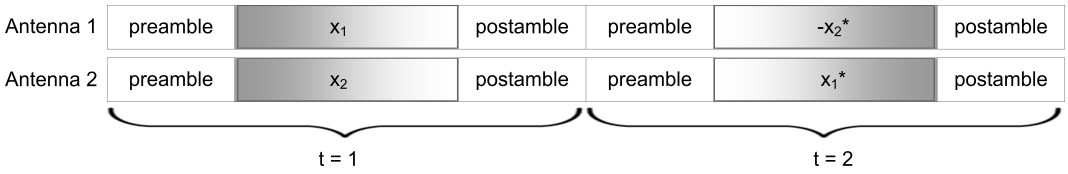

Figure 2.4: OSTBC in frequency-selective channels showing time-reversal of symbol streams in the second time slot.

The propagation channel between transmit antenna m and receiver antenna n is denoted by

$$\mathbf{h}_{nm} = h_{nm}[k] = \Big[h_{nm}[0] \quad h_{nm}[1] \quad \dots \quad h_{nm}[L_h],\Big] \tag{2.18}$$

where $h_{nm}[l]$ for $l = 0, ..., L_h$ denotes the l-th symbol tap in the frequency-selective channel and L_h is the length of the channel delay. The taps are assumed to be quasi-static for the period of $T = 2$ signalling intervals. The

channel matrix for the MIMO system is denoted by

$$\underset{\sim}{\mathbf{H}} = \left[\underset{\sim}{\mathbf{h}}_{nm}\right]_{n=1,...N_r,m=1,...N_t}, \tag{2.19a}$$

$$\underset{\sim}{\mathbf{h}}_{nm} : 1 \times (L_h + 1). \tag{2.19b}$$

with

$$\underset{\sim}{h}_{(n,1)(m,l+1)} = h_{nm}[l], \tag{2.20}$$

for $l = 0, ..., L_h$. The matrix representation for the frequency-selective Alamouti system is

$$\underset{\sim}{\mathbf{Y}} = \underset{\sim}{\mathbf{H}} \otimes \underset{\sim}{\mathbf{S}} + \underset{\sim}{\mathbf{V}}, \tag{2.21}$$

where

$$\underset{\sim}{\mathbf{Y}} = \left[\underset{\sim}{\mathbf{y}}_{nt}\right]_{n=1,...N_r,t=1,...T}, \tag{2.22a}$$

$$\underset{\sim}{\mathbf{y}}_{nt} : 1 \times (L_s + L_h), \tag{2.22b}$$

is the received partitioned matrix with $\underset{\sim}{\mathbf{y}}_{nt}$ denoting the $1 \times (L_s + L_h)$ symbol stream received at time slot t by receive antenna n and

$$\underset{\sim}{\mathbf{V}} = \left[\underset{\sim}{\mathbf{v}}_{nt}\right]_{n=1,...N_r,m=1,...T}, \tag{2.23a}$$

$$\underset{\sim}{\mathbf{v}}_{nt} : 1 \times (L_s + L_h), \tag{2.23b}$$

is the noise partitioned matrix with $\underset{\sim}{\mathbf{v}}_{nt}$ denoting the $1 \times (L_s + L_h)$ stream of

AWGN variables at receive antenna n during time slot t.

Partitioned matrix convolution operates very similarly to matrix multiplication where the subvector entries within a row are convolved with the associated subvector entries within a column of the second partitioned matrix. Addition sums the corresponding submatrices and subvectors together and therefore the vector entries in Equation (**??**) are equivalent to

$$\underset{\sim}{\mathbf{y}}_{nt} = \sum_{m=1}^{N_t} \underset{\sim}{\mathbf{h}}_{nm} \otimes \underset{\sim}{\mathbf{s}}_{mt} + \underset{\sim}{\mathbf{v}}_{nt}, \tag{2.24}$$

for $n = 1, ..., N_r$ and $t = 1, ...T$. Convolution of two sequences is given as

$$h_{nm}[k] \otimes s_{mt}[k] = \sum_{l=1}^{L_s} h_{nm}[k - l + 1] s_{mt}[l]. \tag{2.25}$$

A pictorial representation showing the convolution of a signal with a multi-tapped channel is depicted in Figure **??** displaying the presence of ISI in the received symbol stream over $L_s + L_h$ symbols.

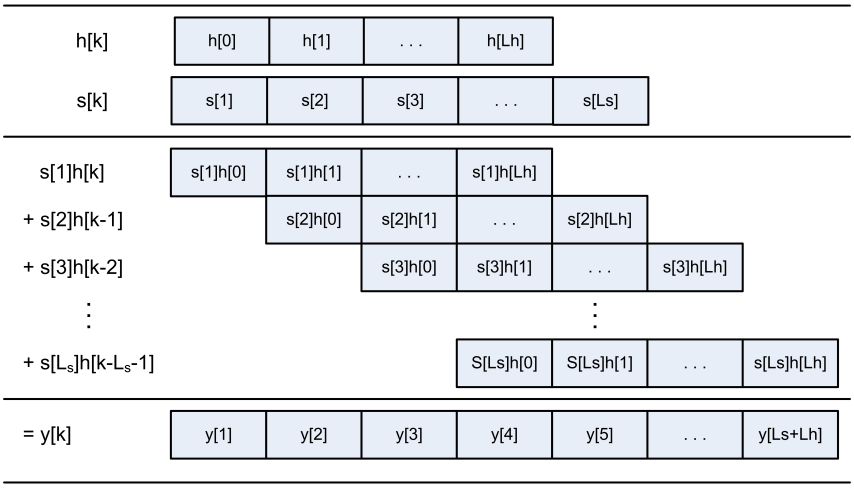

Figure 2.5: Diagram depicting a block of L_s data symbols transmitted through a frequency-selective channel with $L_h + 1$ taps.

Linear combining can be applied to the system at a block level to decouple the data symbol streams

$$\begin{aligned}\hat{\mathbf{y}}_1 &= \sum_{n=1}^{N_r}(\mathbf{h}_{n1}^* \otimes \mathbf{y}_{n1} + \mathbf{h}_{n2} \otimes \mathbf{y}_{n2}^*) \\ &= \boldsymbol{H} \otimes \mathbf{x}_1 + noise, \end{aligned} \tag{2.26a}$$

$$\begin{aligned}\hat{\mathbf{y}}_2 &= \sum_{n=1}^{N_r}(\mathbf{h}_{n2}^* \otimes \mathbf{y}_{n1} - \mathbf{h}_{n1} \otimes \mathbf{y}_{n2}^* \\ &= \boldsymbol{H} \otimes \mathbf{x}_2 + noise, \end{aligned} \tag{2.26b}$$

where $\boldsymbol{H} \in \mathbb{C}^{1\times(2L_h+1)}$ is the sum of the channels convolved with itself, given by

$$\boldsymbol{H} = \sum_{n=1}^{N_r}(\mathbf{h}_{n1} \otimes \mathbf{h}_{n1} + \mathbf{h}_{n2} \otimes \mathbf{h}_{n2}). \tag{2.27}$$

A ML decoder is used to detect the sequences $\mathbf{x}_1$ and $\mathbf{x}_2$, which is described in the following section and shown to increase in complexity with the length of the channel. The rate of the Alamouti STBC in frequency-selective channels is

$$R = \frac{QL_x}{TL_s}, \tag{2.28}$$

which converges to full rate $R = \dfrac{Q}{T} = 1$ as the ratio of data symbols to the preambles and postambles converges to one. The performance of the TR-STBC in frequency-selective channels is displayed in Figure **??** with the channels normalised to $E[\sum_{l=0}^{L_h} \|h_{nm}[l]\|^2] = 1$, where $E[\cdot]$ denotes the average mean. The results are plotted against SNR with noise variance normalised according

to Equation (??) and show frequency diversity is achieved by longer dispersive channels. The memory of the ML Viterbi decoder depends on the length of equation Equation (??). Therefore, the number of states in the Viterbi trellis is M^{2L_h} for the TR-STBC making it unsuitable for highly dispersive channels.

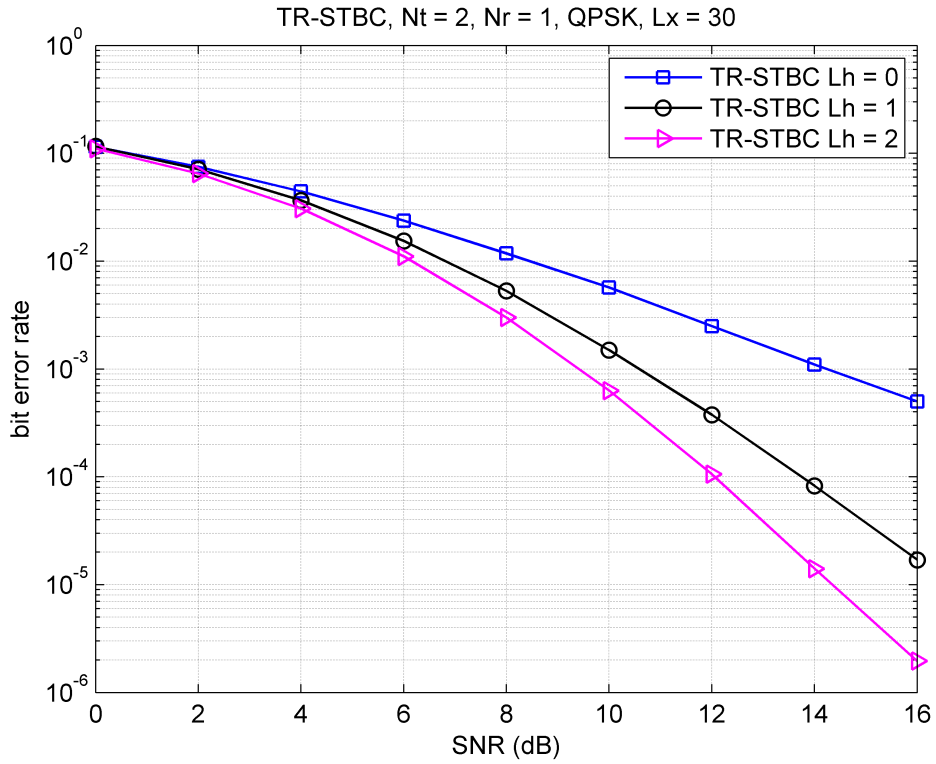

Figure 2.6: OSTBC versus channel length for $N_t = 2, N_r = 2$ and $L_x = 30$ using QPSK modulation.

2.2.2.1 Maximum Likelihood Sequence Detection

The dispersed symbols caused by frequency-selectivity contain valuable information. As a consequence, disregarding ISI in the process of detection can be detrimental to performance. Consideration of ISI is achieved through a process

known as maximum likelihood sequence estimation (MLSE)[**?**]. Therefore, it is performed on the decoupled sequences, $\hat{\mathbf{y}}_q$ from Equation (**??**) which estimates the most likely transmitted sequences $\hat{\mathbf{x}}_q$ with the largest probability density function [**?**] using

$$\hat{\mathbf{x}}_q = \arg \max_{m \in M^{L_x}} f(\hat{\mathbf{y}}_q | \hat{\mathbf{a}}_m, \mathbf{H}), \quad q = 1, ..., Q, \tag{2.29}$$

where $\hat{\mathbf{a}}_m \ \forall \ m = 1, ...M^{Lx}$ belongs to the set of all possible symbol combinations of the transmitted signal stream. The receiver is assumed to have full knowledge of $\mathbf{H}$. The probability density function of Equation (**??**) can be expressed as the Gaussian function

$$f(\hat{\mathbf{y}} | \hat{\mathbf{a}}_m, \mathbf{H}) = Ke^{-\frac{\|\mathbf{y} - \mathbf{H}\hat{\mathbf{a}}_m\|^2}{\sigma^2}}, \tag{2.30}$$

where K is a constant independent of $\hat{\mathbf{y}}$. This is equivalent to finding the sequence with the minimum Euclidean distance given by

$$\hat{\mathbf{x}}_q = \arg \min_{m \in M^{L_x}} \|\mathbf{y} - \mathbf{H}\hat{\mathbf{a}}_m\|^2. \tag{2.31}$$

The decoder must exhaustively search through M^{L_x} possible sequences, which increases exponentially with the length of the data sequence. This computational complexity is prohibitive for long data sequences.

The Viterbi algorithm is a form of dynamic programming that was first designed as a convolutional ML decoder [**?**]. As a result of its success in complexity reduction, it has been adapted for other applications including

MLSE of data streams in the presence of ISI [**?** **?**]. The algorithm of [**?**] is an efficient MLSE detection scheme that computes one symbol in the stream at a time with the ability to equalise ISI. The Viterbi algorithm finds the sequence with the minimum cost path in a structured trellis where cost metrics can include Hamming distance for hard decoding and Euclidean distance for soft decoding. The Viterbi algorithm will now be outlined using an example of a transmit sequence **s** passing through a frequency-selective channel **h** in the presence of noise, **v**, giving received sequence

$$\mathbf{y} = \mathbf{h} \otimes \mathbf{s} + \mathbf{v}. \tag{2.32}$$

Consider a data stream with $L_x = 5$ data symbols chosen from a $M = 2$-ary modulation and a frequency-selective channel with a delay spread of $L_h = 2$ symbols. The data stream is appended with a preamble and postamble of $L_p = L_h = 2$ zero symbols. Convolution of the transmit stream **s** with $L_s = L_x + 2L_p = 9$ symbols and the $L_h + 1 = 3$ multi-tap channel **h** is shown in Figure **??**. The output signal is a stream of $L_r = L_s + L_h = 11$ symbols, where symbols $y[3], ..., y[9]$ contain signal information.

A trellis is formed comprising of states, nodes and branches where the number of nodes at each stage determines the receiver complexity. The channel spread, L_h, signifies the channel memory and therefore dictates the number of symbols in each state. The number of states at each stage or time t in the trellis is fixed except at the beginning and end when the symbols are known. Figure **??** shows the state transitions for the example of Equation (**??**) from time t to $t' = t + 1$. The states are permutations of the M modulated symbols $a_1, ..., a_M$

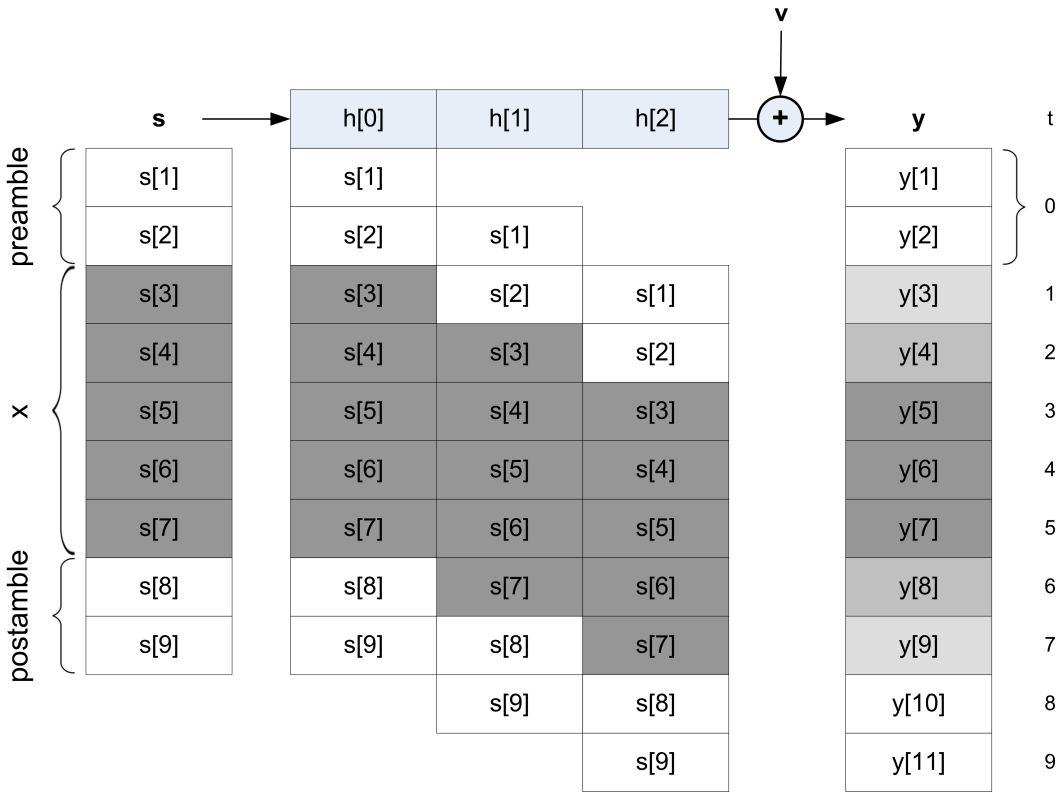

Figure 2.7: Example of convolution for $L_x = 5$, $L_h = L_p = 2$ and $M = 2$.

of the memory length in the channel, L_h. Each node in the trellis denotes a state, z at a point in time, t which is also denoted by a path metric value, $U_z^{(t)}$. At each node, M state transition metrics or branch metrics are computed for the next possible symbol in the sequence, $V_m^{(z)}(t')$, where $m = 1, ..., M$ denotes the m-th branch from state z at time t to t'. Thus, M branches enter the nodes at time t'. Each branch entering a node at t' is summed with the path metric from the originating state. A decision is made at each node at t' to select the path with the best metric while the remaining $M-1$ paths are eliminated from the trellis. The process is repeated until the whole sequence is detected and the winning path at the end of the trellis is chosen as the estimated sequence.

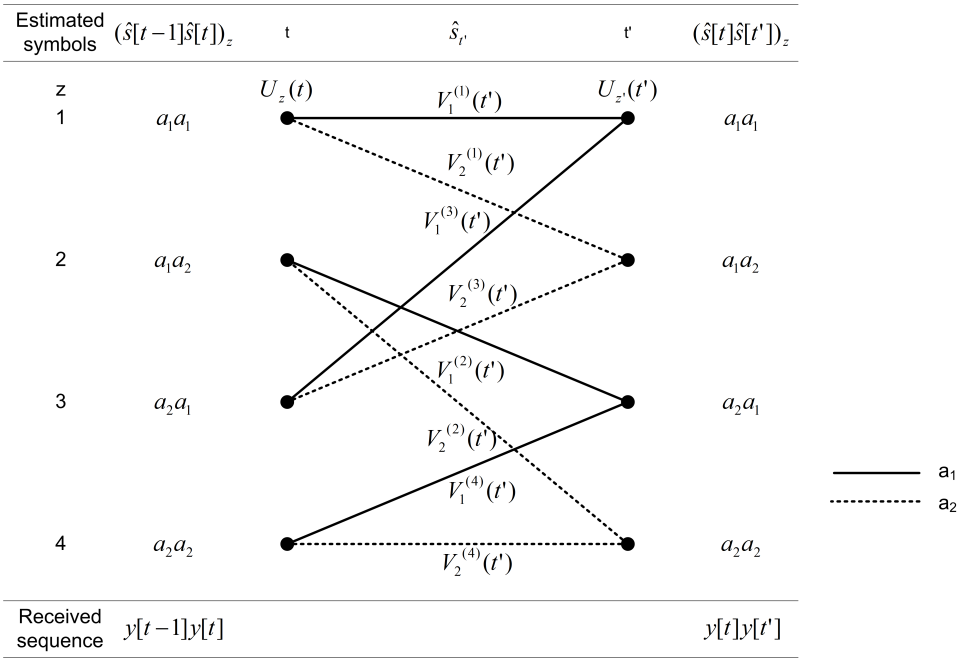

Figure 2.8: States and state transitions for $L_h = L_p = 2$ and $M = 2$.

The steps in the algorithm are described for the example of Equation (??) with $L_p = L_h = 2$ and $L_x = 5$. The trellis diagram is shown in Figure ??.

Compute the path metric at t=0 using

$$U_z^{(t)} = \sum_{l=1}^{L_p} \|y[l] - \sum_{i=0}^{l-1}(h[i]\hat{s}[l-i])_z\|^2, \tag{2.33}$$

for $z = 1$. Example: $L_p = 2$ gives

$$U_1^{(0)} = \underbrace{\|y[1] - h[0]s[1]\|^2}_{l=1} + \underbrace{\|y[2] - (h[0]s[2] + h[1]s[1])\|^2}_{l=2}. \tag{2.34}$$

2. t = 1,...L_h: Calculate the state transition branch metric using

$$V_m^{(z)}(t') = \|y[L_p + t] - (h[0]a_m + \sum_{i=1}^{L_h} h[i]\hat{s}[t-i]_z)\|^2, \tag{2.35}$$

for $z = 1, \ldots, M^{(t-1)}$ and $m = 1, \ldots, M$. The path metric at time t' is given by

$$U_z^{(t')} = V_m^{(z)}(t') + U_z^{(t)}, \tag{2.36}$$

where t' denotes the time at $t + 1$. The path with the minimum value of $U_z^{(t')}$ for each state, z at time t' is kept as the surviving path while the other $M - 1$ paths are eliminated from the trellis.

Example: $L_h = L_p = 2$ gives

$$t = 1: \quad V_m^{(z)}(2) = \|y[3] - (h[0]a_m + \sum_{i=1}^{2} h[i]\hat{s}[t-i]_z)\|^2$$
$$\forall \quad z = 1, m = 1, ...2, \text{ and} \tag{2.37a}$$

$$t = 2: \quad V_m^{(z)}(3) = \|y[4] - (h[0]a_m + \sum_{i=1}^{2} h[i]\hat{s}[t-i]_z)\|^2$$
$$\forall \quad z = 1, ..., 2, m = 1, ...2. \tag{2.37b}$$

3. $t = L_h + 1, \ldots, L_x$: Repeat Step **??**. for $z = 1, \ldots, M^{L_h}$ and $m = 1, \ldots, M$. Example:

$$t = 3, ..., 5: \quad V_m^{(z)}(t') = \|y[L_p + t] - (h[0]a_m + \sum_{i=1}^{2} h[i]\hat{s}[t-i]_z)\|^2$$
$$\forall \quad z = 1, ..., 4, m = 1, ...2. \tag{2.38}$$

4. $t = L_x + 1, ..., L_x + L_h$: The sequence tails off to the postamble state so the number of states decreases, giving

$$V_m^{(z)}(t') = \|y[L_p + t'] - \sum_{i=0}^{L_h} h[i]\hat{s}[t-i]_z\|^2 \tag{2.39}$$

for $z = 1, \ldots, M^{L_x + L_h - t}$ and $m = 0$.

Example: t' = 6, 7

$$t' = 6: \quad V_0^{(z)}(7) = \|y[8] + \sum_{i=0}^{2} h[i]\hat{s}[t-i]_z\|^2 \quad \forall \quad z = 1, 2, \tag{2.40a}$$

and

$$t' = 7: \quad V_0^{(z)}(8) = \|y[9] + \sum_{i=0}^{2} h[i]\hat{s}[t-i]_z\|^2 \quad \forall \quad z = 1. \tag{2.40b}$$

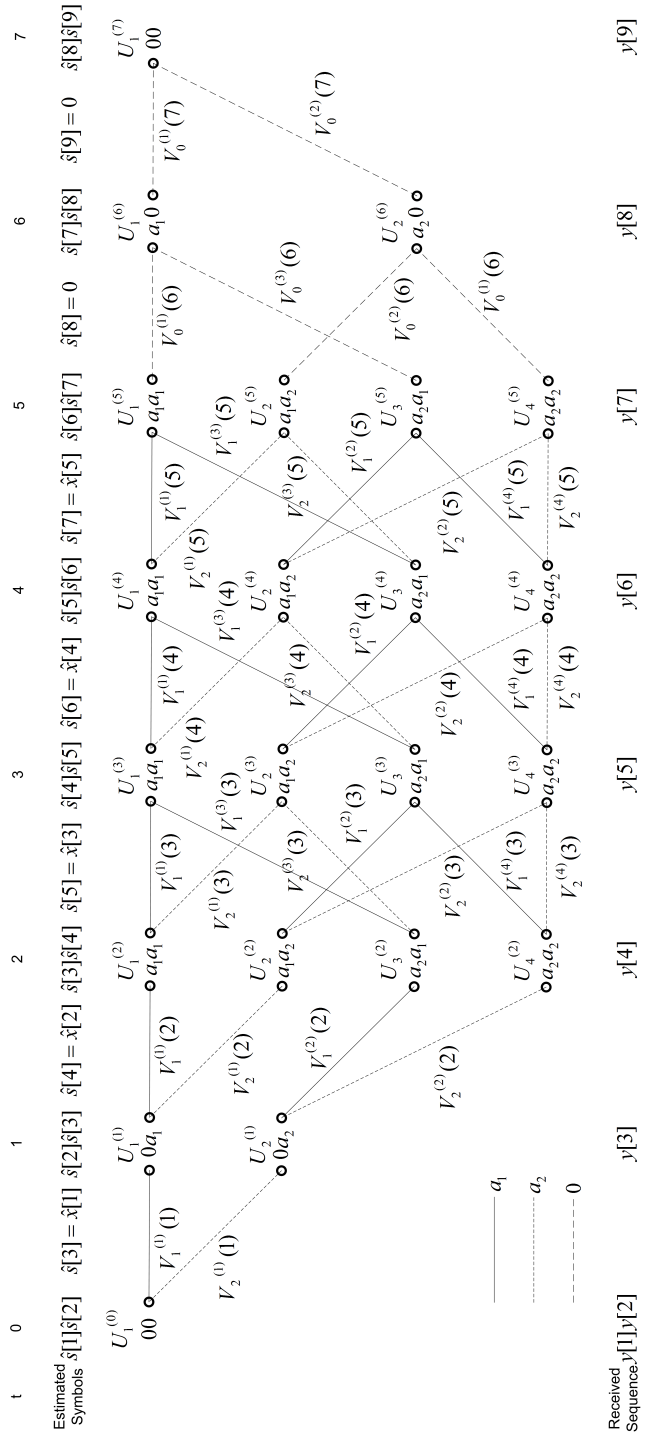

Figure 2.9: Viterbi trellis diagram for $L_h = L_p = 3$ and $M = 2$.

2.3 Vertical BLAST

The rate oriented STBCs sacrifice diversity by exploiting multipath to send different information across space and time. V-BLAST [**?**] is one such design which was developed by Foschini at Lucent Technologies Bell Laboratories which can handle large volumes of traffic and offers a simple sub-optimal detection method at the receiver. The V-BLAST architecture is described in the next section in both frequency-flat and frequency-selective environments using a layered detection scheme.

2.3.1 V-BLAST in Flat Fading Channels

The V-BLAST architecture is shown in Figure **??** where the modulated data is demultiplexed into N_t sub-streams and transmitted via the respective channels. During each symbol interval, a symbol is received at each of the N_r receive antennas. The symbol received at the n-th receive antenna at time t is given by

$$y_{nt} = \sum_{m=1}^{N_t} h_{nm} s_{mt} + v_{nt}, \tag{2.41}$$

where h_{nm} is the channel tap from the m-th transmit antenna to the n-th receive antenna, s_{nt} is the symbol from the m-th transmit antenna at time t and v_{nt} is the AWGN at the n-th receiver at time t. The subscript t can be dropped from the notation since there is no coding across time and therefore, systems in each time slot can be processed independently from those in other symbol time slots. The matrix representation for the system during a symbol

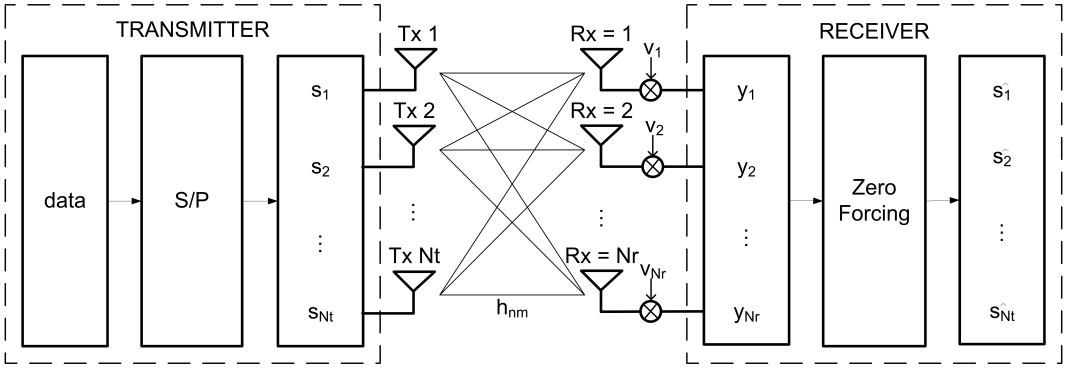

Figure 2.10: V-BLAST multiplexing system where each transmit antenna sends a data symbol s_m in one symbol period.

period is

$$\begin{bmatrix} y_1 \\ y_2 \\ \vdots \\ y_{N_r} \end{bmatrix} = \begin{bmatrix} h_{11} & h_{12} & \cdots & h_{1N_t} \\ h_{21} & h_{22} & \cdots & h_{2N_t} \\ \vdots & \vdots & \ddots & \vdots \\ h_{N_r1} & h_{N_r2} & \cdots & h_{N_rN_t} \end{bmatrix} \begin{bmatrix} s_1 \\ s_2 \\ \vdots \\ s_{N_r} \end{bmatrix} + \begin{bmatrix} v_1 \\ v_2 \\ \vdots \\ v_{N_r} \end{bmatrix}, \tag{2.42a}$$

$$\mathbf{y} = \mathbf{H}\mathbf{s} + \mathbf{v}. \tag{2.42b}$$

Joint ML detection of $Q = N_t$ symbols would require exhaustive search over M^Q codewords. Complexity can be reduced by using a zero forcing (ZF) approach [**?**], where each symbol in the received vector $\mathbf{y}$ is considered in turn as the desired signal, while the remaining symbols are regarded as unwanted interference. Suppose symbol s_a is being detected first, Figure **??** shows that interference can be removed if a zero forcing matrix, $\mathbf{G}$, exists that can force all the channels h_{nm}, for $m \neq a$ to zero. There are different methods for computing $\mathbf{G}$, the most popular being minimum mean square error (MMSE) and ZF. ZF is a simpler scheme [**?**] and therefore will be used to detect

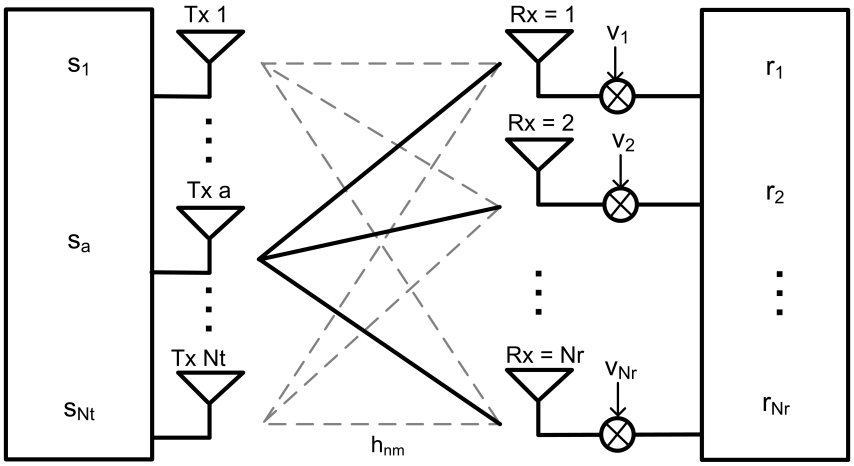

Figure 2.11: Nulling Interference in V-BLAST s_a as the desired signal

the V-BLAST system. The ZF matrix is computed from the Moore-Penrose pseudoinverse

$$\mathbf{G} = (\mathbf{H}^H\mathbf{H})^{-1}\mathbf{H}^H, \tag{2.43}$$

which has the property

$$\mathbf{GH} = \mathbf{I}_{N_t}, \tag{2.44}$$

where $\mathbf{I}_N$ is an identity matrix of size $N \times N$. The nulling matrix exists when $\mathbf{H}$ is not rank deficient or overloaded. Assuming there is full channel knowledge at the receiver, the interference can be zeroed out by multiplying the nulling matrix with the received signal

$$\hat{\mathbf{s}} = \mathbf{Gy} = \mathbf{s} + \mathbf{Gv}, \tag{2.45}$$

and therefore, $\hat{s}_q$ for $q = 1, ..., N_t$ can be successively detected. The decoder reduces to QM computations. Improvements can be achieved by subtracting each detected symbol from the system before the next symbol is estimated.

Interference is reduced in the new received vector

$$\mathbf{y}' = \mathbf{y} - s_m \mathbf{h}_m, \tag{2.46}$$

where $\mathbf{h}_m$ is the m-th column of matrix $\mathbf{H}$. The whole process is repeated until $Q = N_t$ symbols are detected. This detection scheme is called zero-forcing with successive interference cancellation (ZF-SIC).

Better performance can be gained if the symbols are detected in the order of highest post-detection signal to noise ratio (SNR) power. In other words, the symbols with fewer errors are detected first [**?**]. The post detection SNR is proportional to $\frac{1}{\|\mathbf{g}_m\|^2}$, where $\mathbf{g}_m$ is the m-th row of $\mathbf{G}$. Therefore, zero-forcing, ordered successive interference cancellation (ZF-OSIC) recursively detects and cancels the symbols with $min\left\{\frac{1}{\|\mathbf{g}_m\|^2}\right\}$.

The BER performance for the V-BLAST detection schemes in flat fading channels against SNR with noise variance of Equation (**??**) is shown in Figure **??**. ML detection achieves the best performance and is suitable for any system configuration, however, it is computationally complex. Diversity is lost for reduced complexity. These schemes require a nulling matrix which only exists for determinant systems, which means the number of receive antennas has to be equal to or greater than the number of transmitters in the flat fading V-BLAST system.

Figure **??** depicts the ML performance of the OSTBC and the high-rate uncoded V-BLAST system. These schemes demonstrate the advantages of STBCs and the trade-off between diversity gain and high throughput.

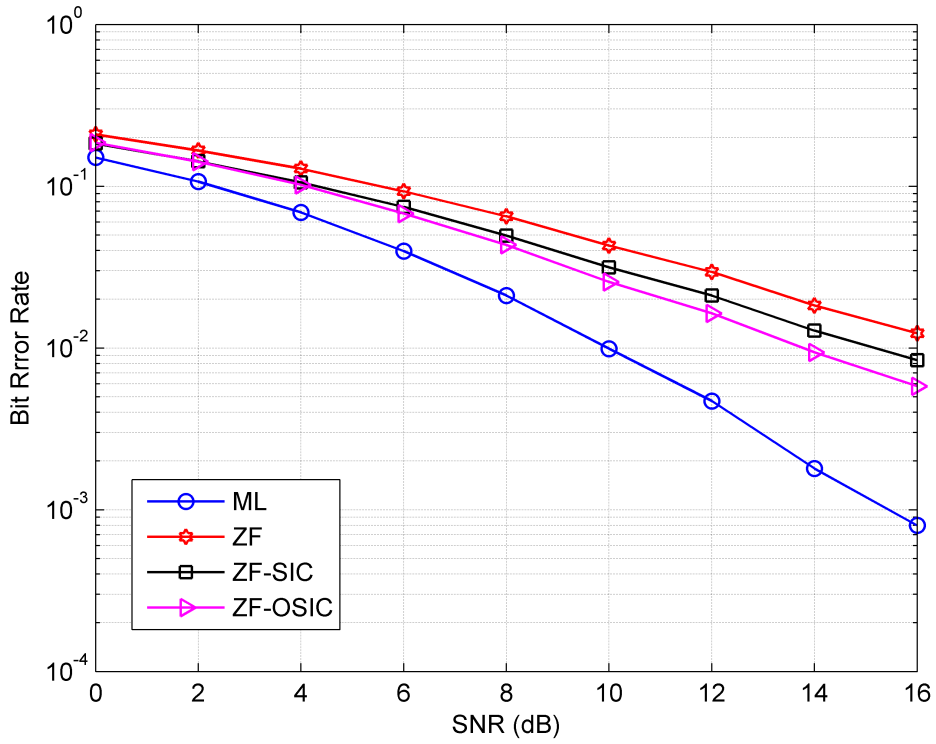

Figure 2.12: BER performance of V-BLAST for various detection schemes in flat fading channels for $N_t = 2, N_r = 2$ and QPSK modulation.

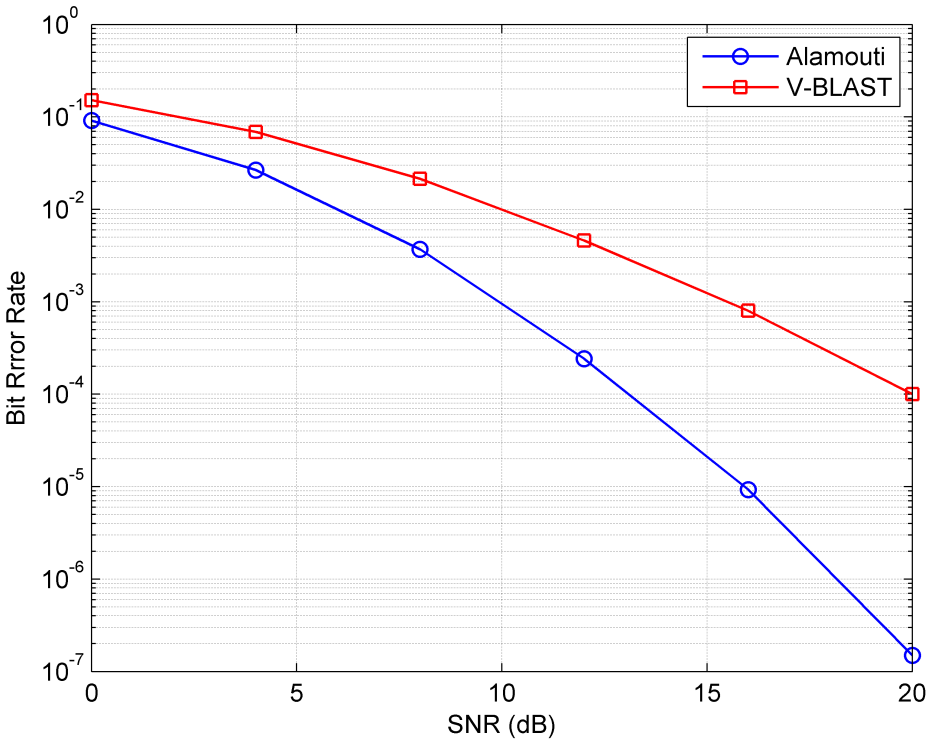

Figure 2.13: BER performance of high-rate V-BLAST versus Alamouti STBC in flat fading channels for $N_t = 2, N_r = 2$, QPSK modulation and ML detection.

2.3.2 V-BLAST in Frequency-Selective Channels

The V-BLAST system in frequency-selective environments can also be represented by the system in Figure **??** and can be denoted by the matrix system

$$\underset{\sim}{\mathbf{Y}} = \underset{\sim}{\mathbf{H}} \otimes \underset{\sim}{\mathbf{S}} + \underset{\sim}{\mathbf{V}}, \tag{2.47}$$

where the received partitioned matrix is given by

$$\underset{\sim}{\mathbf{Y}} = \left[\underset{\sim}{\mathbf{y}}_{nt}\right]_{n=1,\ldots N_r, t=1,\ldots T}, \tag{2.48a}$$

$$\underset{\sim}{\mathbf{y}}_n : 1 \times (L_s + L_h), \tag{2.48b}$$

with index $\underset{\sim}{\mathbf{y}}_n \in \mathbb{C}^{1\times(L_s+L_h)}$, denoting the signal stream received by the n-th receiver antenna. Since $T = 1$, the time subscript is dropped from the notation. The partitioned channel matrix is given by

$$\underset{\sim}{\mathbf{H}} = \left[\underset{\sim}{\mathbf{h}}_{nm}\right]_{n=1,\ldots N_r, m=1,\ldots N_t}, \tag{2.49a}$$

$$\underset{\sim}{\mathbf{y}}_{nm} : 1 \times (L_h + 1), \tag{2.49b}$$

with index $\underset{\sim}{\mathbf{h}}_{nm} \in \mathbb{C}^{1\times(L_h+1)}$ denoting the frequency-selective channel from the m-th transmit antenna to the n-th receive antenna and L_h is the channel delay in symbols. The partitioned transmit signal is given by

$$\underset{\sim}{\mathbf{S}} = \left[\underset{\sim}{\mathbf{s}}_{mt}\right]_{m=1,\ldots N_t, t=1,\ldots T}, \tag{2.50a}$$

$$\underset{\sim}{\mathbf{s}}_m : 1 \times L_s, \tag{2.50b}$$

with $\underset{\sim}{\mathbf{s}}_m \in \mathbb{C}^{1\times L_s}$ denoting the stream of $L_s = L_x + 2L_p$ symbols transmitted by the m-th transmit antenna and t is also dropped from the subscript as the transmitted data is independent across time. Lastly, the noise partitioned matrix is given by

$$\underset{\sim}{\mathbf{V}} = \left[\underset{\sim}{\mathbf{v}}_{nt}\right]_{n=1,...N_r,t=1,...T}, \tag{2.51a}$$

$$\underset{\sim}{\mathbf{v}}_n : 1 \times (L_s + L_h), \tag{2.51b}$$

with index $\underset{\sim}{\mathbf{v}}_n \in \mathbb{C}^{1\times(L_s+L_h)}$ denoting the noise at the n-th receive antenna at signalling interval t, which is also dropped from the notation. The convolution and addition operations on the partitioned system of Equation (**??**) is equivalent to

$$\underset{\sim}{\mathbf{y}}_n = \sum_{m=1}^{N_t} \underset{\sim}{\mathbf{h}}_{nm} \otimes \underset{\sim}{\mathbf{s}}_m + \underset{\sim}{\mathbf{v}}_n. \tag{2.52}$$

The system is converted to an equivalent flat fading system to enable interference nulling. A single-input, single-output (SISO) frequency-selective channel $\underset{\sim}{\mathbf{h}}_{nm}$ can be represented by an equivalent flat fading system with $L_h + 1$ virtual transmit antennas sending a delayed version of the corresponding symbol stream $\underset{\sim}{\mathbf{s}}_m$ to a single receive antenna [**?**]. The variable, $h_{nm}[l]$ denotes the l-th channel tap from transmit antenna m to receive antenna n which is equivalent to

$$h_{nm}[l] = \underset{\sim}{h}_{(n,a)(m,l+1)} \tag{2.53}$$

of the partitioned channel matrix from Equation (**??**) for $l = 0, ..., L_h$. The

tap models a single flat fading channel sending the symbol stream

$$\mathbf{s}_m^{(l)} = \begin{bmatrix} \mathbf{0}_l & \mathbf{s}_m & \mathbf{0}_{L_h-l} \end{bmatrix}, \in \mathbb{R}^{1\times(L_s+L_h)}, \tag{2.54}$$

where $\mathbf{0}_L$ denotes an all zero vector of length $1 \times L$. The equivalent system is a multiple-input, single-output (MISO) flat fading system with $L_h + 1$ transmit antennas sending data over $L_s + L_h$ symbol slots. The transmitting block for the flat fading MISO system is given as

$$\mathbf{S}_m = \begin{bmatrix} \mathbf{s}_m^{(0)} \\ \mathbf{s}_m^{(1)} \\ \vdots \\ \mathbf{s}_m^{(L_h)} \end{bmatrix}, \in \mathbb{R}^{(L_h+1)\times(L_s+L_h)}, \tag{2.55}$$

for the m-th frequency-selective channel, $\underset{\sim}{\mathbf{h}}_{nm}$, for all $n = 1, ..., N_r$. The equivalent flat fading system of Equation (**??**) can be written as

$$\mathbf{Y} = \mathbf{H}\mathbf{S}_T + \mathbf{V}, \tag{2.56}$$

where $\mathbf{Y} \in \mathbb{R}^{N_r\times(L_s+L_h)}$ and $\mathbf{V} \in \mathbb{R}^{N_r\times(L_s+L_h)}$ are the unpartitioned received and noise matrices of Equation (**??**) and Equation (**??**), respectively, with elements in the n-th row and l-th column equivalent to the partitioned matrices

$$y_{nl} = \underset{\sim}{y}_{(n,1)(1,l)}, \tag{2.57}$$

and

$$v_{nl} = \underset{\sim}{v}_{(n,1)(1,l)}, \tag{2.58}$$

for $l = 1, ..., (L_s + L_h)$ and $n = 1, ..., N_r$. $\mathbf{H} \in \mathbb{R}^{N_r \times N_t(L_h+1)}$ is the unpartitioned channel matrix with the equivalent elements

$$h_{n'm'} = h_{nm}[l] = \underset{\sim}{h}_{(n,1)(m,l+1)}, \tag{2.59}$$

for $l = 0, ..., L_h$, $n = 1, ..., N_r$ and

$$m' = l + 1 + (m-1)(L_h + 1), \tag{2.60a}$$

$$n' = n, \tag{2.60b}$$

denote the m'-th row and n'-th column of $\mathbf{H}$. The total transmit matrix for the equivalent flat fading system is given as

$$\mathbf{S}_T = \begin{bmatrix} \mathbf{S}_1 \\ \mathbf{S}_2 \\ \vdots \\ \mathbf{S}_{N_t} \end{bmatrix}, \in \mathbb{R}^{Q(L_h+1)\times(L_s+L_h)}, \tag{2.61}$$

where $\mathbf{S}_m$ is the matrix from Equation (**??**) with delayed versions of the signal stream, $\mathbf{s}_m$, transmitted from the virtual transmit antennas.

A layered detection scheme similar to the V-BLAST scheme of Section **??** can be applied to this system, where each layer $\mathbf{S}_m$ is detected at one time.

Suppose $\mathbf{S}_a$ is being detected, the nulling vector needs to zero out all indices $h_{n'm'}$ for $m \neq a$. This nulling matrix exists when

$$N_r > N_t(L_h + 1) - (L_h + 1). \tag{2.62}$$

The performance of V-BLAST in frequency-selective channels is shown in Figure **??** for different channel delays. Contrary to the results from the TR-STBC scheme, higher performance is achieved by shorter channels. This is explained by the criterion in Equation (**??**) where increasing the channel length, L_h, reduces the number of linear equations in the system. Therefore, the frequency diversity gain is mitigated by the increased loading in the system.

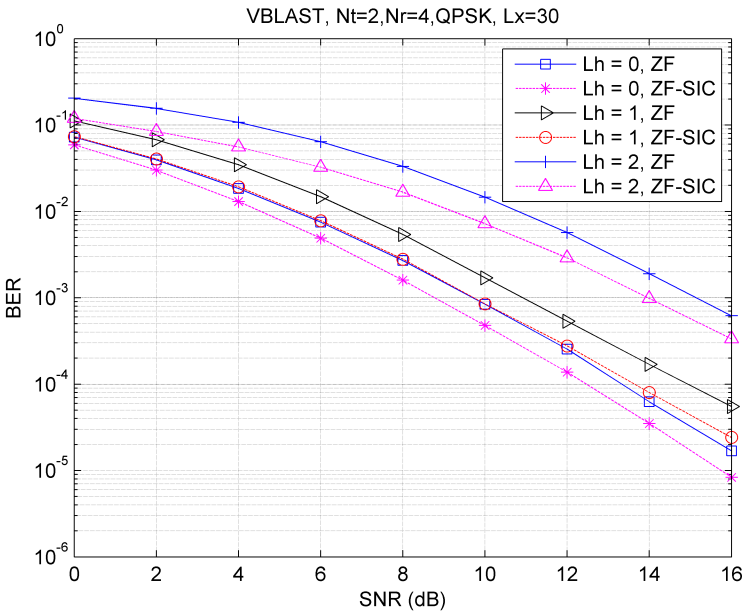

Figure 2.14: V-BLAST versus channel length for $N_t = 2, N_r = 4, L_x = 30$ using QPSK modulation.

2.4 Linear Dispersion Codes

The general structure of LDCs in flat fading channels has been presented in many papers [**?**], [**?**], [**?**] and textbooks [**?**], [**?**] and is also described in this section. LDCs are block codes whose entries are linear combinations of the transmit symbols, $x_1, x_2, ..., x_Q$ chosen from an arbitrary constellation. An LDC, $\mathbf{S} \in \mathbb{C}^{T \times N_t}$ is given by

$$\mathbf{S} = \sum_{q=1}^{Q} (\alpha_q \mathbf{A}_q + j\beta_q \mathbf{B}_q), \tag{2.63}$$

with index s_{tm} denoting the symbol transmitted by the m-th transmit antenna at time t. Variables α_q and β_q denote the real and imaginary components from the transmit symbol x_q for $q = 1, ..., Q$, where Q is the number of transmit symbols dispersed in the LDC. The dispersion matrices governing the distribution of α_q and β_q in space and time are given by

$$\mathbf{A}_q = \begin{bmatrix} a_{11}^{(q)} & \dots & a_{1N_t}^{(q)} \\ \vdots & \ddots & \vdots \\ a_{T1}^{(q)} & \dots & a_{TN_t}^{(q)} \end{bmatrix}, \in \mathbb{C}^{T \times N_t}, \tag{2.64a}$$

$$\mathbf{B}_q = \begin{bmatrix} b_{11}^{(q)} & \dots & b_{1N_t}^{(q)} \\ \vdots & \ddots & \vdots \\ b_{T1}^{(q)} & \dots & b_{TN_t}^{(q)} \end{bmatrix}, \in \mathbb{C}^{T \times N_t}, \tag{2.64b}$$

These matrices are designed to maximise the mutual information between the data symbols $\mathbf{x} = x_1, x_2, ..., x_Q$ and the received signal. The design criterion is

subjected to one of the following constraints [**?**],

$$\sum_{q=1}^{Q}(tr\mathbf{A}_q^*\mathbf{A} + tr\mathbf{B}_q^*\mathbf{B}) = 2TN_t \tag{2.65}$$

$$tr\mathbf{A}_q^*\mathbf{A} = tr\mathbf{B}_q^*\mathbf{B} = \frac{TN_t}{Q}, q = 1, \dots Q \tag{2.66}$$

$$\mathbf{A}_q^*\mathbf{A} = \mathbf{B}_q^*\mathbf{B} = \frac{T}{Q}\mathbf{I}_{N_t}, q = 1, \dots Q. \tag{2.67}$$

The received signal is the sum of N_t transmit symbols across the independent flat fading channels and can be represented by the matrix notation

$$\mathbf{R} = \mathbf{S}\mathbf{H}' + \mathbf{V}, \tag{2.68}$$

where $\mathbf{R} \in \mathbb{C}^{T\times N_r}$ is the received matrix with r_{tn} denoting the n-th received symbol at time t, $\mathbf{H} \in \mathbb{C}^{N_r\times N_t}$ is the channel matrix which is assumed to be constant for T symbol intervals and known by the receiver with h_{nm} denoting the channel tap between transmit antenna m and receive antenna n and $\mathbf{V} \in \mathbb{C}^{T\times N_r}$ is the noise matrix with v_{tn} denoting AWGN at the n-th receiver seen at time t.

2.4.1 Decoding

Optimal detection of any STBCs demands exhaustive search over all possible codewords. For a LDC, the number of searches in the codebook is M^Q, which is impractical for large modulations or systems with high throughput. Fortunately, the variables α, β are linear in the STBC and can be extracted out from the block code to form an equivalent real system of equations, where

perfect phase coherence is assumed. The new system is structurally similar to V-BLAST and thus, the detection complexity can be reduced by ZF. The equivalent real system is first described. The STBC from Equation (**??**) is substituted into the LDC system of Equation (**??**) to give

$$\mathbf{R} = \sum_{q=1}^{Q} (\alpha_q \mathbf{A}_q + j\beta_q \mathbf{B}_q)\mathbf{H}' + \mathbf{V}. \tag{2.69}$$

Expanding and decomposing into real and imaginary terms gives

$$\mathbf{R}^{\mathbb{R}} = \sum_{q=1}^{Q} \left[(\mathbf{A}_q^{\mathbb{R}} \mathbf{H}'^{\mathbb{R}} - \mathbf{A}_q^{\mathbb{I}} \mathbf{H}'^{\mathbb{I}})\alpha_q + (-\mathbf{B}_q^{\mathbb{I}} \mathbf{H}'^{\mathbb{R}} - \mathbf{B}_q \mathbb{R} \mathbf{H}'^{\mathbb{I}})\beta_q \right] + \mathbf{V}^{\mathbb{R}} \tag{2.70a}$$

$$\mathbf{R}^{\mathbb{I}} = \sum_{q=1}^{Q} \left[(\mathbf{A}_q^{\mathbb{I}} \mathbf{H}'^{\mathbb{R}} + \mathbf{A}_q^{\mathbb{R}} \mathbf{H}'^{\mathbb{I}})\alpha_q + (\mathbf{B}_q^{\mathbb{R}} \mathbf{H}'^{\mathbb{R}} - \mathbf{B}_q^{\mathbb{I}} \mathbf{H}'^{\mathbb{I}})\beta_q \right] + \mathbf{V}^{\mathbb{I}}. \tag{2.70b}$$

Let $\mathbf{R}^{\mathbb{R}}$, $\mathbf{R}^{\mathbb{I}}$, $\mathbf{V}^{\mathbb{R}}$ and $\mathbf{V}^{\mathbb{I}} \in \mathbb{R}^{T \times Nr}$ be the real and imaginary components of matrix $\mathbf{R}$ and $\mathbf{V}$, then $\mathbf{r}_n^{\mathbb{R}}$, $\mathbf{r}_n^{\mathbb{I}}$, $\mathbf{v}_n^{\mathbb{R}}$ and $\mathbf{v}_n^{\mathbb{I}}$ are the n-th column of $\mathbf{R}^{\mathbb{R}}$,$\mathbf{R}^{\mathbb{I}}$, $\mathbf{V}^{\mathbb{R}}$ and $\mathbf{V}^{\mathbb{I}}$, respectively. The columns can be arranged to form the new LDC system

$$\begin{bmatrix} \mathbf{r}_1^{\mathbb{R}} \\ \mathbf{r}_1^{\mathbb{I}} \\ \vdots \\ \mathbf{r}_{N_r}^{\mathbb{R}} \\ \mathbf{r}_{N_r}^{\mathbb{I}} \end{bmatrix} = \boldsymbol{\mathcal{H}} \begin{bmatrix} \alpha_1 \\ \beta_1 \\ \vdots \\ \alpha_Q \\ \beta_Q \end{bmatrix} + \begin{bmatrix} \mathbf{v}_1^{\mathbb{R}} \\ \mathbf{v}_1^{\mathbb{I}} \\ \vdots \\ \mathbf{v}_{N_r}^{\mathbb{R}} \\ \mathbf{v}_{N_r}^{\mathbb{I}} \end{bmatrix}, \tag{2.71a}$$

$$\mathbf{r} = \boldsymbol{\mathcal{H}}\mathbf{x} + \mathbf{v}, \tag{2.71b}$$

where $\boldsymbol{\mathcal{H}} \in \mathbb{R}^{2N_rT \times 2Q}$ is also a modified channel matrix

$$\boldsymbol{\mathcal{H}} = \begin{bmatrix} \boldsymbol{\mathcal{A}}_1\mathbf{h}_1 & \boldsymbol{\mathcal{B}}_1\mathbf{h}_1 & \cdots & \boldsymbol{\mathcal{A}}_Q\mathbf{h}_1 & \boldsymbol{\mathcal{B}}_Q\mathbf{h}_1 \\ \vdots & \vdots & \ddots & \vdots & \vdots \\ \boldsymbol{\mathcal{A}}_1\mathbf{h}_{N_r} & \boldsymbol{\mathcal{B}}_1\mathbf{h}_{N_r} & \cdots & \boldsymbol{\mathcal{A}}_Q\mathbf{h}_{N_r} & \boldsymbol{\mathcal{B}}_Q\mathbf{h}_{N_r} \end{bmatrix}. \tag{2.72}$$

The channel matrix contains the dispersion matrices given by

$$\boldsymbol{\mathcal{A}}_q = \begin{bmatrix} \mathbf{A}_q^{\mathbb{R}} & -\mathbf{A}_q^{\mathbb{I}} \\ \mathbf{A}_q^{\mathbb{I}} & \mathbf{A}_q^{\mathbb{R}} \end{bmatrix}, \in \mathbb{R}^{2T \times 2N_t}, \tag{2.73}$$

$$\boldsymbol{\mathcal{B}}_q = \begin{bmatrix} -\mathbf{B}_q^{\mathbb{I}} & -\mathbf{B}_q^{\mathbb{R}} \\ \mathbf{B}_q^{\mathbb{R}} & -\mathbf{B}_q^{\mathbb{I}} \end{bmatrix}, \in \mathbb{R}^{2T \times 2N_t}, \tag{2.74}$$

and channel vector given by

$$\mathbf{h}_n = \begin{bmatrix} \mathbf{h}_n^{\mathbb{R}} \\ \mathbf{h}_n^{\mathbb{I}} \end{bmatrix}, \in \mathbb{R}^{2N_t \times 1}, \quad n = 1, \ldots, N_r \tag{2.75}$$

where $\mathbf{h}_n^{\mathbb{R}} \in \mathbb{R}^{N_t \times 1}$ and $\mathbf{h}_n^{\mathbb{I}} \in \mathbb{R}^{N_t \times 1}$ are the n-th real and imaginary columns of the matrix $\mathbf{H}$. Equation (**??**) can be decoded using ZF provided $N_rT \geqslant Q$ is satisfied.

2.4.2 A High-Rate LDC

The mutual information between the transmit and receive symbols affects the performance. Therefore, the design of dispersion codes is crucial. As mentioned previously, LDCs subsume as special cases both the Alamouti STBC

and V-BLAST. The Alamouti STBC can be written as a LDC with dispersion matrices

$$\mathbf{A}_1 = \begin{bmatrix} 1 & 0 \\ 0 & 1 \end{bmatrix}, \mathbf{A}_2 = \begin{bmatrix} 0 & -1 \\ -1 & 0 \end{bmatrix}, \tag{2.76a}$$

$$\mathbf{B}_1 = \begin{bmatrix} 1 & 0 \\ 0 & -1 \end{bmatrix}, \mathbf{B}_2 = \begin{bmatrix} 0 & 1 \\ 1 & 0 \end{bmatrix} \tag{2.76b}$$

for $T = N_t = Q = 2$. V-BLAST corresponds to a LDC with $Q = N_t T$ with the dispersion matrices

$$\begin{aligned} \mathbf{A}_{N_t(\tau-1)+m} = \mathbf{B}_{N_t(\tau-1)+m} = \zeta_\tau \eta_m \\ \tau = 1, ..., T, m = 1, ...N_t, \end{aligned} \tag{2.77}$$

where ζ_τ and η_m are T- and N_t- dimensional column and row vectors, respectively, with one in the τth and mth entries and zeros elsewhere. The design from Hassibi in [**?**] is able to attain the same rate as V-BLAST for a $Q = N_t T = 4$ system, but uses the dispersion code given by

$$\begin{aligned} \mathbf{A}_{N_t(k-1)+l} = \mathbf{B}_{N_t(l-1)+1} = \frac{1}{N_t} D^{k-1} \Pi^{l-1} \\ k = 1, ...N_t, l = 1, ..., N_t, \end{aligned} \tag{2.78}$$

where

$$D = \begin{bmatrix} 1 & 0 & \cdots & 0 \\ 0 & e^{j\frac{2\pi}{N_t}} & 0 & \cdots \\ \vdots & & \ddots & \\ 0 & & & e^{j\frac{2\pi(N_t-1)}{N_t}} \end{bmatrix}, \tag{2.79}$$

and

$$\Pi = \begin{bmatrix} 0 & \cdots & & 0 & 1 \\ 1 & 0 & \cdots & & 0 \\ 0 & 1 & 0 & \cdots & 0 \\ \vdots & & \ddots & & \vdots \\ 0 & \cdots & 0 & 1 & 0 \end{bmatrix}. \tag{2.80}$$

The performance of the Alamouti STBC and the LDC of Equation (**??**) are compared in Figure **??** for a system with $N_t = 2$ transmit antennas and $N_r = 2$ receive antennas in flat fading environments. ML detection and ZF-SIC of the LDC both achieve the same optimum Alamouti performance.

The performance of the LDCs with V-BLAST dispersion matrices in Equation (**??**) and Hassibi's dispersion matrices in Equation (**??**) are compared in Figure **??** with a standard $N_t = 2$ by $N_r = 2$ V-BLAST system in flat fading systems. All systems achieve the same high-rate of $R = N_t$. ML detection is shown to achieve better performance over ZF detection but with higher decoding complexity. ML decoding shows the system of Equation (**??**) achieves a small diversity gain over the the uncoded ML detected V-BLAST system. ZF detection gives the same performance in all three systems. The

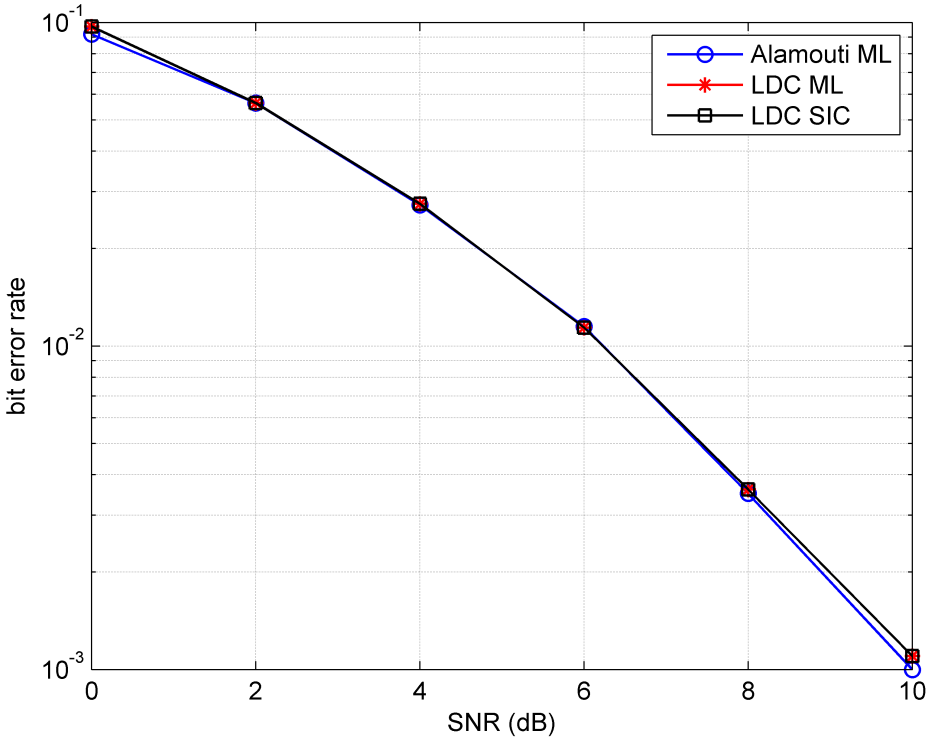

Figure 2.15: BER performance of Alamouti STBC versus orthogonal LDC for $N_t = 2$ and $N_r = 2$ using QPSK modulation in flat fading channels.

LDC framework is presented as a general scheme for designers to select the desired trade-off between low error rate and high throughput. This thesis is interested in high-rate STBCs. Therefore, the next chapter develops the LDC framework in frequency-selective channels and analyses the system using the example of Equation (**??**).

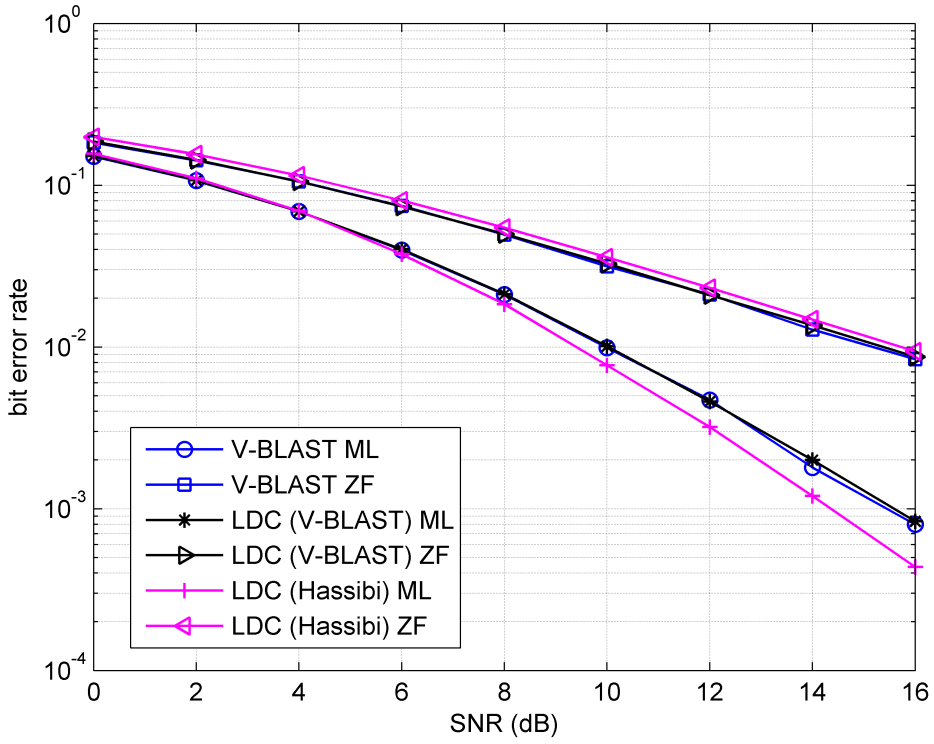

Figure 2.16: BER performance of V-BLAST versus LDCs with the same rate for $N_t = 2$, $N_r = 2$ and QPSK modulation in flat fading channels.

2.5 Summary

The OSTBC has been proven to achieve better performance than uncoded V-BLAST and offers simple linear decoding at the receiver. The Alamouti STBC

sends two symbols over four available spatial-time slots so it has throughput of one symbol per time slot. OSTBCs can be applied to bigger systems, however, only two transmit antenna schemes achieve full rate of one symbol per time slot. On the other hand, multiplexing schemes trade diversity for higher throughputs. V-BLAST utilises every available slot in space and time to transmit data and achieves rate $R = N_t$ in the MIMO system. These schemes illustrate the extremes of the diversity-multiplexing trade-off. A general framework that encompasses both OSTBC and V-BLAST, namely LDCs, is described and shown to provide flexibility in performance selection.

The extension OSTBC and VBLAST systems to frequency-selective channels is also considered in this thesis. The dispersive environment requires sequence processing which is demanding for joint detection. Therefore, linear decoupling or zero-forcing of interfering symbols is necessary at the decoder. Linear decoupling is limited to orthogonal STBCs, but provides optimal performance. ZF degrades performance, but is suitable for any LDCs provided the system is not overloaded. In the next chapter, the LDC is extended to operate in channels with non-zero delay spreads.

Chapter 3

High-Rate STBC in Frequency-Selective Channels

> "If we knew what it was we were doing, it would not be called research, would it?"
>
> *Albert Einstein*

3.1 Introduction

The convenience of wireless technology has played a massive role in the increasing popularity of wireless communication. However, time delay dispersion from multipath propagation is detrimental to the quality of service in the wireless channel [**?**]. The delay spread gives rise to multiple received replicas of the signal and leads to destructive behaviours in out of phase signal components. The time delay dispersion results in time-domain intersymbol interference (ISI). In the frequency-domain, it results in frequency-selectivity [**?**], where different

frequency components of the signal experience different attenuations.

The rapid technological advance and development of high-speed applications have pushed the need for higher data rates. Limited wireless spectrum seeks better spectral efficiency. High data-rates also translate to wider signal bandwidths that tend to be greater than the channel coherence bandwidth. This results in channel delay spreads greater than the transmit symbol period. Thus, the design of high-rate space-time block codes (STBCs) in frequency-selective channels is important for modern day wireless communication. Orthogonal frequency division multiplexing (OFDM) [**?**] is a popular method for combating ISI by dividing the frequency-selective channel into multiple single-tapped sub-channels. However, OFDM is not suitable for channels with small bandwidths where dividing the frequency-selective channels into narrowband sub-channels may not be possible. In this chapter, a high-rate coding scheme is proposed for operating over comparatively narrow frequency-selective channels.

Linear dispersion codes (LDCs) provide the option to design high-rate STBCs and subsume as special cases the orthogonal STBC and the Vertical Bell Laboratories Layered Space-Time (V-BLAST) schemes in frequency non-selective channels. A linear design from Hassibi [**?**] achieved rates comparable with the high-rate V-BLAST multiplexing architecture. Since LDCs can be designed to achieve the same rate as spatial multiplexing systems, this chapter endeavours to extend LDCs to operate in frequency-selective channels. High-rate STBCs at greater than one data symbol per time slot, lack orthogonality and therefore detection complexity is an issue. As a result, a general detection framework with practical complexity that has the ability to equalize ISI and

mitigate inter-block interference is required.

This chapter develops a general framework for LDCs in frequency-selective environments and studies various detection approaches. In addition, the limitations of LDCs in frequency-selective channels are investigated.

3.2 LDCs in Frequency-Selective Channels

As mentioned in Section **??**, LDCs have been developed in many papers for flat Rayleigh fading channels. However, extension of LDCs to frequency-selective environments is limited in the literature. The presence of ISI makes detection difficult. Variants of the multicarrier OFDM [**?**] scheme have been used to combat ISI. OFDM performs inverse Fourier transform to split the frequency-selective channel into multiple parallel flat sub-channels and protects the signal from frequency-selectivity. In addition to its unsuitability for narrowband channels, OFDM also has a high peak-to-average power ratio requiring costly power amplifiers and is sensitive to carrier frequency offset and phase noise [**?**]. OFDM is also disadvantaged by the maximum data packet size being limited by the Fourier transform block length. This affects the spectral efficiency for short packet transmissions [**?**].

Single carrier modulations with time or frequency-domain equalisation (FDE) have reduced peak to average ratio requirements and therefore do not require costly power amplifiers. FDE [**?**] operates on a Fourier transformed block of data and has the same performance and low complexity as OFDM [**?**]. Figure **??** shows the complexity comparison between different forms of equalisation [**?**]. The complexity of time-domain equalisation exceeds that of

FDE and OFDM with increasing channel lengths, however, it does not require Fourier transformation and therefore it is attractive for equalising frequency-selective channels with a small number of taps.

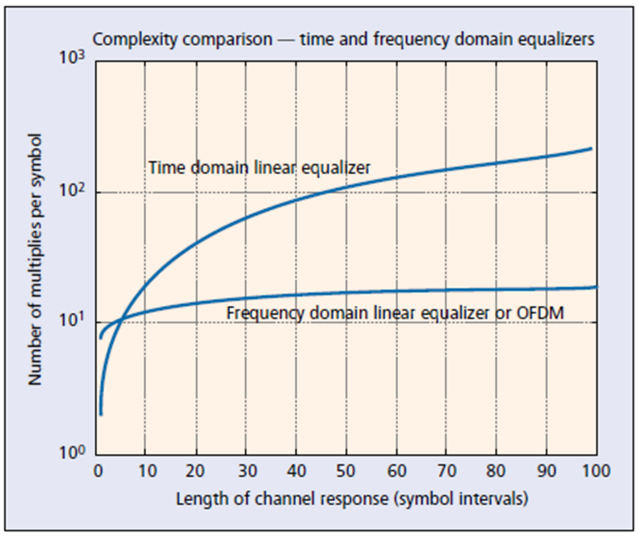

Figure 3.1: Complexity comparison of equalisers in time and frequency-domain taken from [**?**].

LDCs have been extended using OFDM in [**?**] and frequency-domain equalisation in [**?**]. These approaches are suitable for wideband channels. On the other hand, Ghaderipoor's high-rate LDC in [**?**] is more appropriate for narrowband dispersive channels with time-domain detection. However, it avoids the problem of ISI by transmitting only one symbol every four symbol periods across a four tap frequency-selective channel. This avoids ISI at the cost of significantly reducing the transmission rate.

In this chapter, the general LDC framework for short dispersive channels is developed in a phase coherent system. The structure supports block processing of signal streams through frequency-selective channels. Single-carrier time-domain equalisation is investigated for quasi-static channels where chan-

nel gains are constant over the period it takes to transmit the LDC.

3.2.1 General Structure

Single-carrier STBC transmissions across frequency-selective channels are typically based on sequences or blocks of symbols instead of individual symbols, which presents challenges and additional complexity to the LDC structure. It involves the manipulation of partitioned matrices which are matrices with entries consisting of blocks of smaller matrices or smaller vectors [**?**].

The LDC data structure is displayed in Figure **??**. It shows that N_t transmit antennas are used to send dispersed information over T time slots. The LDC is represented using a partitioned matrix, where each entry is a subvector denoting a stream of symbols sent over a fixed time interval from a particular transmit antenna in the MIMO link. Each time slot per antenna is able to transmit a stream of $L_s = 2L_p + L_x$ symbols, where L_x symbols contain data information which will be defined later and L_p known symbols are appended to each end of the data symbols to prevent interference between consecutive data symbol blocks sent in time.

The partitioned LDC in matrix form is given by

$$\underset{\sim}{\mathbf{S}} = \begin{bmatrix} \mathbb{s}_{11} & \cdots & \mathbb{s}_{1N_t} \\ \vdots & \ddots & \vdots \\ \mathbb{s}_{T1} & \cdots & \mathbb{s}_{TN_t} \end{bmatrix}, \tag{3.1}$$

where $\underset{\sim}{\cdot}$ signifies a partitioned matrix with subvector $\mathbb{s}_{tm} \in \mathbb{C}^{1\times L_s}$ denoting the symbol stream transmitted from transmit antenna m during time slot t. The

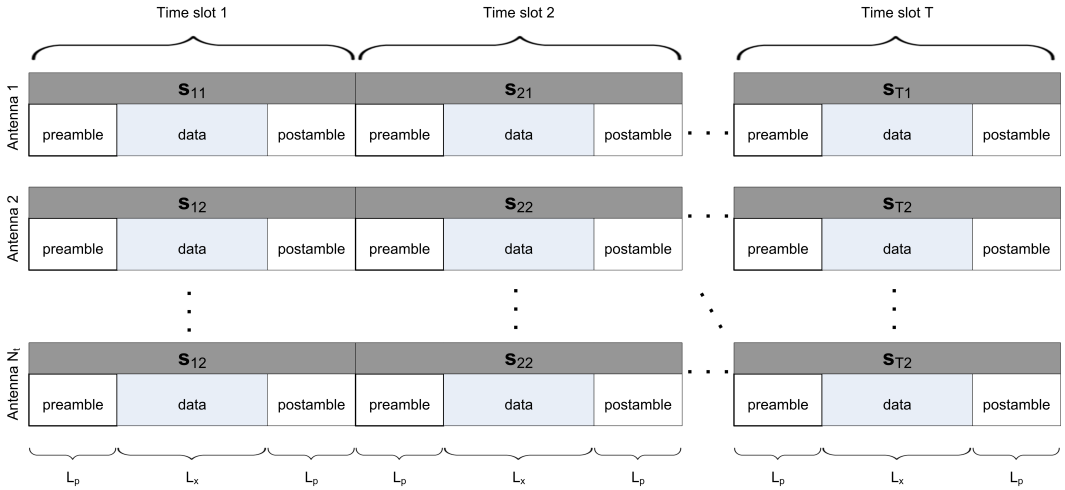

Figure 3.2: Diagram showing the LDC symbol streams.

partitioned matrix of Equation (**??**) is also denoted by

$$\underset{\sim}{\mathbf{S}} = \left[\underset{\sim}{\mathbf{s}}_{tm}\right]_{t=1,...T,m=1,...N_t} \tag{3.2a}$$

$$\underset{\sim}{\mathbf{s}}_{tm} : p_t \times q_m = 1 \times L_s. \tag{3.2b}$$

This indicates that the partitioned matrix $\underset{\sim}{\mathbf{S}}$ is made up of T rows and N_t columns of sub-blocks $\underset{\sim}{\mathbf{s}}_{tm}$, which have p_t rows and q_m columns. In this instance, $p_t = 1$ and $q_m = L_s$ for $t = 1, ...T$ and $m = 1, .., N_t$ and entries $\underset{\sim}{\mathbf{s}}_{tm}$ are row vectors in the partitioned matrix. Refer to Section **??** for the notations to index a partitioned matrix.

In flat fading LDCs, there are Q dispersion matrices governing the distribution of data symbols across space and time, where Q is the number of data symbols dispersed in a LDC. The distribution of Q symbol streams across N_t transmit antennas and T time slots is governed by partitioned dispersion codes which are extended from the dispersion matrices in flat fading channels.

The partitioned dispersion matrices are denoted by

$$\underset{\sim}{\mathbf{A}}_q^{(L_s)} = \left[\underset{\sim}{\mathbf{A}}_{tm}^{(q)}\right]_{t=1,...T,m=1,...N_t} \tag{3.3a}$$

$$\underset{\sim}{\mathbf{B}}_q^{(L_s)} = \left[\underset{\sim}{\mathbf{B}}_{tm}^{(q)}\right]_{t=1,...T,m=1,...N_t} \tag{3.3b}$$

$$\{\underset{\sim}{\mathbf{A}}_{tm}^{(q)}, \underset{\sim}{\mathbf{B}}_{tm}^{(q)}\} : L_s \times L_s, \tag{3.3c}$$

for $q = 1, ..., Q$, where the submatrices $\{\underset{\sim}{\mathbf{A}}_{tm}^{(q)}, \underset{\sim}{\mathbf{B}}_{tm}^{(q)}\}$, for $t = 1, ..., T$ and $m = 1, ..., N_t$, are identity matrices scaled by the respective dispersion matrix elements in Equation (**??**) giving

$$\underset{\sim}{\mathbf{A}}_{tm}^{(q)} = a_{tm}^{(q)}\mathbf{I}_{Ls}, \tag{3.4a}$$

$$\underset{\sim}{\mathbf{B}}_{tm}^{(q)} = b_{tm}^{(q)}\mathbf{I}_{Ls}, \tag{3.4b}$$

where $\mathbf{I}_{L_s}$ denotes an identity matrix of size $L_s \times L_s$. The data streams $\mathbf{x}_q$, for $q = 1, ...Q$, consist of L_x modulated symbols which are appended with preamble and postamble vectors of length L_p symbols as shown in Figure **??**.

At the encoder, the symbol streams of length $L_s = 2L_p + L_x$ are separated into real and imaginary stream components before they are linearly dispersed across space and time. The signal components are denoted by

$$\boldsymbol{\alpha}_q = \mathcal{R}\{[\text{preamble} \quad \mathbf{x}_q \quad \text{postamble}]\}, \in \mathbb{R}^{1\times L_s}, \tag{3.5a}$$

$$\boldsymbol{\beta}_q = \mathcal{I}\{[\text{preamble} \quad \mathbf{x}_q \quad \text{postamble}]\}, \in \mathbb{R}^{1\times L_s}, \tag{3.5b}$$

for $q = 1, ...Q$, and $\mathcal{R}\{\cdot\}$ and $\mathcal{I}\{\cdot\}$ denote the real and imaginary components,

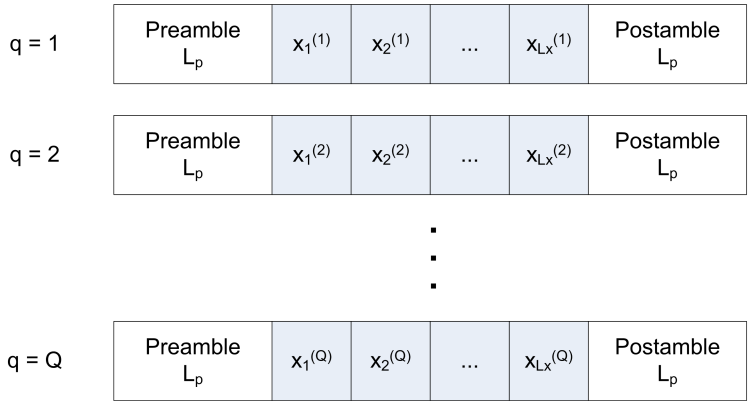

Figure 3.3: Diagram showing Q data symbol streams appended with preambles and postambles before they are encoded across space and time

respectively. The LDC from Equation (**??**) can now be defined as a linear combination of the data streams in Equation (**??**) as governed by the dispersion matrices in Equation (**??**), giving

$$\underset{\sim}{\mathbf{S}} = \sum_{q=1}^{Q} (\boldsymbol{\alpha}_q \underset{\sim}{\mathbf{A}}_q^{(L_s)} + j\boldsymbol{\beta}_q \underset{\sim}{\mathbf{B}}_q^{(L_s)}). \tag{3.6}$$

Addition of the partitioned matrices sums the corresponding submatrices and subvectors together and therefore

$$\underset{\sim}{\mathbf{s}}_{tm} = \sum_{q=1}^{Q} (\boldsymbol{\alpha}_q \underset{\sim}{\mathbf{A}}_{tm}^{(q)} + j\boldsymbol{\beta}_q \underset{\sim}{\mathbf{B}}_{tm}^{(q)}), \tag{3.7}$$

for $t = 1, ..., T$ and $m = 1, ..., N_t$. The identity matrices in $\{\underset{\sim}{\mathbf{A}}_{tm}^{(q)}, \underset{\sim}{\mathbf{B}}_{tm}^{(q)}\}$ do not alter the order of the data symbols in each stream.

The frequency-selective MIMO channel is represented by the parti-

tioned matrix

$$\underset{\sim}{\mathbf{H}} = \left[\underset{\sim}{\mathbf{h}}_{mn}\right]_{m=1,...N_t,n=1,...N_r} \tag{3.8a}$$

$$\underset{\sim}{\mathbf{h}}_{mn} : 1 \times (L_h + 1), \tag{3.8b}$$

where the subvector

$$\underset{\sim}{\mathbf{h}}_{mn} = \left[h_{mn}[0], ..., h_{mn}[L_h]\right], \tag{3.9}$$

denotes the frequency-selective channel with L_h+1 taps from transmit antenna m to receive antenna n. Each individual channel tap is equivalent to

$$h_{mn}[l] = \underset{\sim}{h}_{(m,1)(n,l+1)}, \quad l = 0, ..., L_h, \tag{3.10}$$

in the partitioned matrix of Equation (**??**).

A quasi-static frequency-selective channel model is considered, where the channel taps remain constant for T time slots and are normalised to $\sum_{l=0}^{L_h} \|h_{mn}^{(l)}\|^2 = 1$. The received matrix can be written as

$$\underset{\sim}{\mathbf{Y}} = \underset{\sim}{\mathbf{S}} \otimes \underset{\sim}{\mathbf{H}} + \underset{\sim}{\mathbf{V}}. \tag{3.11}$$

Partitioned matrix convolution operates very similarly to matrix multiplication where the subvector entries within a row are convolved with the associated subvector entries within a column of the second partitioned matrix and summing the results. Therefore, the vector entries in Equation (**??**) are equivalent

to

$$\underset{\sim}{\mathbf{y}}_{tn} = \sum_{m=1}^{Nt} \underset{\sim}{\mathbf{s}}_{tm} \otimes \underset{\sim}{\mathbf{h}}_{mn} + \underset{\sim}{\mathbf{v}}_{tn}, \tag{3.12}$$

for $t = 1, ..., T$ and $n = 1, ..., N_r$. The received partitioned matrix

$$\underset{\sim}{\mathbf{Y}} = \left[\underset{\sim}{\mathbf{y}}_{tn}\right]_{t=1,...T,n=1,...N_r} \tag{3.13a}$$

$$\underset{\sim}{\mathbf{y}}_{tn} : 1 \times (L_s + L_h), \tag{3.13b}$$

and the AWGN noise partitioned matrix

$$\underset{\sim}{\mathbf{V}} = \left[\underset{\sim}{\mathbf{v}}_{tn}\right]_{t=1,...T,n=1,...N_r} \tag{3.14a}$$

$$\underset{\sim}{\mathbf{v}}_{tn} : 1 \times (L_s + L_h), \tag{3.14b}$$

have subvectors with $L_r = L_s + L_h$ symbols as a result of the convolution of the symbol streams with the frequency-selective fading channels.

3.2.2 Decoding

In this section, joint MLSE for high-rate LDCs in frequency-selective channels is shown to be impractical for modern day receivers. Consequently, detection complexity is reduced by sacrificing system reliability. Linear restructuring of the partitioned LDC system of Equation (**??**) is described, modifying the linearly dispersed system into a V-BLAST-like system. Hence, a layered, zero-forcing technique can be used to decode the LDC in frequency-selective channels. Limitations of the zero forcing scheme are discussed later.

The Viterbi algorithm is a promising scheme because it is efficient and has the ability to combat ISI. However, with no preprocessing of the system in Equation (**??**), the algorithm would be required to jointly process all Q data streams. This equates to M^{QL_h} states in the trellis and for a QPSK signal with a channel length of $L_h = 2$, the number of states is 65536, significantly too large to be processed by the receiver.

Each transmit stream, $\underset{\sim}{\mathbf{s}}_{tm}$, in the LDC may contain compositions of any of the Q symbol sequences as governed by the dispersion codes. Linear extraction of the symbol components of Equation (**??**) into a multiplexing-like code structure allows the matrix system to be processed so that single stream detection is possible. This section presents the manipulation of partitioned matrices to do this.

Let the n-th block column vector of the partitioned channel matrix $\underset{\sim}{\mathbf{H}}$ be denoted by $\underset{\sim}{\mathbf{h}}_{:n} = [\underset{\sim}{\mathbf{h}}_{1n}, ..., \underset{\sim}{\mathbf{h}}_{N_t n}]^T$. The following partitioned matrices are formed by stacking the real and imaginary components of the n-th channel block column

$$\underset{\sim}{\mathfrak{h}}_n = \begin{bmatrix} \mathcal{R}\{\underset{\sim}{\mathbf{h}}_{:n}\} \\ \mathcal{I}\{\underset{\sim}{\mathbf{h}}_{:n}\} \end{bmatrix} = \left[\underset{\sim}{\mathfrak{h}}_v^{(n)} \right]_{v=1,...,2N_t} \tag{3.15a}$$

$$\underset{\sim}{\mathfrak{h}}_v^{(n)} : 1 \times (L_h + 1), \tag{3.15b}$$

for $n = 1, ...N_r$ and the subscript denoting the column block is omitted indicating it is a single block column of $2N_t$ blocks. The real partitioned dispersion

matrices are

$$\underset{\sim}{\mathcal{A}}_q = \begin{bmatrix} \mathcal{R}\{\underset{\sim}{\mathbf{A}}_q^{(L_h+1)}\} & -\mathcal{I}\{\underset{\sim}{\mathbf{A}}_q^{(L_h+1)}\} \\ \mathcal{I}\{\underset{\sim}{\mathbf{A}}_q^{(L_h+1)}\} & \mathcal{R}\{\underset{\sim}{\mathbf{A}}_q^{(L_h+1)}\} \end{bmatrix} = \left[\underset{\sim}{\mathfrak{a}}_{uv}^{(q)}\right]_{u=1,\ldots,2T,v=1,\ldots,2N_t} \tag{3.16a}$$

$$\underset{\sim}{\mathfrak{a}}_{uv}^{(q)} : 1 \times (L_h+1), \tag{3.16b}$$

and

$$\underset{\sim}{\mathcal{B}}_q = \begin{bmatrix} \mathcal{I}\{\underset{\sim}{\mathbf{B}}_q^{(L_h+1)}\} & -\mathcal{R}\{\underset{\sim}{\mathbf{B}}_q^{(L_h+1)}\} \\ \mathcal{R}\{\underset{\sim}{\mathbf{B}}_q^{(L_h+1)}\} & -\mathcal{I}\{\underset{\sim}{\mathbf{B}}_q^{(L_h+1)}\} \end{bmatrix} = \left[\underset{\sim}{\mathfrak{b}}_{uv}^{(q)}\right]_{u=1,\ldots,2T,v=1,\ldots,2N_t} \tag{3.17a}$$

$$\underset{\sim}{\mathfrak{b}}_{uv}^{(q)} : 1 \times (L_h+1), \tag{3.17b}$$

for $q = 1, \ldots Q$. Note that $\underset{\sim}{\mathbf{A}}_q^{(L_h+1)}$ and $\underset{\sim}{\mathbf{B}}_q^{(L_h+1)}$ differ from Equation (**??**) in that the submatrices are scaled identity matrices of dimensions $(L_h+1) \times (L_h+1)$. Multiplication of the $2T \times 2N_t$ partitioned matrices of Equation (**??**) and Equation (**??**) with $2N_t \times 1$ partitioned column blocks of Equation (**??**) results in the $2T \times 1$ partitioned column matrices,

$$\underset{\sim}{\mathcal{A}}_q \, \underset{\sim}{\mathfrak{h}}_n = \left[\underset{\sim}{\mathfrak{C}}_u^{(qn)}\right]_{u=1,..2T} \tag{3.18a}$$

$$\underset{\sim}{\mathcal{B}}_q \underset{\sim}{\mathfrak{h}}_n = \left[\underset{\sim}{\mathfrak{D}}_u^{(qn)}\right]_{u=1,\ldots,2T} \tag{3.18b}$$

$$\underset{\sim}{\mathfrak{C}}_u^{(qn)} : 1 \times (L_h+1) \tag{3.18c}$$

$$\underset{\sim}{\mathfrak{D}}_u^{(qn)} : 1 \times (L_h+1) \tag{3.18d}$$

for $q = 1, \ldots Q$, $n = 1, \ldots, N_r$, where partitioned matrix multiplication is given

as

$$\underset{\sim}{\mathfrak{C}}_u^{(qn)} = \sum_{v=1}^{2N_t} \underset{\sim}{\mathfrak{h}}_v^{(n)} \underset{\sim}{\mathfrak{a}}_{uv}^{(q)}, \tag{3.19a}$$

$$\underset{\sim}{\mathfrak{D}}_u^{(qn)} = \sum_{v=1}^{2N_t} \underset{\sim}{\mathfrak{h}}_v^{(n)} \underset{\sim}{\mathfrak{b}}_{uv}^{(q)}, \tag{3.19b}$$

and together they form a new partitioned channel matrix

$$\underset{\sim}{\mathfrak{H}} = \begin{bmatrix} \mathfrak{A}_1 \underset{\sim}{\mathfrak{h}}_1 & \mathfrak{B}_1 \underset{\sim}{\mathfrak{h}}_1 & \cdots & \mathfrak{A}_Q \underset{\sim}{\mathfrak{h}}_1 & \mathfrak{B}_Q \underset{\sim}{\mathfrak{h}}_1 \\ \vdots & \vdots & \ddots & \vdots & \vdots \\ \mathfrak{A}_1 \underset{\sim}{\mathfrak{h}}_{N_r} & \mathfrak{B}_1 \underset{\sim}{\mathfrak{h}}_{N_r} & \cdots & \mathfrak{A}_Q \underset{\sim}{\mathfrak{h}}_{N_r} & \mathfrak{B}_Q \underset{\sim}{\mathfrak{h}}_{N_r} \end{bmatrix} = \left[\underset{\sim}{\mathfrak{h}}_{wz} \right]_{w=1,\ldots,2TN_r, z=1,\ldots,2Q}, \tag{3.20a}$$

$$\underset{\sim}{\mathfrak{h}}_{wz} : 1 \times (L_h + 1). \tag{3.20b}$$

The dispersion codes in the transmit block are extracted from the transmit block into the new channel to form the equivalent system

$$\underset{\sim}{\mathfrak{Y}} = \underset{\sim}{\mathfrak{H}} \otimes \underset{\sim}{\mathfrak{X}} + \underset{\sim}{\mathfrak{V}}, \tag{3.21}$$

where $\underset{\sim}{\mathfrak{X}}$ is the the signal components denoted by

$$\underset{\sim}{\mathfrak{X}} = \begin{bmatrix} \boldsymbol{\alpha}_1 \\ \boldsymbol{\beta}_1 \\ \vdots \\ \boldsymbol{\alpha}_Q \\ \boldsymbol{\beta}_Q \end{bmatrix} = \left[\underset{\sim}{\mathfrak{x}}_z \right]_{z=1,\ldots,2Q}, \tag{3.22a}$$

$$\underset{\sim}{\mathfrak{x}}_z : 1 \times L_s, \tag{3.22b}$$

$\mathfrak{Y}$ is the equivalent received block matrix

$$\underset{\sim}{\mathfrak{Y}} = \begin{bmatrix} \mathcal{R}\{\underset{\sim}{\mathbf{y}}_{:1}\} \\ \mathcal{I}\{\underset{\sim}{\mathbf{y}}_{:1}\} \\ \vdots \\ \mathcal{R}\{\underset{\sim}{\mathbf{y}}_{:N_r}\} \\ \mathcal{I}\{\underset{\sim}{\mathbf{y}}_{:N_r}\} \end{bmatrix} = \left[\underset{\sim}{\mathfrak{y}}_w \right]_{w=1,\ldots,2TN_r} \tag{3.23a}$$

$$\underset{\sim}{\mathfrak{y}}_w : 1 \times L_r, \tag{3.23b}$$

and $\underset{\sim}{\mathcal{Y}}$ is the equivalent noise block matrix

$$\underset{\sim}{\mathcal{V}} = \begin{bmatrix} \mathcal{R}\{\underset{\sim}{\mathbf{v}}_{:1}\} \\ \mathcal{I}\{\underset{\sim}{\mathbf{v}}_{:1}\} \\ \vdots \\ \mathcal{R}\{\underset{\sim}{\mathbf{v}}_{:N_r}\} \\ \mathcal{I}\{\underset{\sim}{\mathbf{v}}_{:N_r}\} \end{bmatrix} = \Big[\underset{\sim}{\mathfrak{v}}_w\Big]_{w=1,\ldots,2TN_r} \tag{3.24a}$$

$$\underset{\sim}{\mathfrak{v}}_w : 1 \times (L_r). \tag{3.24b}$$

with $\underset{\sim}{\mathbf{y}}_{:n}$ and $\underset{\sim}{\mathbf{v}}_{:n}$ denoting the n-th column block of $\underset{\sim}{\mathbf{Y}}$ and $\underset{\sim}{\mathbf{V}}$, respectively. The new equivalent LDC system is shown in Fig **??**.

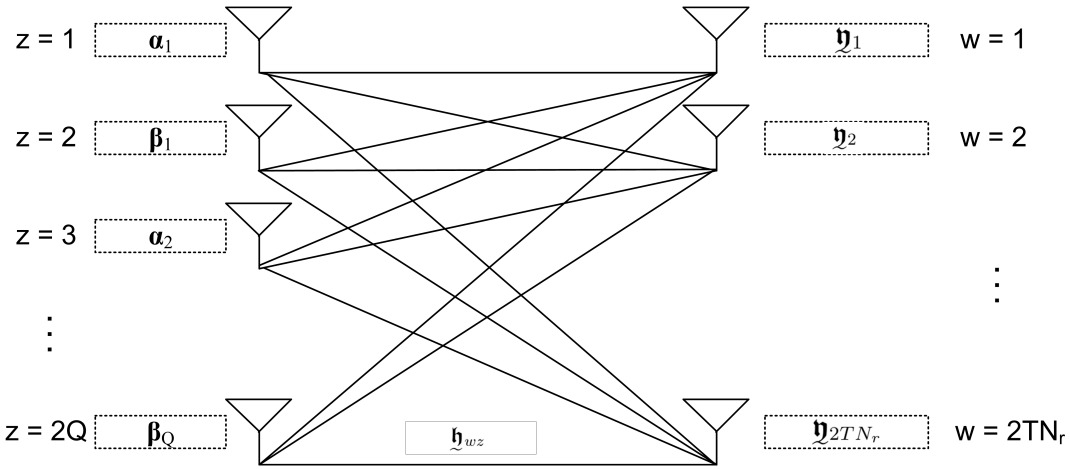

Figure 3.4: Equivalent LDC system after restructuring of the system.

3.2.3 Detection of Non-orthogonal LDCs

Performing joint ML sequence estimation of Q data streams exceeds the current capability of modern receivers. Therefore, sub-optimum detection is required to reduce the processing complexity. The zero-forcing detection scheme used

for V-BLAST systems is adopted for the modified LDC system in Equation (**??**).

A single-input, single-output (SISO) frequency-selective channel $\underset{\sim}{\mathfrak{h}}_{wz}$ from Equation (**??**) can be represented by an equivalent flat fading system with $L_h + 1$ transmit antennas sending a delayed version of the corresponding symbol stream $\underset{\sim}{\mathfrak{x}}_z$ to a single receive antenna [**?**]. The variable $\mathfrak{h}_{wz}[l]$ denotes the l-th channel tap from transmit antenna z to receive antenna w which represents a single flat fading channel and sends the delayed symbol stream

$$\mathbf{s}_z^{(l)} = \begin{bmatrix} \mathbf{0}_l & \underset{\sim}{\mathfrak{x}}_z & \mathbf{0}_{L_h - l} \end{bmatrix}, \quad \in \quad \mathbb{R}^{1 \times (L_s + L_h)}, \tag{3.25}$$

where $\mathbf{0}_L$ denotes an all zero vector of length L. The equivalent system is a multiple-input, single-output (MISO) flat fading system. The matrix

$$\mathbf{S}_z = \begin{bmatrix} \mathbf{s}_z^{(0)} \\ \mathbf{s}_z^{(1)} \\ \vdots \\ \mathbf{s}_z^{(L_h)} \end{bmatrix}, \quad \in \quad \mathbb{R}^{(L_h+1) \times (L_s + L_h)} \tag{3.26}$$

forms the transmit block code for the z-th equivalent flat fading MISO system with $L_h + 1$ transmit antennas and one receive antenna, where $z = 1, ..., 2Q$. The equivalent flat fading system of Equation (**??**) can be written as

$$\mathcal{Y} = \mathcal{H}\mathcal{S} + \mathcal{V}, \tag{3.27}$$

where $\mathcal{Y} \in \mathbb{R}^{2TN_r \times (L_s + L_h)}$ is the unpartitioned received matrix of Equation (**??**)

with the corresponding equivalent element entries

$$y_{wl} = \underset{\sim}{\mathfrak{y}}_{(w,1)(1,l)}, \tag{3.28}$$

$\boldsymbol{\mathcal{V}} \in \mathbb{R}^{2TN_r \times (L_s+L_h)}$ is the unpartitioned noise matrix of Equation (**??**) with the equivalent element entries

$$v_{wl} = \underset{\sim}{\mathfrak{v}}_{(w,1)(1,l)}, \tag{3.29}$$

for $l = 1, ..., (L_s + L_h)$, $\boldsymbol{\mathcal{H}} \in \mathbb{R}^{2N_rT \times 2Q(L_h+1)}$ is the channel matrix with the equivalent entries

$$h_{w'z'} = \mathfrak{h}_{wz}[l] = \underset{\sim}{\mathfrak{h}}_{(w,1)(z,l+1)}, \tag{3.30}$$

for $l = 0, ..., L_h$, $w = 1, ..., 2TN_r$ and $z = 1, ..., 2Q$, with the element in the w'-th row and z'-th column of $\boldsymbol{\mathcal{H}}$ equivalent to

$$w' = w, \tag{3.31a}$$

$$z' = (z-1)(L_h+1) + l + 1, \tag{3.31b}$$

and the transmit matrix is an unpartitioned matrix of Equation (**??**) stacked

into

$$\boldsymbol{\mathcal{S}} = \begin{bmatrix} \mathbf{S}_1 \\ \mathbf{S}_2 \\ \vdots \\ \mathbf{S}_{2Q} \end{bmatrix}, \in \mathbb{R}^{2Q(L_h+1)\times(L_s+L_h)}. \tag{3.32}$$

The equivalent flat fading system is shown in Figure **??**.

The zero-forcing detection scheme estimates a symbol block one layer at a time by nulling out the interfering signals. Suppose block $\mathbf{S}_a$ is being detected, then let $\boldsymbol{\mathcal{H}}_a$ be all the channels that are transmitting the symbol stream $\mathfrak{x}_a$ as shown in Figure **??**. This includes all channel taps $\mathfrak{h}_{wz}[l]$ for $z = a$. The remaining channels that are not transmitting $\mathbf{S}_a$ are considered as interfering signals and are denoted $\boldsymbol{\mathcal{H}}'_a$. The interference signals can be cancelled out by the nulling matrix

$$\mathbf{G}_a = \text{null}(\boldsymbol{\mathcal{H}}'_a), \tag{3.33}$$

where

$$\mathbf{G}_a \boldsymbol{\mathcal{H}}'_a = \mathbf{0}. \tag{3.34}$$

The nulling matrix is able to mitigate interference from other symbol streams by using

$$\mathbf{G}_a \boldsymbol{\mathcal{Y}} = \mathbf{G}_a \boldsymbol{\mathcal{H}}_a \mathbf{S}_a + \mathbf{G}_a \boldsymbol{\mathcal{V}}, \tag{3.35}$$

so that single stream detection is possible. The Viterbi algorithm reduces to M^{L_h} states which is a significant improvement from M^{QL_h}. The nulling

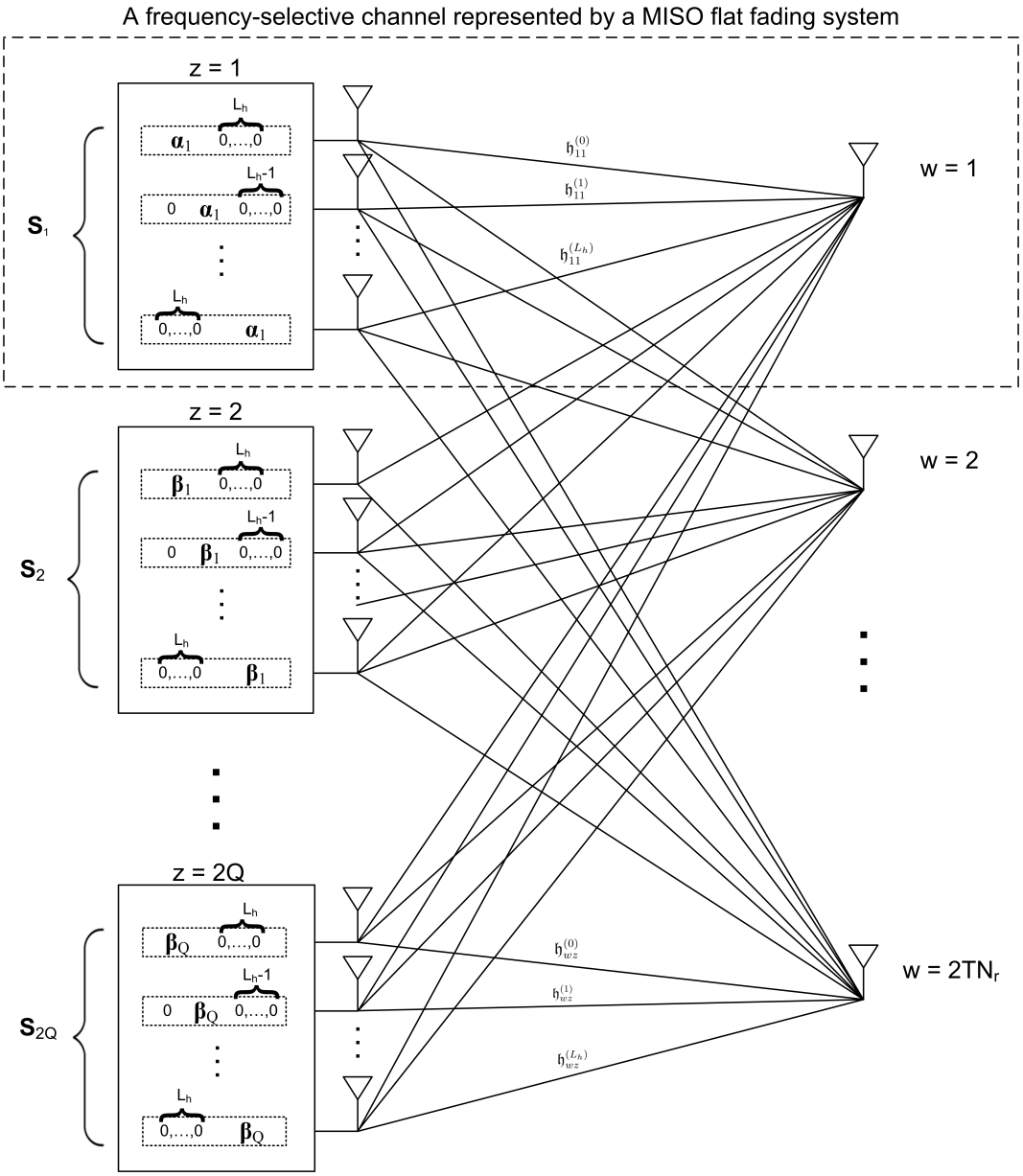

Figure 3.5: Equivalent flat fading system for a LDC.

process, unfortunately, is limited by system dimensionality and has to satisfy

$$N_r T > Q(L_h + 1) - \frac{(L_h + 1)}{2}. \tag{3.36}$$

3.2.4 Detection of Orthogonal LDCs

Mitigation of signal interference on the LDC system can also be performed by linear decoupling if the matrix of Equation (**??**) is orthogonal. The orthogonal dispersion matrices of Equation (**??**) give rise to the following property for the channel matrix

$$\underset{\sim}{\mathcal{F}} = \underset{\sim}{\mathcal{H}}' \otimes \underset{\sim}{\mathcal{H}} = \left[\underset{\sim}{\mathfrak{f}}_{ab}\right]_{a=1,\ldots,2Q,b=1,\ldots,2Q}, \tag{3.37a}$$

$$\underset{\sim}{\mathfrak{f}}_{ab} : 1 \times (2L_h + 1), \tag{3.37b}$$

$$\underset{\sim}{\mathfrak{f}}_{ab} = \mathbf{0} \quad for \quad a \neq b, \tag{3.37c}$$

where $(\underset{\sim}{\cdot})'$ denotes partitioned matrix transpose given as

$$\underset{\sim}{\mathcal{H}}' = \left[\underset{\sim}{\mathfrak{h}}_{wz}\right]' = \left[\underset{\sim}{\mathfrak{h}}_{zw}\right]_{z=1,\ldots,2Q,w=1,\ldots,2TN_r}, \tag{3.38a}$$

$$\underset{\sim}{\mathfrak{h}}_{zw} : 1 \times (L_h + 1). \tag{3.38b}$$

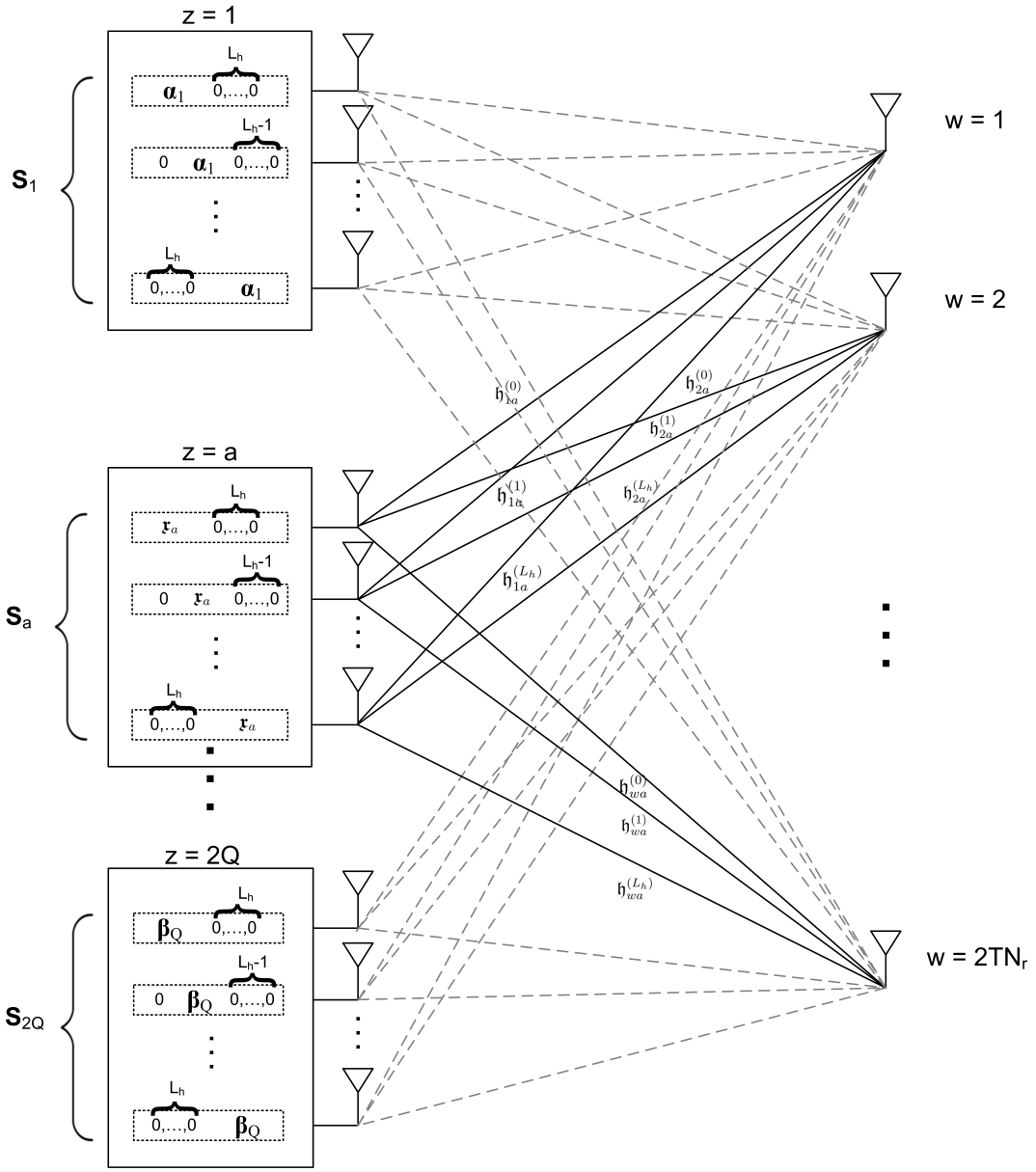

Figure 3.6: Equivalent flat fading system for a LDC.

Therefore, orthogonality can be exploited in LDCs to take advantage of linear decoupling. This is achieved by using

$$\underset{\sim}{\mathcal{H}}' \otimes \underset{\sim}{\mathcal{Y}} = \underset{\sim}{\mathfrak{f}}_{zz} \otimes \underset{\sim}{\mathfrak{X}} + \underset{\sim}{\mathfrak{f}}_{zz} \otimes \underset{\sim}{\mathcal{V}} = \left[\underset{\sim}{\mathfrak{r}}_z\right]_{z=1,\ldots,2Q}, \tag{3.39}$$

$$\underset{\sim}{\mathfrak{r}}_z : 1 \times (L_s + 2L_h + 1). \tag{3.40}$$

to give the decoupled sequences

$$\underset{\sim}{\mathfrak{r}}_z = \underset{\sim}{\mathfrak{f}}_{zz} \otimes \underset{\sim}{\mathfrak{x}}_z + \underset{\sim}{\mathfrak{f}}_{z:} \otimes \underset{\sim}{\mathfrak{v}}_z, \tag{3.41}$$

for $z = 1, ..., 2Q$, which are equalized individually by the Viterbi decoder. The channel of Equation (**??**) is doubled in length and increases the memory of the Viterbi algorithm.

3.3 Results and Discussion

This section illustrates the bit-error-rate (BER) performance for different STBCs in frequency-selective channels against signal to noise ratio (SNR). SNR is defined as

$$SNR_{dB} = 10\, log_{10}\left(\frac{E_s}{N_0}\right), \tag{3.42}$$

where E_s is the average symbol energy and N_0 is the power spectral density of the AWGN noise. The noise variance is defined as

$$\sigma^2 = \frac{N_0}{2} = \frac{E_s}{2 \cdot 10^{SNR_{dB}/10}}. \tag{3.43}$$

Unless stated otherwise, all the schemes discussed in this section have a signalling interval that transmits a symbol stream of $L_x = 30$ QPSK symbols appended with zero vectors of length $L_p = L_h = 1$ symbol. This results in a stream of $L_s = 32$ symbols transmitted within one signalling interval. The dispersive channel is quasi-static for T signalling slots and $L_h + 1 = 2$ channel taps. Each frequency-selective channel from transmit antenna m to receive antenna n is normalised to $E[\sum_{l=0}^{L_h} \|h_{nm}[l]\|^2] = 1$.

Figure **??** illustrates the BER performance of an OSTBC with $N_t = 2$ transmit antennas over $T = 2$ signalling intervals for different numbers of receive antennas in a frequency-selective environment. Figure **??** shows the performance of the TR-STBC from Section **??**, an OSTBC with time-reversal of symbol streams in the second signalling interval. Detection in both schemes takes advantage of orthogonality to linearly decouple $Q = 2$ symbol streams which are then independently equalized by the Viterbi decoder. These schemes are extensions of the Alamouti STBC in Equation (**??**) to frequency-selective channels and the results show receive diversity is achieved by both schemes with and without time-reversal.

Performance comparisons between the OSTBC and TR-STBC are shown in Figure **??** for different numbers of receive antennas. Time-reversal inverts the order of the data symbols transmitted in the second signalling interval, effectively achieving channel diversity by taking advantage of the uncorrelated channel taps. The results show performance is gained from time-reversal.

Figure **??** illustrates the BER performance of the LDC with orthogonal dispersion matrices from Equation (**??**) for different number of receive antennas over frequency-selective channels. Detection is ZF with successive

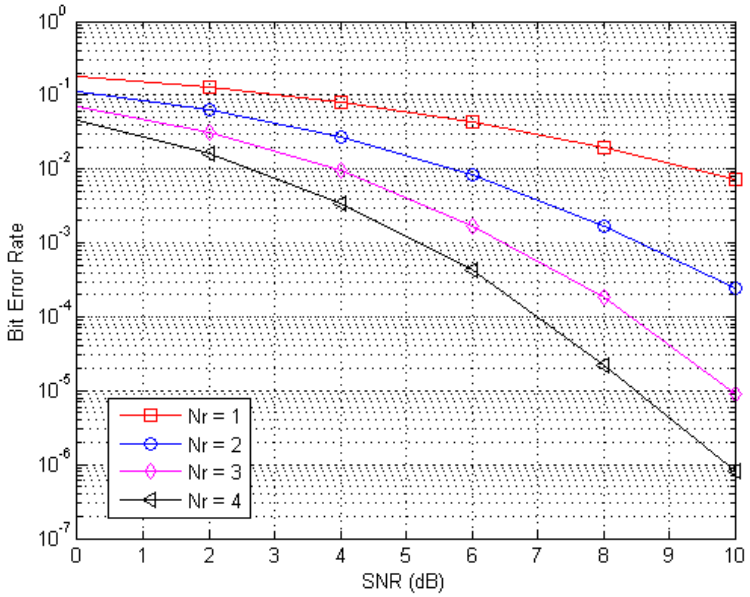

(a) Without time-reversal.

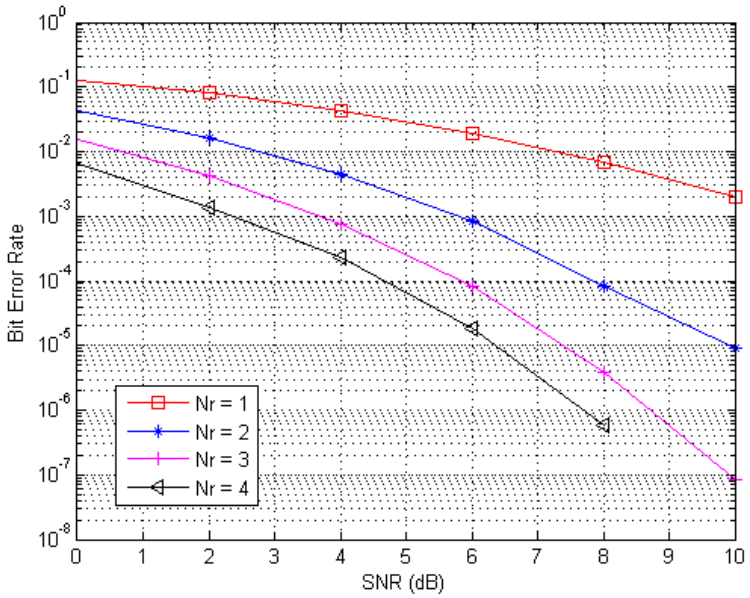

(b) With time-reversal.

Figure 3.7: BER performance of an orthogonal STBC versus different number of receive antennas over a frequency-selective channel with and without time reversal of symbol streams transmitted in the second signalling interval.

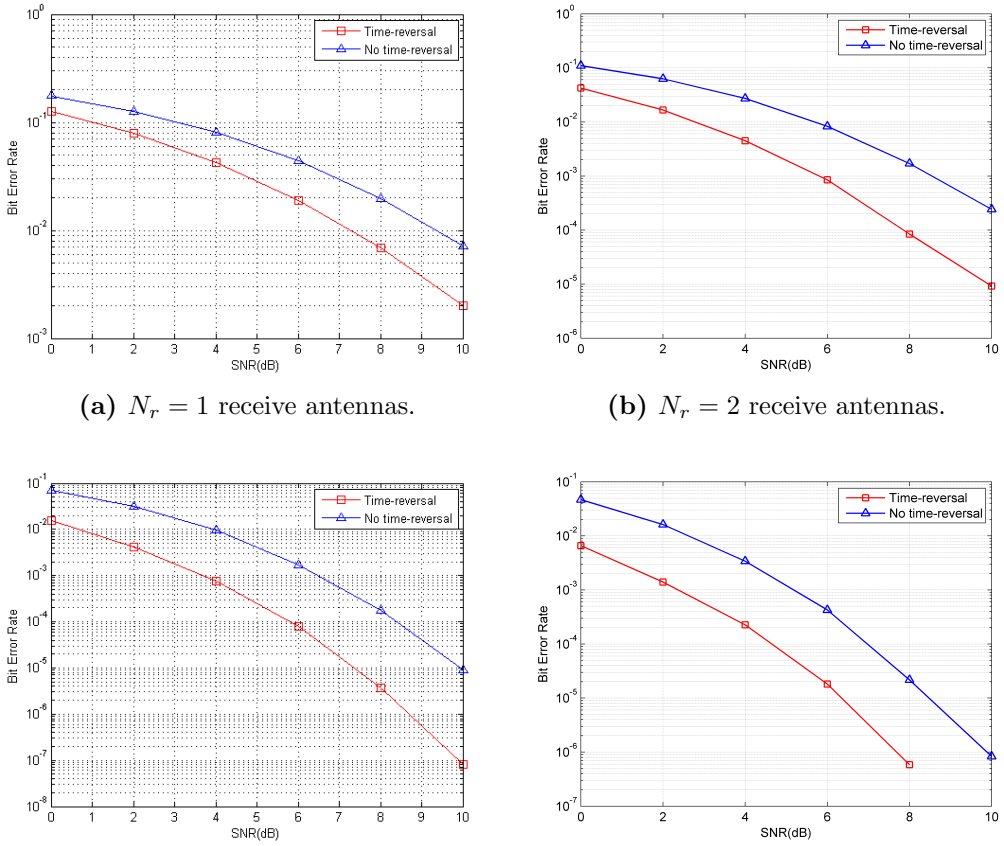

(a) $N_r = 1$ receive antennas.

(b) $N_r = 2$ receive antennas.

(c) $N_r = 3$ receive antennas.

(d) $N_r = 4$ receive antennas.

Figure 3.8: Comparing BER performance of OSTBC with and without time-reversal for different number of receive antennas.

interference cancellation (SIC) over $2Q$ stages. An attempt to time-reverse the symbol streams transmitted in the second signalling interval of the LDC appears to have no effect on performance. Zero forcing detection must satisfy dimensionality criterion of Equation (**??**) and therefore the LDC requires a minimum of two receive antennas.

Linear processing, on the other hand, supports any number of receive antennas in the system. Figure **??** illustrates the BER performance of the orthogonal LDC as considered above with linear processing detection. Orthogonality is exploited to linearly decouple the LDC system as discussed in Section **??**. The results show both ZF and linear detection achieve receive diversity. Thus far, the schemes presented achieve the same throughput rate of

$$R = \frac{QL_x}{TL_s} = 0.9375. \tag{3.44}$$

Performance comparisons of these high-rate codes will be explored next.

In Figure **??**, the BER performance of the OSTBC, TR-STBC and LDC with linear processing and LDC with ZF are compared for different number of receive antennas. Figure **??** is an overloaded system that does not support ZF detection. TR-STBC exhibits the best performance of all the systems regardless of the number of antennas at the receiver. LDC with linear detection is shown to achieve the same performance as the OSTBC with no reversal of symbol streams. This resembles the results from Figure **??** of the equivalent STBCs in flat fading channels. The results show LDC with linear detection will always have higher error rates than TR-STBC. The sub-optimal ZF de-

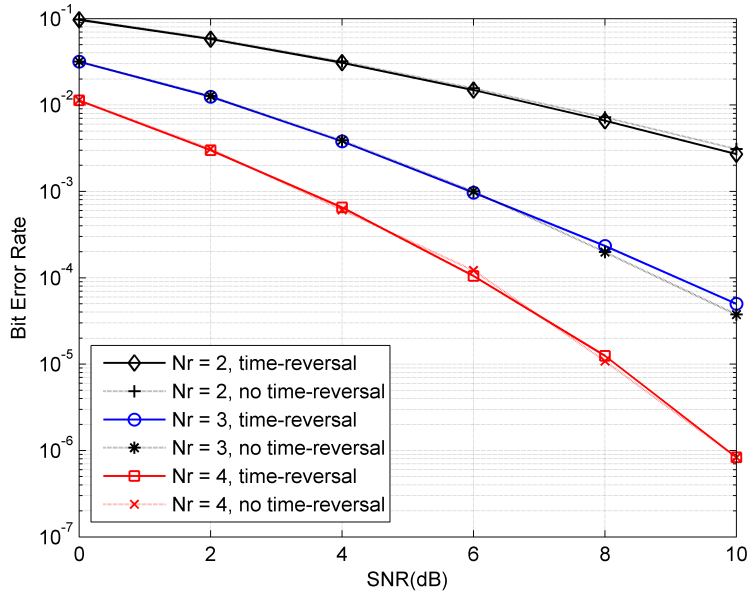

(a) ZF-SIC detection.

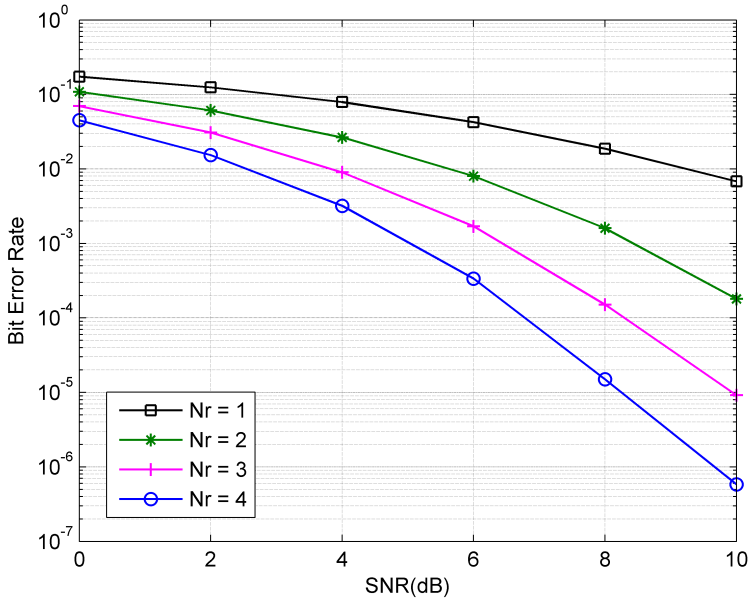

(b) Linear detection.

Figure 3.9: BER performance of an orthogonal LDC versus different number of receive antennas over a frequency-selective channel with $N_t = 2$ transmit antennas.

tection, on the other hand, achieves a lower diversity however, decreasing the loading of the system allows it to improve in performance significantly, surpassing linear detection at low SNRs. In summary, the system configuration and SNR determine the best detection scheme with regards to reliability. Linear detection is suited for more heavily loaded systems and high SNRs whereas ZF can outweigh performance of linear detection for underloaded systems at low SNRs. Next, complexity of the two detection schemes is discussed.

STBCs in frequency-selective channels give rise to ISI which is equalized by Viterbi decoders. Preprocessing of the received signals is necessary to remove interference from other symbol streams yielding a single stream for the equalizer. Viterbi algorithm complexity increases significantly when joint equalisation is required. The Viterbi algorithm dominates the computational power requirements in the receiver. The number of trellis states in the Viterbi algorithm is therefore an indication of receiver complexity. The decoders for linear and zero-forcing detection schemes equalize a single stream at a time. However, linear decoupling involves a more complex decoder since the channel that is fed into the decoder given in Equation (**??**) is double the symbol length of the frequency-selective channel. Therefore, the number of states in the decoder for linear decoupling is M^{2L_h}, compared with M^{L_h} for zero-forcing detection. This shows complexity increases exponentially with channel length. Table **??** gives an indication of the number of states in the Viterbi algorithm for the two detection schemes.

ZF detection has been stated to not work for rank-deficient or overloaded systems, which arise when the number of unknowns is greater than the number of independent equations in the system. It must satisfy certain sys-

Detection	M	$L_h = 1$	$L_h = 2$	$L_h = 3$	$L_h = 4$
Zero-forcing	2	2	4	8	6
	4	4	16	64	256
Linear processing	2	4	16	64	256
	4	16	256	4096	65536

Table 3.1: Number of states in the Viterbi equaliser for ZF and linear detection.

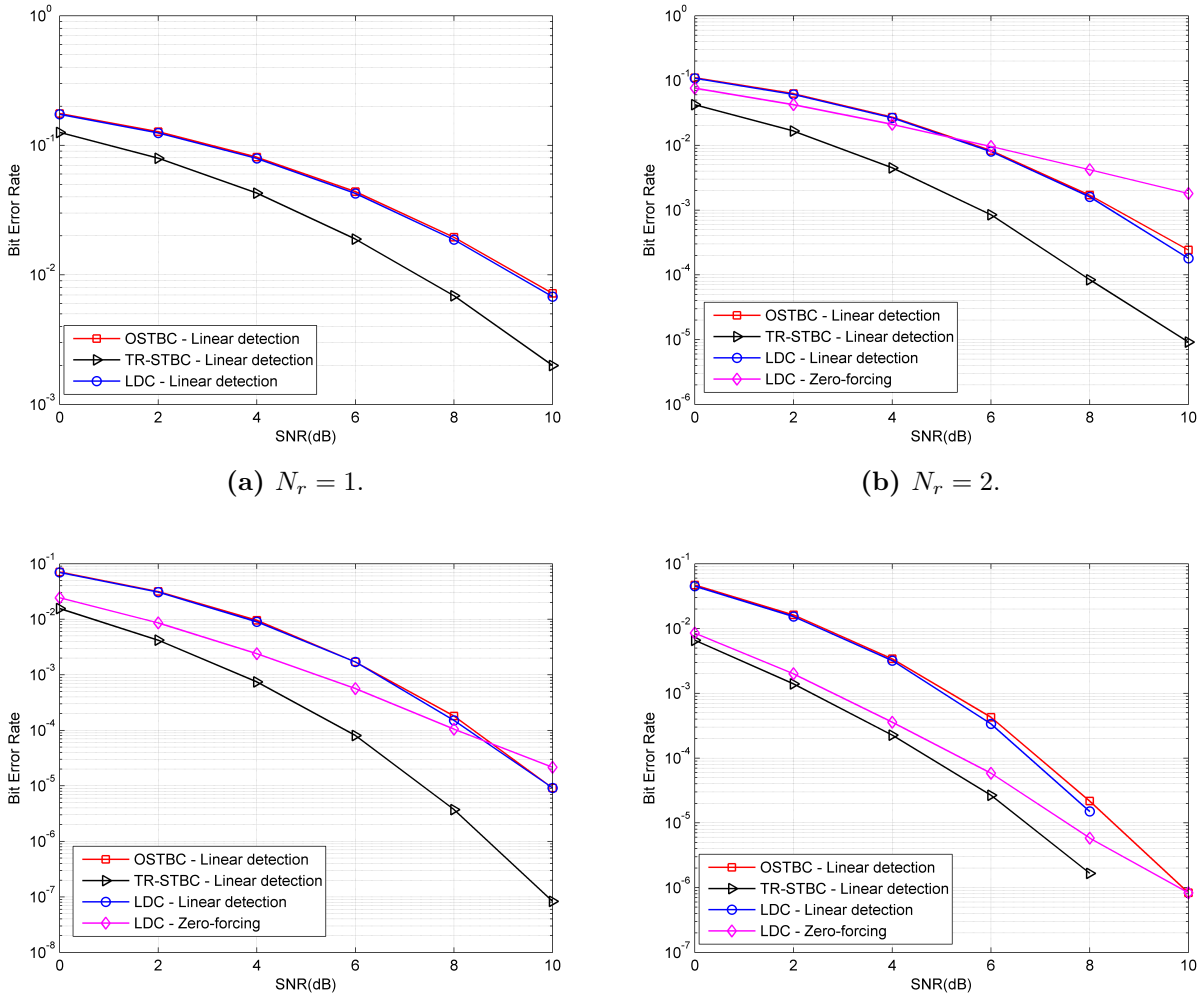

(a) $N_r = 1$.

(b) $N_r = 2$.

(c) $N_r = 3$.

(d) $N_r = 4$.

Figure 3.10: Performance comparisons of an OSTBC and a LDC using linear detection and SIC for different number of receive antennas.

tem dimensions to avoid overloading, but can handle non-orthogonal codes. In addition, decoder complexity does not increase as significantly as with linear decoupling with the length of the frequency-selective channel.

High-rate STBCs in frequency-selective channels are now investigated. Zero-forcing of interfering signals is the only possible detection scheme for these non-orthogonal block codes. Figure **??** illustrates the performance of the V-BLAST system from Section **??** for different numbers of receive antennas. The system has $N_t = 2$ transmit antennas and transmits $Q = N_t$ symbol streams in $T = 1$ signalling interval. Therefore the rate achieved is $R = 1.875$, double the rate of the OSTBC. ZF at the decoder nulls the interfering symbol streams in the uncoded multiplexing system over $Q = 2$ successive layers. Thus, single sequence detection using the Viterbi equalizer is possible. ZF, however does not work when the system of Equation (**??**) is overloaded. This is avoided as long as the dimensions satisfy

$$N_r > N_t(L_h + 1) - (L_h + 1). \tag{3.45}$$

Therefore, the two transmit antenna V-BLAST system requires a minimum of three receive antennas to achieve single stream equalisation across a two tap frequency-selective channel. The V-BLAST scheme is shown to achieve receive diversity gain.

Figure **??** shows the performance of the high-rate LDC from Hassibi [**?**] using $N_t = 2$ transmit antennas over $T = 2$ signalling intervals in frequency-selective channels. The LDC partitioned block code is a linear combination of $Q = 4$ symbol streams and achieves the same multiplexing rate of $R = 1.875$

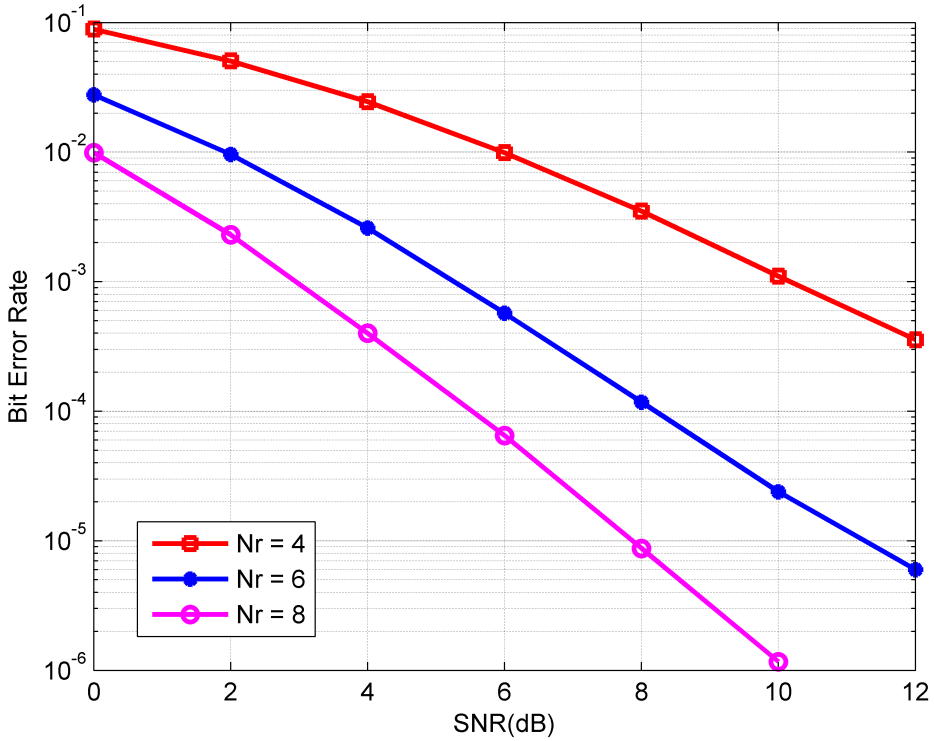

Figure 3.11: BER performance of V-BLAST in frequency-selective channels versus different number of receive antennas with $N_t = 2$ transmit antennas and successive interference cancelling.

as the V-BLAST system. ZF is also used to detect the system of Equation (**??**), where the sequences have been split into real signal components. The restructured LDC channel contains the channel taps and the dispersion matrices. The new system has the structure of a multiplexing scheme where $2Q$ successive layers are required to detect each of the signal component streams which are selected from $log_2(M)$ real points in the constellation map. The number of states in the Viterbi decoder is equivalent to the V-BLAST scheme where $(log_2 M)^{2QL_h} = M^{QL_h}$. The system of Equation (**??**) must also meet the

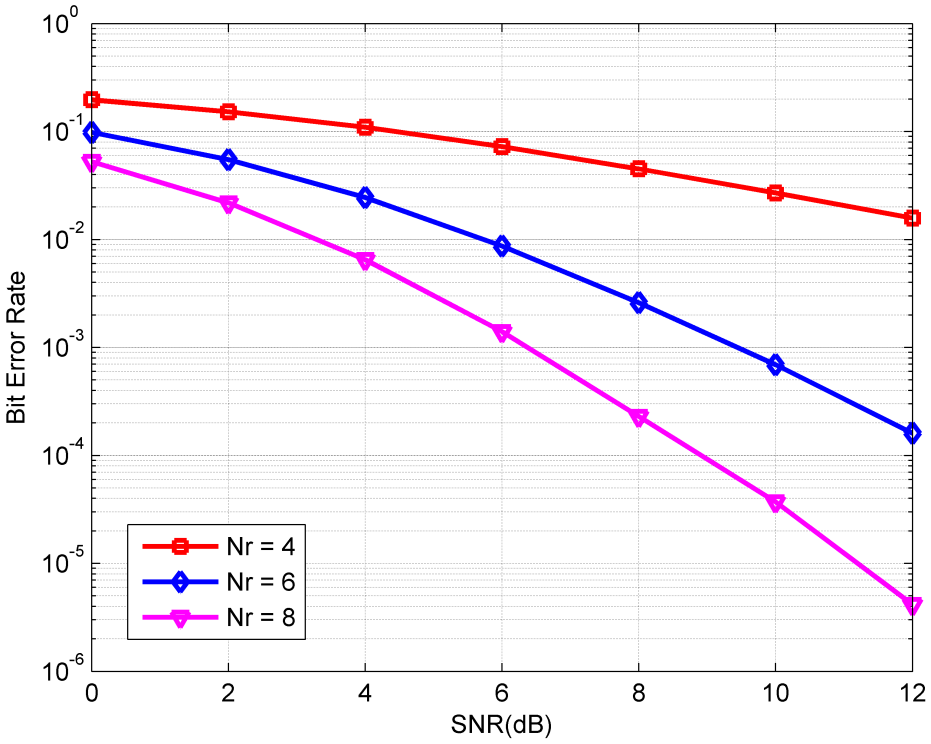

Figure 3.12: BER performance of Hassibi's LDC in frequency-selective channels versus different number of receive antennas using $N_t = 2$ transmit antennas and successive interference cancellation.

criterion of Equation (**??**), making the minimum number of receive antennas

$$N_r > N_t(L_h + 1) - \frac{(L_h + 1)}{2T}, \tag{3.46}$$

when rate is maintained at the V-BLAST rate of $Q = N_t T$. The results for the high-rate LDC also shows receive diversity is achieved.

Comparing the criteria of Equation (**??**) and Equation (**??**), it is evident that for the same number of transmit antennas, the LDC is more overloaded than the V-BLAST system for a given small number of receive antennas as a result of coding across time. However, as more receive antennas are added

into the system, the dimensionality evens out in both schemes. This is shown by the figures in **??**, which show worse performance for the LDC when four receive antennas, but performance approaches that of V-BLAST as more receive antennas are added to the system.

High-rate LDCs require a large number of receive antennas to achieve equivalent performance to the uncoded V-BLAST system. The number of receive antennas required to achieve a coding gain increases with the rate and the length of the channel delay. Up to this point, frequency-selective channels have been modelled by a uniform power profile as shown in Figure **??**. Suppose an exponential decay power delay profile [**?**] is used to model the dispersive channel where the channel taps decrease in power and are normalised to $\sum_{l=0}^{L_h} \|h[l]\|^2 = 1$. The number of receive antennas required to achieve good performance can be reduced if the frequency-selective channel can be assumed to have a shorter length by ignoring the taps with low power. The performance of the LDC is examined for the power delay profiles plotted in Figure **??**. Figure **??** compares the BER performance of different power delay profiles for Hassibi's LDC over a frequency-selective channel with $L_h + 1 = 3$ taps which are all known and used by the equalizer. The results show that the channel profiles do not significantly affect the performance of the system when all taps are used by the decoder.

However, Figure **??** compares the performance of Hassibi's LDC when $L'_h + 1 = 2$ taps are passed through the equalizer in a frequency-selective channel with $L_h + 1 = 3$ taps, and L'_h is the assumed channel length by the equalizer. The last tap in the channel is ignored by the decoder. Therefore, performance is significantly degraded when the channel is modelled by the

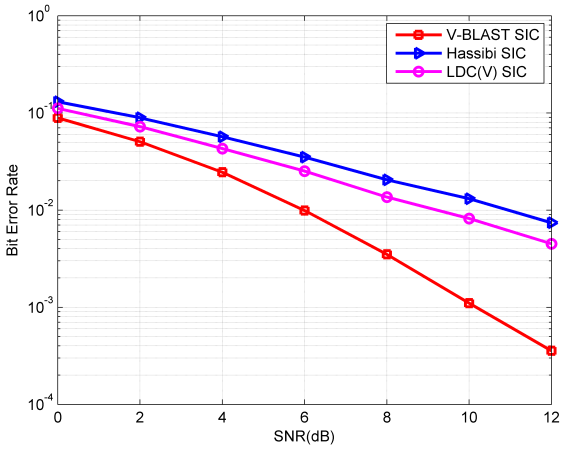

(a) $Nr = 4$

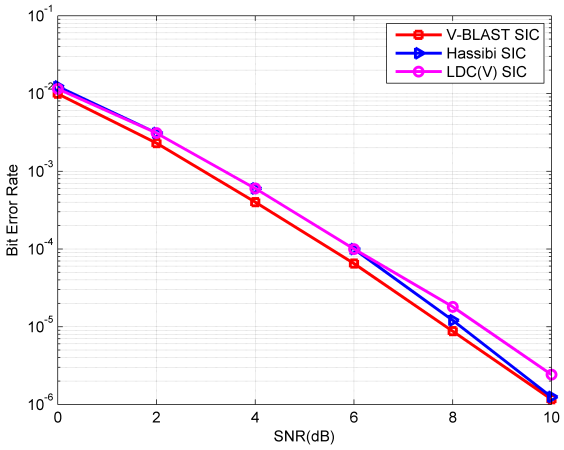

(b) $Nr = 8$

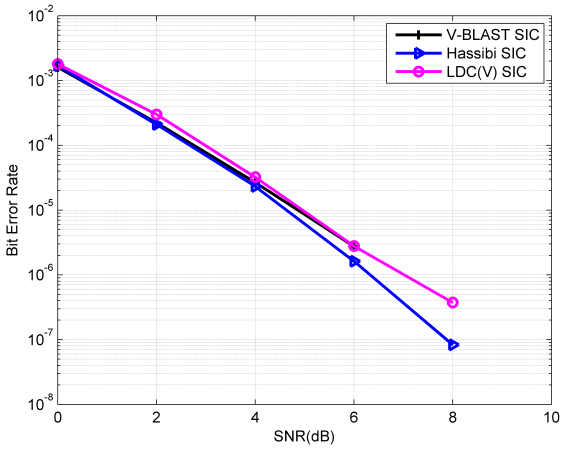

(c) $Nr = 12$

Figure 3.13: BER performance of two high-rate STBCs in frequency-selective channels versus different number of receive antennas.

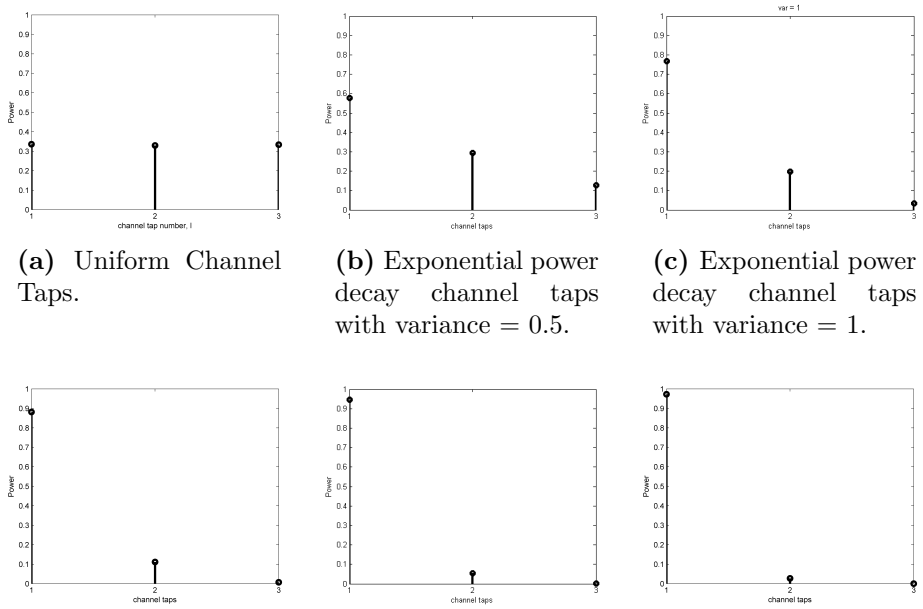

(a) Uniform Channel Taps.

(b) Exponential power decay channel taps with variance = 0.5.

(c) Exponential power decay channel taps with variance = 1.

(d) Exponential power decay channel taps with variance = 1.5.

(e) Exponential power decay channel taps with variance = 2.

(f) Exponential power decay channel taps with variance = 2.5.

Figure 3.14: Different power profiles for a frequency-selective channel with $Lh = 2$ symbols.

uniform delay profile where a third of the power is lost. The greater the variance of the exponential decay, the less power is carried by the unused tap and thus the performance improves with increasing decay variance. As the variance gets bigger, the frequency-selective channel begins to model a shorter channel until it eventually forms a flat fading channel as shown in Figure **??**. Therefore, the performance of a system with exponential decay channels tends towards the performance of a L'_h system. The resulting investigation shows that assuming a smaller channel length is beneficial for the ZF receiver if truncated taps have small energy, as it reduces the loading on the system This allows better performance to be achieved with a smaller number of receive antennas.

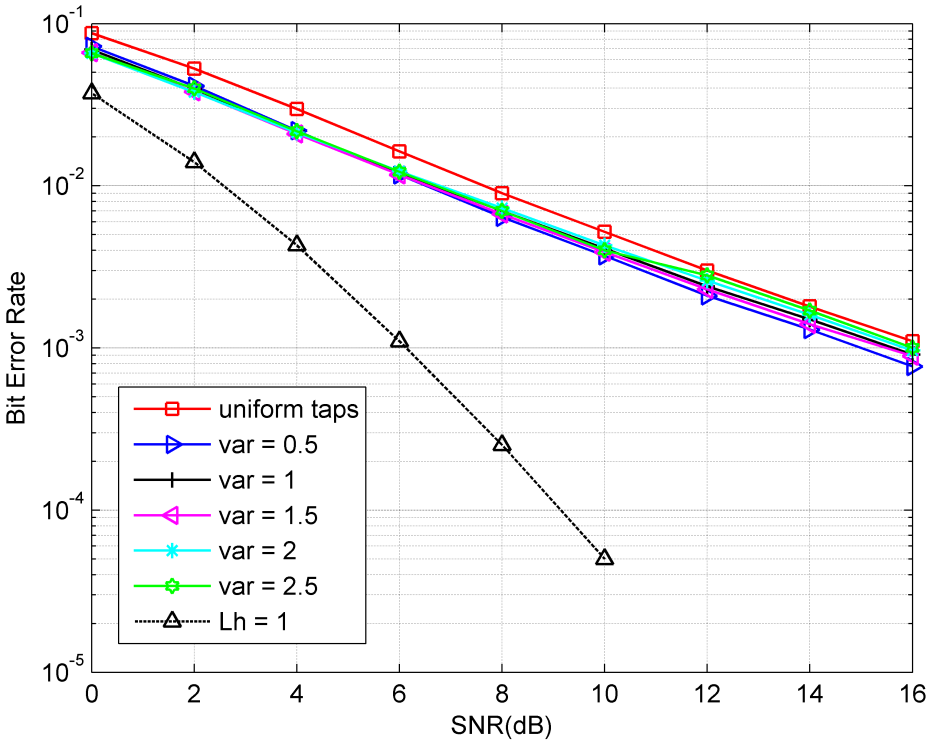

Figure 3.15: Performance of a high-rate LDC versus varying decaying channels with $N_r = 6$ receive antennas and $L'_h = L_h = 2$ channel assumed by the decoder.

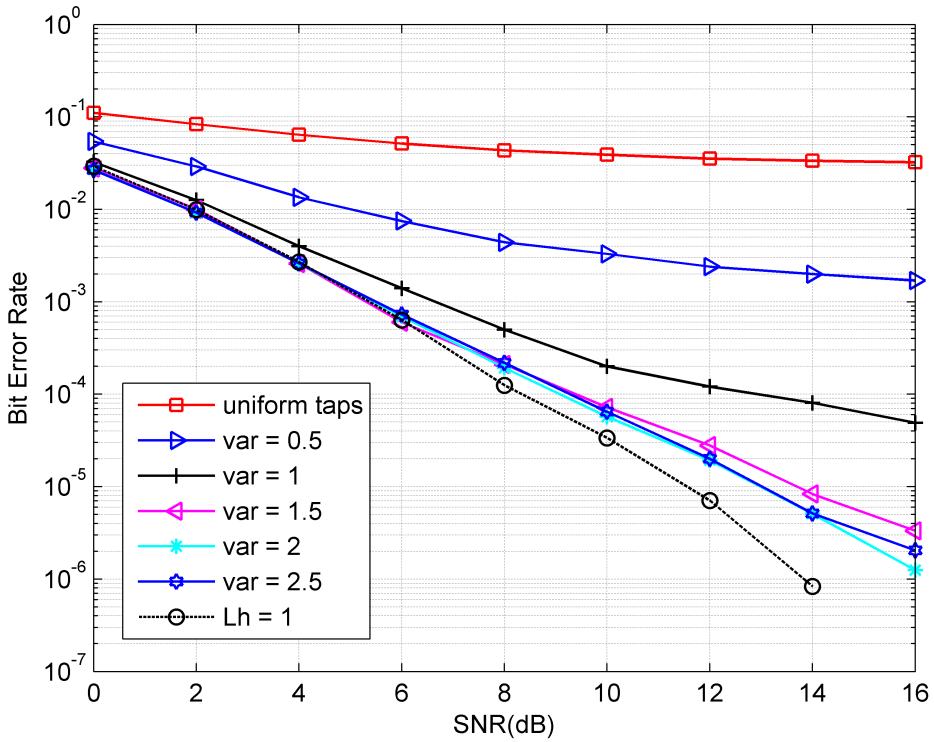

Figure 3.16: Performance of a high-rate LDC versus varying decaying channels with $N_r = 6$ receive antennas and $L'_h = 1$ channel assumed by the decoder in a frequency-selective channel with $L_h = 2$.

3.4 Summary

This chapter summarises several contributions to the thesis. The structure of the LDC in frequency-selective channels and the manipulation of the partitioned LDC system into an equivalent real V-BLAST-like system are introduced followed by discussions on suitable detection schemes.

The frequency-selective channel produces ISI in the detected signal which is mitigated by MLSE processing in the Viterbi decoder. Joint detection of symbol streams cannot be practically accomplished by the receiver when detection also demands ISI equalisation. Therefore, two detection schemes with the ability to mitigate interfering signals are investigated. The two schemes are linear and ZF detection.

For high-rate LDCs in frequency-selective channels, high complexity is unavoidable. ZF sacrifices reliability by cancelling the unwanted signals to achieve a significant complexity reduction. Nulling of interfering signals allows the receiver to process a single stream at a time and does not require orthogonality in the block code. However, ZF only works for underloaded linear systems where there are more independent linear equations than the number of unknowns in the system. For high-rate codes in long dispersive frequency-selective channels, this criterion is satisfied by a large number of receive antennas which is not practical for many devices.

Linear decoding of the LDC system cannot be combined with time-reversal. Therefore, an orthogonal LDC with linear detection does not benefit from the extra LDC preprocessing when TR-STBC is able to exploit channel diversity. Linear detection, however, doubles the memory of the Viterbi

decoder and therefore is only suitable for low level modulations or very short response dispersive channels. ZF is therefore proven to be a more suitable general detection scheme for high-rate LDCs in narrowband frequency-selective channels.

The last section of the chapter further investigates the ZF detection scheme, which has the disadvantage of requiring a large number of receive antennas to compensate for the dispersive channel. Modelling of frequency-selective channels with exponential power delay profiles allows the equalizer to assume a shorter channel length, thus giving better performance and decreasing the required number of receive antennas in the system.

In this chapter, a high-rate STBC scheme in frequency-selective channels is proposed in the form of LDCs. ZF detection is used as it is more applicable to a wide range of channel delays and non-orthogonal high-rate codes. Although the scheme is hindered by dimensionality, it can be ameliorated by using fewer taps in the equaliser when the channel is modelled by an exponential delay profile.

Chapter 4

Multiuser Cooperation in Frequency-Selective Fading Channels

> "If you can't explain it simply, you don't understand it well enough."
>
> *Albert Einstein*

4.1 Introduction

Multi-antenna systems have been demonstrated to achieve lower error rate and higher throughput in wireless fading channels. In spite of this, constraints on size, weight and hardware design restrict the number of antennas in many devices. Fortunately, communication networks generally consist of clusters of user nodes where users are able to hear transmissions from other broadcasting nodes in the vicinity. An alternate means of achieving diversity is to exploit

cooperation of multiple users [? ?] in the network to reduce error rate.

In Chapter ??, linear dispersion codes (LDCs) were investigated in frequency-selective environments. The presence of intersymbol interference (ISI) from dispersive channels requires block processing and sequence estimation at the receiver. Unfortunately, joint maximum likelihood processing of multiple symbol streams in combination with ISI equalization is computationally intensive and impractical for most modern day receivers. Zero forcing (ZF) mitigates interfering symbol streams to enable single stream equalization of each layer. However, it does not work for overloaded systems where the number of unknown symbols exceed the number of linear equations in the system. In frequency-selective channels, the channel length adds to the loading of the system and increases the minimum requirement of the number of receive antennas which can easily become impractical. On the other hand, orthogonal LDCs [?] support linear processing and resolves the problem of system overloading. In this chapter, a multi-user cooperation scheme is developed for frequency-selectivity channels. The users transmit LDCs and form an overall system that supports linear and ZF detection.

4.2 Multi-user Cooperation System

The idea of cooperation was first presented in [?] where diversity was achieved by a simple three terminal relay channel consisting of a source, a destination and a relay. The relay was a nearby terminal that forwarded information from the source to the destination. Direct transmission from source to destination and an additional relay path provided two independent channels for the signal

and thus increased the probability of correct signal detection at the destination receiver. The classical relay channel and other extended relay networks [**?** **?** **?**] form virtual antenna arrays [**?**] to achieve spatial diversity.

The relay is an inactive user node assisting another user, known as the source node to transmit data to the destination. Cooperation between multiple active nodes where all users have information to transmit can also work together to achieve diversity. Most existing multiuser cooperative systems have predominantly focused on flat fading wireless channels [**?**], [**?**]. Current multiuser cooperative schemes in frequency-selective channels combine with OFDM [**?**], [**?**] or use frequency-domain equalization [**?** **?** **?**] to detect signals in the presence of ISI. These schemes are more suited for wideband channels with large channel delays. A time-reversal multiuser cooperative scheme has been developed in [**?**] for sensor networks. The transmission scheme involves two source nodes where they maximise the channel peak power by modulating a time-reversed version of the estimated channel with the transmit data. The users cooperate by using a training phase to exchange channel information.

In this section, a novel two-user cooperative scheme is developed for narrowband dispersive channels. A cooperative multiple-access half-duplex channel is assumed where two users exchange data and then cooperatively forward all the information to a common destination. Both linear decoupling and ZF detection are combined with Viterbi equalization and investigated for the multiuser system. The scheme is described in this section.

The proposed multiuser scheme is designed for the cooperation of two user nodes. A narrow bandwidth is allocated to each pair of cooperating

users to transmit to a common destination. Every node is equipped with two transmit antennas and has data to transmit to the destination, which could be another user or a base station. The multiuser system is shown in Figure **??** showing the transmission states over one cooperative frame consisting of $T_b = 3$ consecutive block codes. Half-duplex transmission means the antennas are capable of unidirectional communication where an active node is either transmitting or receiving at any point in time. The arrows indicate the direction of transmission from the transmit to the receive antenna during each block interval, for $t_b = 1, ..., T_b$. Each user transmits $Q = 2$ symbol streams giving a total throughput of $2Q$ data streams over one transmission frame.

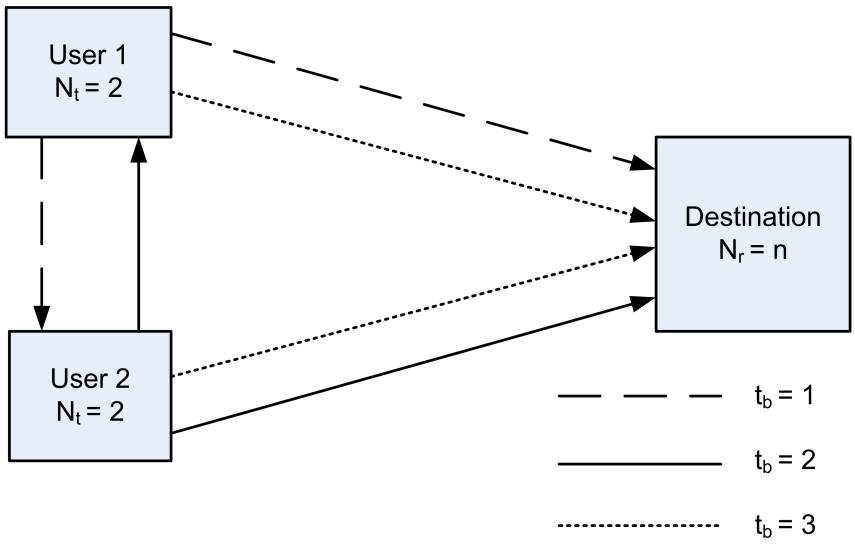

Figure 4.1: Proposed multiuser system showing the transmission states over three block intervals which form one cooperative frame. The two source nodes are equipped with two transmit antennas and cooperate together to transmit to one common destination.

Figure **??** depicts the symbols transmitted by the users over one cooperative frame. Let $\mathbf{x}_q^{(u)}$, for $q = 1, ...Q$, be the signal streams from User u, where $u = 1$ and 2 denote a source node in the system. The signal streams contain L_x

modulated symbols which are appended with preamble and postamble vectors of L_p known symbols to prevent interblock interference. Each block code is a LDC with dispersed signals over $T_s = 2$ successive signalling intervals and across $N_t = 2$ transmit antennas. Therefore, all signal streams transmitted in the $t_s = 1, ...T_s$ signalling intervals have a fixed length of $L_s = L_x + 2L_p$ symbols.

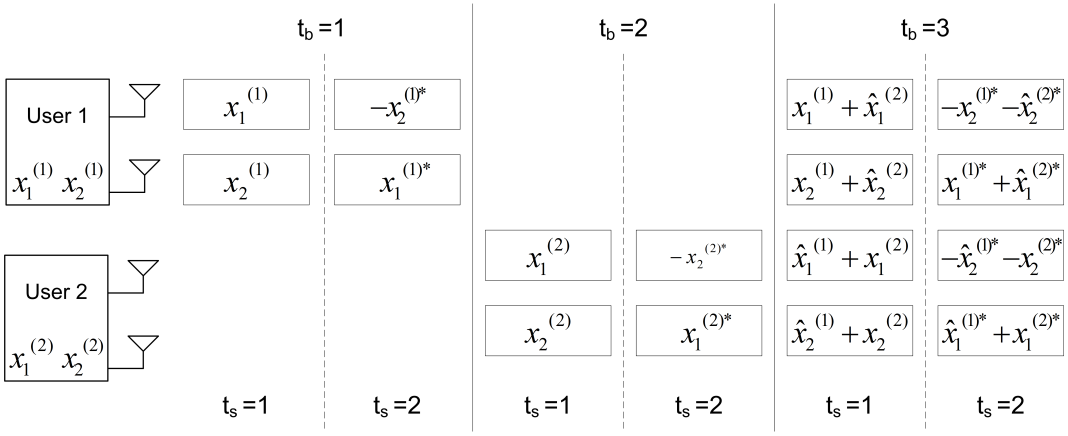

Figure 4.2: Multiuser system showing symbols transmitted during each time block interval.

In the first block interval, User 1 transmits an orthogonal LDC containing its own information, $\mathbf{x}_q^{(1)}, q = 1, ..., Q$ which is heard by User 2 and the destination node. User 2 detects the signals, $\hat{\mathbf{x}}_q^{(1)}, q = 1, ..., Q$ using ML linear processing while the destination node stores the received signal. In the second time block, User 2 sends the same LDC structure embedded with its own data streams, $\mathbf{x}_q^{(2)}, q = 1, ..., Q$ while User 1 receives and detects the signal, $\hat{\mathbf{x}}_q^{(2)}$, q=1,...,Q, and the destination stores the received signal. In the last time block, both users transmit a LDC containing its information plus the detected data from the other user and thus doubles the number of signal streams in the LDC to $2Q$. The destination node receives the signal and processes all the

data from the three time blocks to detect the signals from User 1 and User 2.

The mathematical representation for the multiuser cooperative system is described here and assumes phase coherence within each block. For more information on the notations and operations of partitioned matrices, refer to Section **??**. The real and imaginary signal components are denoted by

$$\boldsymbol{\alpha}_q^{(u)} = \mathcal{R}\{\mathbf{x}_q^{(u)}\}, \tag{4.1a}$$

$$\boldsymbol{\beta}_q^{(u)} = \mathcal{I}\{\mathbf{x}_q^{(u)}\}, \tag{4.1b}$$

for $u = 1$ and 2 and $q = 1, ..., Q$. The dispersion matrices for the multiuser system are

$$\mathbf{A}_q = \begin{bmatrix} a_{11}^{(q)} & a_{12}^{(q)} \\ a_{21}^{(q)} & a_{22}^{(q)} \end{bmatrix} = \begin{cases} \begin{bmatrix} 1 & 0 \\ 0 & 1 \end{bmatrix} & \text{for} \quad q = 1, \\ \begin{bmatrix} 0 & -1 \\ 1 & 0 \end{bmatrix} & \text{for} \quad q = 2, \end{cases} \tag{4.2}$$

$$\mathbf{B}_q = \begin{bmatrix} b_{11}^{(q)} & b_{12}^{(q)} \\ b_{21}^{(q)} & b_{22}^{(q)} \end{bmatrix} = \begin{cases} \begin{bmatrix} 1 & 0 \\ 0 & 1 \end{bmatrix} & \text{for} \quad q = 1, \\ \begin{bmatrix} 0 & -1 \\ 1 & 0 \end{bmatrix} & \text{for} \quad q = 2, \end{cases} \tag{4.3}$$

which are used to compute the partitioned dispersion matrices

$$\underset{\sim}{\mathbf{A}}_q^{(L_s)} = \left[\underset{\sim}{\mathbf{A}}_{t_s m}^{(q)}\right]_{t_s=1,...T_s, m=1,...N_t} \tag{4.4a}$$

$$\underset{\sim}{\mathbf{B}}_q^{(L_s)} = \left[\underset{\sim}{\mathbf{B}}_{t_s m}^{(q)}\right]_{t_s=1,...T_s, m=1,...N_t} \tag{4.4b}$$

$$\{\underset{\sim}{\mathbf{A}}_{t_s m}^{(q)}, \underset{\sim}{\mathbf{B}}_{t_s m}^{(q)}\} : L_s \times L_s, \tag{4.4c}$$

for $q = 1, ...Q$. The parameter t_s denotes the signalling interval to transmit a symbol stream with $T_s = 2$ and $N_t = 2$ is the number of transmit antennas at a user node. The subvectors are

$$\underset{\sim}{\mathbf{A}}_{t_s m}^{(q)} = a_{t_s m}^{(q)} \mathbf{I}_{Ls}, \tag{4.5a}$$

$$\underset{\sim}{\mathbf{B}}_{t_s m}^{(q)} = b_{t_s m}^{(q)} \mathbf{I}_{Ls}. \tag{4.5b}$$

The LDCs transmitted by user $u = t_b$ in the first and second block intervals, $t_b = 1$ and 2, are given as

$$\underset{\sim}{\mathbf{S}}_{t_b}^{(u)} = \sum_{q=1}^{Q} (\boldsymbol{\alpha}_q^{(u)} \underset{\sim}{\mathbf{A}}_q^{(Ls)} + j\boldsymbol{\beta}_q^{(u)} \underset{\sim}{\mathbf{B}}_q^{(Ls)}), \tag{4.6}$$

The frequency-selective channels are assumed to be slow fading and quasi-static over a transmission frame. Therefore, the channels from User u to the destination node,

$$\underset{\sim}{\mathbf{H}}_u = \left[\underset{\sim}{\mathbf{h}}_{mn}^{(u)}\right]_{m=1,...N_t, n=1,...N_r} \tag{4.7a}$$

$$\underset{\sim}{\mathbf{h}}_{mn}^{(u)} : 1 \times (L_h + 1), \tag{4.7b}$$

remains the same for $T_b = 3$ block intervals, where N_r is the number of antennas at the destination receiver and L_h is the length of channel dispersion. The signal received at the destination is

$$\underset{\sim}{\mathbf{Y}}_{t_b} = \underset{\sim}{\mathbf{S}}_{t_b}^{(u)} \otimes \underset{\sim}{\mathbf{H}}_u + \underset{\sim}{\mathbf{V}}_{t_b}, \tag{4.8}$$

where

$$\underset{\sim}{\mathbf{Y}}_{t_b} = \left[\underset{\sim}{\mathbf{y}}_{t_s n}^{(t_b)}\right]_{t_s=1,\ldots T_s, n=1,\ldots N_r} \tag{4.9a}$$

$$\underset{\sim}{\mathbf{y}}_{t_s n}^{(t_b)} : 1 \times (L_s + L_h), \tag{4.9b}$$

is the received signal during the t_b-th block interval and

$$\underset{\sim}{\mathbf{V}}_{t_b} = \left[\mathbf{v}_{t_s n}^{(t_b)}\right]_{t_s=1,..T_s, n=1,\ldots N_r} \tag{4.10a}$$

$$\underset{\sim}{\mathbf{v}}_{t_s n}^{(t_b)} : 1 \times (L_s + L_h), \tag{4.10b}$$

is the AWGN at the destination receive antenna at time block t_b. According to Section **??**, Equation (**??**) can be rewritten as

$$\underset{\sim}{\mathcal{Y}}_{t_b} = \underset{\sim}{\mathcal{H}}_u \otimes \underset{\sim}{\mathcal{X}}_{t_b}^{(u)} + \underset{\sim}{\mathcal{V}}_{t_b}, \tag{4.11}$$

where

$$\underset{\sim}{\mathcal{H}}_u = \left[\underset{\sim}{\mathfrak{h}}_{wz}^{(u)}\right]_{w=1,\ldots,2T_s N_r, z=1,\ldots,2Q}, \tag{4.12}$$

$$\underset{\sim}{\mathfrak{h}}_{wz}^{(u)} : 1 \times (L_h + 1). \tag{4.13}$$

is the modified real channel partitioned matrix from User u to the destination during the block interval $t_b = u$ signalling slot. The real partitioned received matrix is given by

$$\underset{\sim t_b}{\mathcal{Y}} = \begin{bmatrix} \mathcal{R}\{\underset{\sim}{\mathbf{y}}_{:1}^{(t_b)}\} \\ \mathcal{I}\{\underset{\sim}{\mathbf{y}}_{:1}^{(t_b)}\} \\ \vdots \\ \mathcal{R}\{\underset{\sim}{\mathbf{y}}_{:N_r}^{(t_b)}\} \\ \mathcal{I}\{\underset{\sim}{\mathbf{y}}_{:N_r}^{(t_b)}\} \end{bmatrix} = \left[\underset{\sim}{\mathfrak{y}}_{w}^{(t_b)}\right]_{w=1,\ldots,2T_sN_r} \tag{4.14}$$

$$\underset{\sim}{\mathfrak{y}}_{w}^{(t_b)} : 1 \times L_r. \tag{4.15}$$

The real noise partitioned matrix is given by

$$\underset{\sim t_b}{\mathcal{V}} = \begin{bmatrix} \mathcal{R}\{\underset{\sim}{\mathbf{v}}_{:1}^{(t_b)}\} \\ \mathcal{I}\{\underset{\sim}{\mathbf{v}}_{:1}^{(t_b)}\} \\ \vdots \\ \mathcal{R}\{\underset{\sim}{\mathbf{v}}_{:N_r}^{(t_b)}\} \\ \mathcal{I}\{\underset{\sim}{\mathbf{v}}_{:N_r}^{(t_b)}\} \end{bmatrix} = \left[\mathfrak{v}_{w}^{(t_b)}\right]_{w=1,\ldots,2T_sN_r} \tag{4.16}$$

$$\underset{\sim}{\mathfrak{v}}_{w}^{(t_b)} : 1 \times (L_r). \tag{4.17}$$

and the stacked real signal components from User u are given by

$$\underset{\sim t_b}{\mathbf{\mathcal{X}}}^{(u)} = \begin{bmatrix} \boldsymbol{\alpha}_1^{(u)} \\ \boldsymbol{\beta}_1^{(u)} \\ \vdots \\ \boldsymbol{\alpha}_Q^{(u)} \\ \boldsymbol{\beta}_Q^{(u)} \end{bmatrix} = \left[\underset{\sim}{\mathbf{\mathcal{x}}}_z^{(u)} \right]_{z=1,\ldots,2Q}, \tag{4.18}$$

$$\underset{\sim}{\mathbf{\mathcal{x}}}_z^{(u)} : 1 \times L_s. \tag{4.19}$$

In the third time block, $t_b = 3$, both users transmit a combination of their own symbol streams and the detected symbol streams from the other user according to

$$\begin{aligned} \underset{\sim}{\mathbf{S}}_3^{(u)} = &\sum_{q=1}^{Q} (\boldsymbol{\alpha}_q^{(u)} \underset{\sim}{\mathbf{A}}_q^{(Ls)} + j\boldsymbol{\beta}_q^{(u)} \underset{\sim}{\mathbf{B}}_q^{(Ls)}) \\ &+ \sum_{q=1}^{Q} (\hat{\boldsymbol{\alpha}}_q^{(u')} \underset{\sim}{\mathbf{A}}_q^{(Ls)} + j\hat{\boldsymbol{\beta}}_q^{(u')} \underset{\sim}{\mathbf{B}}_q^{(Ls)}), \end{aligned} \tag{4.20}$$

where $\hat{\boldsymbol{\alpha}}_q^{(u')}$ and $\hat{\boldsymbol{\beta}}_q^{(u')}$ are the estimated real and imaginary component from User u, for $u = 1, 2$ and $u' = 2, 1$. With the assumption of quasi-static channels during $T_b = 3$ block intervals, the received signal at $t_b = 3$ is given by

$$\underset{\sim}{\mathbf{Y}}_3 = \underset{\sim}{\mathbf{S}}_3^{(1)} \otimes \underset{\sim}{\mathbf{H}}_1 + \underset{\sim}{\mathbf{S}}_3^{(2)} \otimes \underset{\sim}{\mathbf{H}}_2 + \underset{\sim}{\mathbf{V}}_3 \tag{4.21}$$

which is equivalent to

$$\underset{\sim}{\mathbf{\mathcal{Y}}}_3 = \underset{\sim}{\mathbf{\mathcal{H}}}_1 \otimes \underset{\sim}{\mathbf{\mathcal{X}}}_3^{(1)} + \underset{\sim}{\mathbf{\mathcal{H}}}_2 \otimes \underset{\sim}{\mathbf{\mathcal{X}}}_3^{(2)} + \underset{\sim}{\mathbf{\mathcal{V}}}_3, \tag{4.22}$$

where

$$\underset{\sim}{\mathfrak{X}}_3^{(1)} = \begin{bmatrix} \boldsymbol{\alpha}_1^{(1)} \\ \boldsymbol{\beta}_1^{(1)} \\ \vdots \\ \boldsymbol{\alpha}_Q^{(1)} \\ \boldsymbol{\beta}_Q^{(1)} \\ \hat{\boldsymbol{\alpha}}_1^{(2)} \\ \hat{\boldsymbol{\beta}}_1^{(2)} \\ \vdots \\ \hat{\boldsymbol{\alpha}}_Q^{(2)} \\ \hat{\boldsymbol{\beta}}_Q^{(2)} \end{bmatrix} \quad \text{and} \quad \underset{\sim}{\mathfrak{X}}_3^{(2)} = \begin{bmatrix} \hat{\boldsymbol{\alpha}}_1^{(1)} \\ \hat{\boldsymbol{\beta}}_1^{(1)} \\ \vdots \\ \hat{\boldsymbol{\alpha}}_Q^{(1)} \\ \hat{\boldsymbol{\beta}}_Q^{(1)} \\ \boldsymbol{\alpha}_1^{(2)} \\ \boldsymbol{\beta}_1^{(2)} \\ \vdots \\ \boldsymbol{\alpha}_Q^{(2)} \\ \boldsymbol{\beta}_Q^{(2)} \end{bmatrix} \tag{4.23}$$

are the partitioned matrices of the data symbols and the estimated symbols of the users, respectively. Suppose

$$\boldsymbol{\alpha}_q^{(u)} \approx \hat{\boldsymbol{\alpha}}_q^{(u)} \tag{4.24a}$$

$$\boldsymbol{\beta}_q^{(u)} \approx \hat{\boldsymbol{\beta}}_q^{(u)}, \tag{4.24b}$$

for $q = 1, ..., Q$ and $u = 1, 2$, then

$$\underset{\sim}{\mathfrak{X}}_3^{(1)} \approx \underset{\sim}{\mathfrak{X}}_3^{(2)} \approx \begin{bmatrix} \mathfrak{X}_1^{(1)} \\ \mathfrak{X}_2^{(2)}, \end{bmatrix} \tag{4.25}$$

and Equation (**??**) and Equation (**??**) form the combined cooperative system given by

$$\underset{\sim T}{\mathfrak{Y}} = \underset{\sim T}{\mathfrak{H}} \otimes \underset{\sim T}{\mathfrak{X}} + \underset{\sim T}{\mathfrak{V}} \tag{4.26}$$

where

$$\underset{\sim T}{\mathcal{Y}} = \begin{bmatrix} \mathcal{Y}_1 \\ \mathcal{Y}_2 \\ \mathcal{Y}_3 \end{bmatrix} = \left[\underset{\sim}{\mathfrak{y}}_w^{(T)} \right]_{w=1,\ldots,2T_f N_r} \tag{4.27a}$$

$$\underset{\sim}{\mathfrak{y}}_w^{(T)} : 1 \times (L_s + L_h), \tag{4.27b}$$

is the total received signal over $T_f = T_b T_s = 6$ signalling intervals,

$$\underset{\sim T}{\mathcal{H}} = \begin{bmatrix} \mathcal{H}_1 & \mathbf{0} \\ \mathbf{0} & \mathcal{H}_2 \\ \mathcal{H}_1 + \mathcal{H}_2 & \mathcal{H}_1 + \mathcal{H}_2 \end{bmatrix} = \left[\underset{\sim}{\mathfrak{h}}_{wz}^{(T)} \right]_{w=1,\ldots,2T_f N_r, z=1,\ldots,4Q}, \tag{4.28a}$$

$$\underset{\sim}{\mathfrak{h}}_{wz}^{(T)} : 1 \times (L_h + 1) \tag{4.28b}$$

is the equivalent channel matrix over the entire transmission frame,

$$\underset{\sim T}{\mathcal{X}} = \begin{bmatrix} \mathcal{X}_1^{(1)} \\ \mathcal{X}_2^{(2)}, \end{bmatrix} = \left[\underset{\sim}{\mathfrak{x}}_z^{(T)} \right]_{z=1,\ldots,4Q}, \tag{4.29}$$

$$\underset{\sim}{\mathfrak{x}}_z^{(T)} : 1 \times L_s, \tag{4.30}$$

is the stacked symbol blocks of the data streams from both users and

$$\underset{\sim T}{\mathcal{V}} = \begin{bmatrix} \mathcal{V}_1 \\ \mathcal{V}_2 \\ \mathcal{V}_3 \end{bmatrix} = \left[\underset{\sim}{\mathfrak{v}}_w^{(T)} \right]_{w=1,\ldots,2T_f N_r} \tag{4.31a}$$

$$\underset{\sim}{\mathfrak{v}}_w^{(T)} : 1 \times (L_s + L_h), \tag{4.31b}$$

is the AWGN noise matrix over the three block time slots.

4.2.1 Detection and Equalization

The received signal is a linear combination of Q signal streams from User 1 and User 2 which have been degraded by the fading channels and ISI. Joint detection of 2Q signal streams is computationally intensive even when using the Viterbi algorithm. Fortunately, the overall channel has an orthogonal structure with the following property

$$\underset{\sim}{\mathfrak{F}} = \underset{\sim T}{\mathfrak{H}'} \otimes \underset{\sim T}{\mathfrak{H}} = \begin{bmatrix} \mathfrak{a}_1 & \mathfrak{0} & \mathfrak{0} & \mathfrak{0} & \mathfrak{a}_2 & \mathfrak{0} & \mathfrak{0} & \mathfrak{0} \\ \mathfrak{0} & \mathfrak{a}_1 & \mathfrak{0} & \mathfrak{0} & \mathfrak{0} & \mathfrak{a}_2 & \mathfrak{0} & \mathfrak{0} \\ \mathfrak{0} & \mathfrak{0} & \mathfrak{a}_1 & \mathfrak{0} & \mathfrak{0} & \mathfrak{0} & \mathfrak{a}_2 & \mathfrak{0} \\ \mathfrak{0} & \mathfrak{0} & \mathfrak{0} & \mathfrak{a}_1 & \mathfrak{0} & \mathfrak{0} & \mathfrak{0} & \mathfrak{a}_2 \\ \mathfrak{a}_2 & \mathfrak{0} & \mathfrak{0} & \mathfrak{0} & \mathfrak{a}_3 & \mathfrak{0} & \mathfrak{0} & \mathfrak{0} \\ \mathfrak{0} & \mathfrak{a}_2 & \mathfrak{0} & \mathfrak{0} & \mathfrak{0} & \mathfrak{a}_3 & \mathfrak{0} & \mathfrak{0} \\ \mathfrak{0} & \mathfrak{0} & \mathfrak{a}_2 & \mathfrak{0} & \mathfrak{0} & \mathfrak{0} & \mathfrak{a}_3 & \mathfrak{0} \\ \mathfrak{0} & \mathfrak{0} & \mathfrak{0} & \mathfrak{a}_2 & \mathfrak{0} & \mathfrak{0} & \mathfrak{0} & \mathfrak{a}_3 \end{bmatrix} \tag{4.32a}$$

$$= \left[\underset{\sim}{\mathfrak{f}}_{bc} \right]_{b=1,\ldots,4Q, c=1,\ldots,4Q} \tag{4.32b}$$

$$\underset{\sim}{\mathfrak{f}}_{bc} : 1 \times (2L_h + 1) \tag{4.32c}$$

where $(\underset{\sim}{\cdot})'$ denotes partitioned matrix transpose as defined by Equation (**??**) and each zero entry is an all-zero vector of length $1 \times (2L_h + 1)$. Therefore, convolving the partitioned matrix transpose with the received signal, the system

of Equation (??) becomes

$$\underset{\sim}{\hat{\mathfrak{y}}}_T = \underset{\sim}{\mathcal{H}}'_T \otimes \underset{\sim}{\mathfrak{y}}_T = \begin{bmatrix} \mathfrak{a}_1 & \mathfrak{a}_2 \\ \mathfrak{a}_1 & \mathfrak{a}_2 \\ \mathfrak{a}_1 & \mathfrak{a}_2 \\ \mathfrak{a}_1 & \mathfrak{a}_2 \\ \mathfrak{a}_2 & \mathfrak{a}_3 \\ \mathfrak{a}_2 & \mathfrak{a}_3 \\ \mathfrak{a}_2 & \mathfrak{a}_3 \\ \mathfrak{a}_2 & \mathfrak{a}_3 \end{bmatrix} \otimes \begin{bmatrix} \boldsymbol{\alpha}_1^{(1)} & \boldsymbol{\beta}_1^{(1)} & \boldsymbol{\alpha}_2^{(1)} & \boldsymbol{\beta}_2^{(1)} & \boldsymbol{\alpha}_1^{(1)} & \boldsymbol{\beta}_1^{(1)} & \boldsymbol{\alpha}_2^{(1)} & \boldsymbol{\beta}_2^{(1)} \\ \boldsymbol{\alpha}_1^{(2)} & \boldsymbol{\beta}_1^{(2)} & \boldsymbol{\alpha}_2^{(2)} & \boldsymbol{\beta}_2^{(2)} & \boldsymbol{\alpha}_1^{(2)} & \boldsymbol{\beta}_1^{(2)} & \boldsymbol{\alpha}_2^{(2)} & \boldsymbol{\beta}_2^{(2)} \end{bmatrix}$$

$$+ \underset{\sim}{\mathcal{H}}'_T \otimes \underset{\sim}{\mathcal{V}}_T \tag{4.33}$$

$$= \left[\underset{\sim}{\hat{\mathfrak{y}}}_z \right]_{w=1,\ldots,4Q} \tag{4.34}$$

$$\underset{\sim}{\hat{\mathfrak{y}}}_z : 1 \times (L_s + 2L_h), \tag{4.35}$$

which decouples the cooperative system into the four independent systems

$$\begin{bmatrix} \hat{\mathfrak{y}}_1 \\ \hat{\mathfrak{y}}_5 \end{bmatrix} = \begin{bmatrix} \mathfrak{a}_1 & \mathfrak{a}_2 \\ \mathfrak{a}_2 & \mathfrak{a}_3 \end{bmatrix} \otimes \begin{bmatrix} \boldsymbol{\alpha}_1^{(1)} \\ \boldsymbol{\alpha}_1^{(2)} \end{bmatrix} + noise \tag{4.36a}$$

$$\begin{bmatrix} \hat{\mathfrak{y}}_2 \\ \hat{\mathfrak{y}}_6 \end{bmatrix} = \begin{bmatrix} \mathfrak{a}_1 & \mathfrak{a}_2 \\ \mathfrak{a}_2 & \mathfrak{a}_3 \end{bmatrix} \otimes \begin{bmatrix} \boldsymbol{\beta}_1^{(1)} \\ \boldsymbol{\beta}_1^{(2)} \end{bmatrix} + noise \tag{4.36b}$$

$$\begin{bmatrix} \hat{\mathfrak{y}}_3 \\ \hat{\mathfrak{y}}_7 \end{bmatrix} = \begin{bmatrix} \mathfrak{a}_1 & \mathfrak{a}_2 \\ \mathfrak{a}_2 & \mathfrak{a}_3 \end{bmatrix} \otimes \begin{bmatrix} \boldsymbol{\alpha}_2^{(1)} \\ \boldsymbol{\alpha}_2^{(2)} \end{bmatrix} + noise \tag{4.36c}$$

$$\begin{bmatrix} \hat{\mathfrak{y}}_4 \\ \hat{\mathfrak{y}}_8 \end{bmatrix} = \begin{bmatrix} \mathfrak{a}_1 & \mathfrak{a}_2 \\ \mathfrak{a}_2 & \mathfrak{a}_3 \end{bmatrix} \otimes \begin{bmatrix} \boldsymbol{\beta}_2^{(1)} \\ \boldsymbol{\beta}_2^{(2)} \end{bmatrix} + noise \tag{4.36d}$$

where $\underset{\sim}{\hat{\mathfrak{y}}}_z$ is the z-th row block of $\hat{\mathfrak{Y}}_T$. The four decoupled systems are passed successively into a Viterbi decoder which jointly equalizes two signal streams. The joint Viterbi algorithm becomes more complex and is described below.

The trellis states in Section **??** are permutations of L_h data symbols. Joint detection increases the number of permutations to $M'^{L_h Q'}$ where M' is the size of modulation of the signal stream and Q' is the number of joint signal detections. A state in the joint Viterbi trellis is given as

$$\begin{pmatrix} \hat{\mathfrak{s}}_1 \\ \hat{\mathfrak{s}}_2 \\ \vdots \\ \hat{\mathfrak{s}}_{Q'} \end{pmatrix}_z = \left[\hat{\mathfrak{s}}_q\right]^{(z)}_{q=1,\ldots,Q'} \tag{4.37a}$$

$$\underset{\sim}{\hat{\mathfrak{s}}}^{(z)}_q : 1 \times L_h, \tag{4.37b}$$

for $z = 1, ..., M'^{L_h Q'}$. During the state transition from time t to $t' = t + 1$, there are also $m = 1, ..., M'^{Q'}$ branch metrics to be computed for every state z. Each branch, m, is a permutation for the next possible symbols in Q' joint sequences given as

$$\begin{pmatrix} b_1 \\ b_2 \\ \vdots \\ b_{Q'} \end{pmatrix}_m , = b^{(m)}_q \tag{4.38}$$

for $q = 1, ..., Q'$. Equations (**??**), (**??**) and (**??**) become

$$U_z^{(t)} = \sum_{q_1=1}^{Q'} \left(\sum_{l=1}^{L_p} \|y_{q_1}[l] - \sum_{q_2=1}^{Q'} \sum_{i=0}^{l-1} (h_{q_1 q_2}[i] \hat{s}_{q_2}^{(z)}[l-i]) \|^2 \right), \tag{4.39}$$

$$V_m^{(z)}(t) = \sum_{q_1=1}^{Q'} \left(\|y_{q_1}[L_p + t] - \sum_{q_2=1}^{Q'} (h_{q_1 q_2}[0] b_{q2}^{(m)} + \sum_{i=1}^{L_h} h_{q_1 q_2}[i] \hat{s}_{q_2}^{(z)}[t-i]) \|^2 \right), \tag{4.40}$$

and

$$V_m^{(z)}(t) = \sum_{q_1=1}^{Q'} \left(\|y_{q_1}[L_p + t'] - \sum_{q_2=1}^{Q'} \sum_{i=0}^{L_h} h_{q_1 q_2}[i] \hat{s}_{q_2}^{(z)}[t-i] \|^2 \right), \tag{4.41}$$

respectively.

In addition to linear decoupling, the multiuser system in Equation (**??**) can also be detected by ZF which was used to recover the V-BLAST system as well as the LDC in frequency-selective environments. Refer to Section **??** for details of forcing the interfering signals in the multiuser cooperative system to zero. However, a simple description involves converting the system into a bigger transmit array flat fading system and nulling out interfering channels through $4Q$ stages. The multiuser system must meet the following criterion

$$2T_f N_r > 4Q(L_h + 1) - (L_h + 1), \tag{4.42}$$

to satisfy the dimensionality requirement for ZF detection.

4.3 Results and Discussion

This section presents simulation results for the proposed multiuser cooperative transmission scheme in frequency-selective channels. Simulations of the multiuser scheme using both linear processing and ZF detection are examined. Performance comparison with other multiuser schemes is difficult as multiuser schemes vary in their cooperative strategy. However, the first two block intervals in the cooperative frame transmit two non-cooperative orthogonal LDCs. Therefore, it is reasonable to compare the proposed scheme with the non-cooperative scheme where the first two slots of the block transmission are used. Incorporating time-reversal into the orthogonal LDC results in the TR-STBC which is shown in Figure **??** to give better performance. This scheme will be considered as the benchmark for comparing the performance of the proposed cooperative scheme. Both perfect and imperfect detection at the user nodes are investigated. Perfect user detection assumes an ideal inter-user channel with no errors in the received signal.

The definition of signal to noise ratio (SNR) is given in Equation (**??**) with the noise variance defined in Equation (**??**). Unless stated otherwise, the schemes simulated and discussed in this section transmit a symbol stream of $L_x = 30$ QPSK symbols appended with zero vectors of length $L_p = L_h = 1$ symbol, resulting in a stream of $L_s = 32$ symbols transmitted in each signalling interval. The dispersive channel is quasi-static for one transmission frame and has a delay spread of $L_h = 1$ symbol and two channel taps. Each frequency-selective channel from transmit antenna m to receive antenna n is normalized such that $E\left[\sum_{l=0}^{L_h} \|h_{nm}[l]\|^2\right] = 1$ and is assumed to be known perfectly by

the receiver.

Figure **??** illustrates the simulation results for the proposed multiuser cooperation with linear detection at the receiver and perfect detection at the user nodes. Linear detection is suitable for any number of receive antennas at the destination node and is shown to achieve receive diversity gain. However, it is observed from the figure that the multiuser scheme does not achieve an improvement in BER when compared with the performance of the non cooperative TR-STBC. A non cooperative OSTBC scheme with no time-reversal is displayed to show that the cooperative scheme is able to reduce BER. Nevertheless, the proposed cooperative scheme with linear detection cannot contend with the performance gained from time-reversal. Furthermore, incorporating time-reversal into the cooperative scheme by multiplying the permutation matrix with Equation (**??**) to give

$$\underset{\sim}{\mathbf{A}}_{t_s m}^{(q)} = a_{t_s m}^{(q)} \mathbf{P}_{L_s}^{(0)} \mathbf{I}_{Ls}, \tag{4.43a}$$

$$\underset{\sim}{\mathbf{B}}_{t_s m}^{(q)} = b_{t_s m}^{(q)} \mathbf{P}_{L_s}^{(0)} \mathbf{I}_{Ls}. \tag{4.43b}$$

does not decouple the system completely into Equation (**??**). Thus, time-reversal of the multiuser cooperative scheme demands a more complex receiver.

As discussed in Chapter **??**, ZF detection can be adapted to any multiplexing system provided the system is not overloaded with more unknown variables than the number of equations available. This can be avoided for the multiuser system if it satisfies the dimensionality criterion in Equation (**??**). The additional time slot required in the cooperation scheme to transmit the

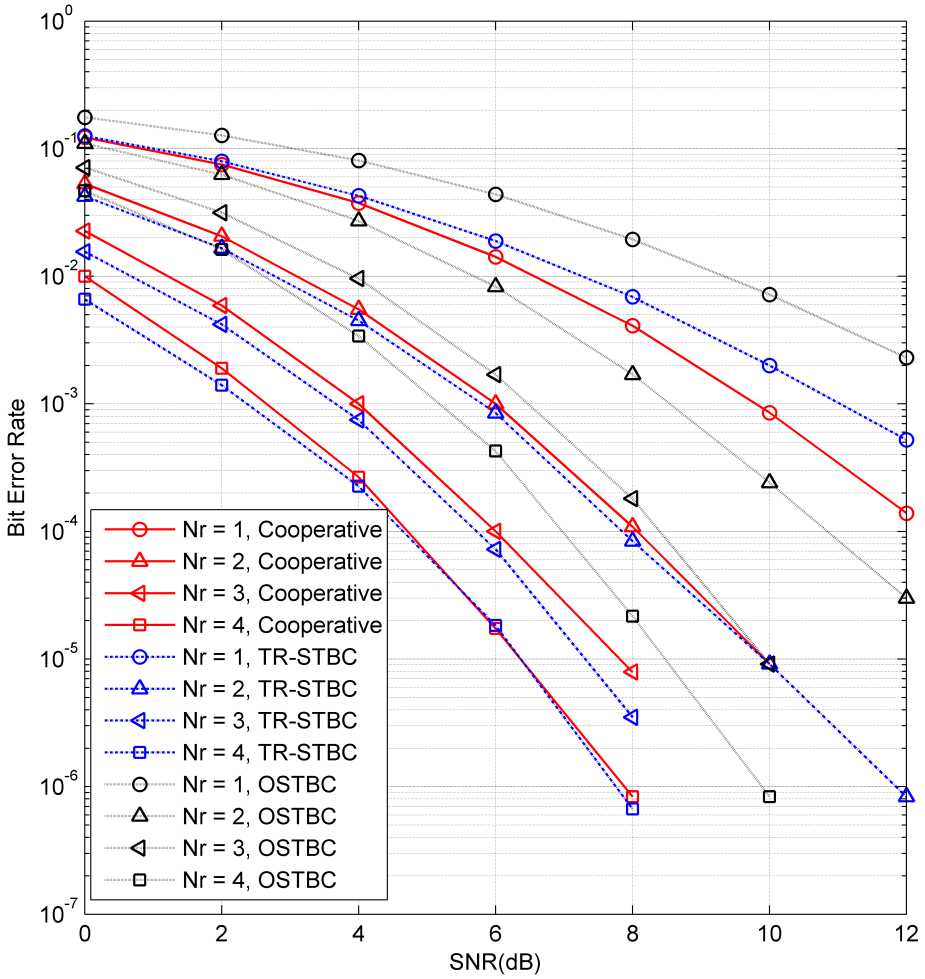

Figure 4.3: BER performance of the multiuser cooperation system versus no cooperation in frequency-selective channels with linear detection.

combined users' information is shown to decrease system loading. Therefore, the multiuser system in channels with lengths, $L_h < 3$ requires a minimum of two receive antennas. Minimizing the loading of the system also minimizes the antenna requirements of the multiuser cooperative system.

Figure **??** compares the performance of the multiuser cooperative system using ZF detection and $T_s = 3$ with the non cooperative TR-STBC using $T_s = 2$. Simulation results show cooperation with ZF detection attains a BER improvement over the TR-STBC uncooperative transmission scheme, which is greater at low SNRs. The performance improvement appears to be a coding gain rather than a diversity gain which is sacrificed for transmitting more data in the last time slot. The multiuser cooperative scheme loses throughput by utilising a third time slot, however, the coding gain improvement justifies its employment. The gain margin between user cooperation and no user cooperation increases with a larger number of receive antennas. The availability of more independent equations, as a result of adding more antennas to the receiver is seen to reduce the system load, thus giving higher coding gain.

Increasing the length of the transmission frame or the number of receive antennas at the destination reduces the load on the multiuser system. This is verified by Equation (**??**) where a larger value on the right side of the equation gives a more heavily loaded system. An underloaded system allows ZF detection to be used and to achieve performance gain with the cooperative system. However, the dispersive length of the channel also contributes to system loading which is illustrated in Figure **??** where the system suffers from a loss in performance when it becomes more loaded with a higher number of channel taps. The system with $L_h = 4$ symbol delays is shown to have

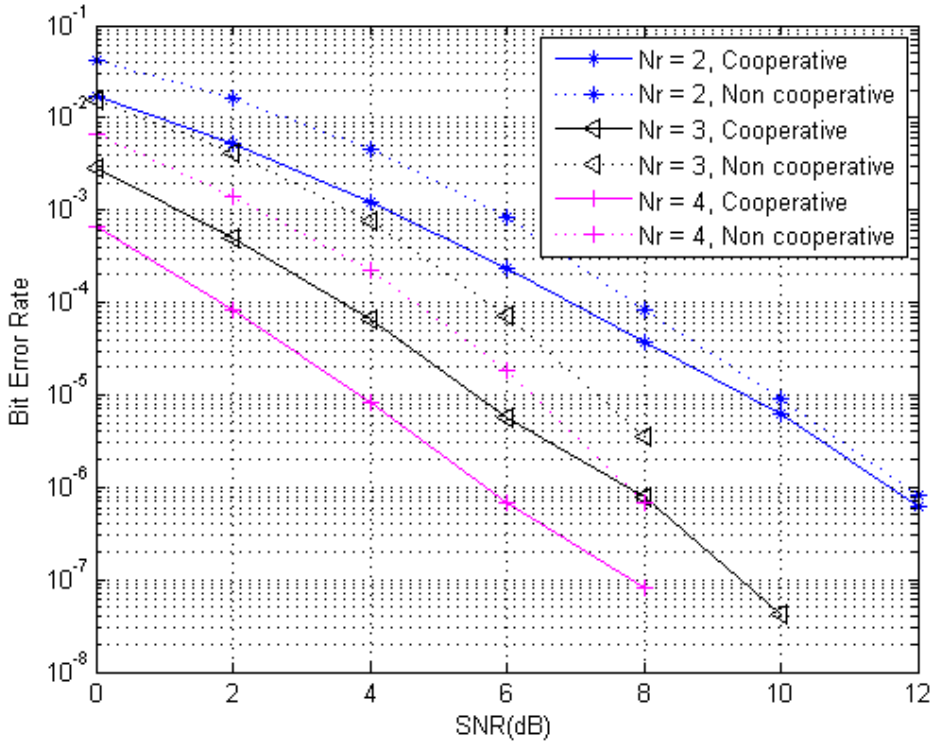

Figure 4.4: BER performance of the multiuser cooperation system versus no cooperation in frequency-selective channels with ZF detection.

a severe degradation in performance as a result of the system being close to overloading. Performance can only be compensated by utilising more receive antenns. Despite this, multiuser cooperation with ZF detection is still more desirable over the non cooperative TR-STBC because it has a lower equalization complexity as discussed in Chapter **??**. The number of Viterbi states for equalizing the TR-STBC in $L_h = 4$ channels is $M^{2L_h} = 65536$, prohibitive for modern day receivers.

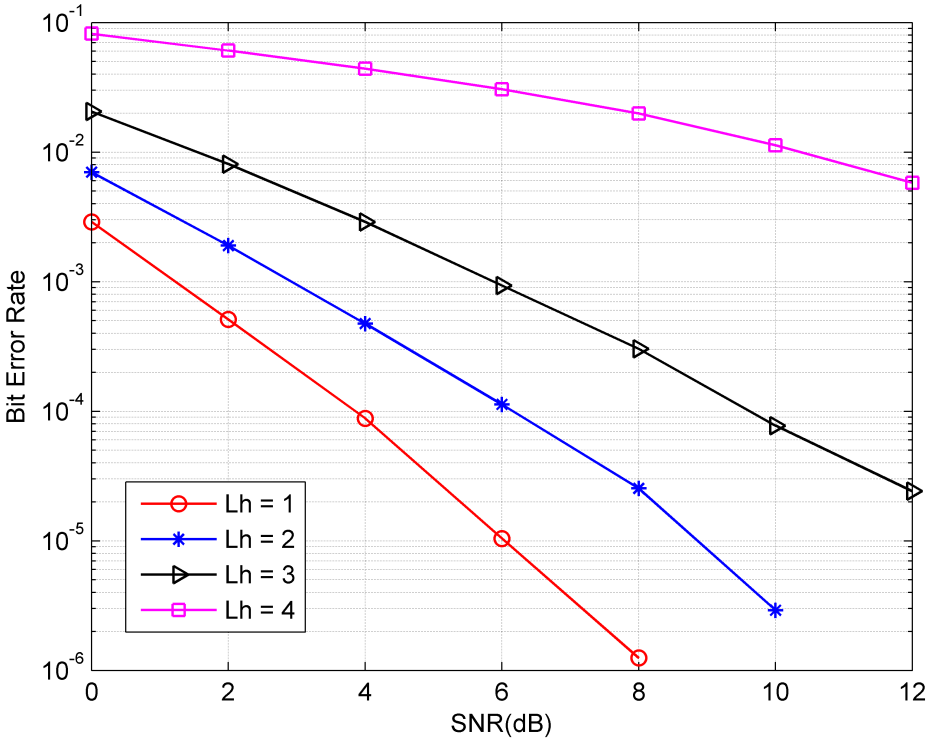

Figure 4.5: BER performance of the multiuser cooperation system with ZF detection versus channel length and $N_r = 3$.

The previous simulations have been investigated in perfect multiuser environments where ideal inter-user channels are assumed. This means the user nodes decode and forward the information perfectly to the destination.

However, this is not realistic in communications systems and therefore, the limitations of the multiuser system are investigated for imperfect user detection. Figure **??** illustrates the BER performance at the destination with $N_r = 2$ receive antennas and an assumption that SNR is constant at the user nodes. The BER curve for the ideal multiuser scheme with $N_r = 2$ receive antennas is also displayed. The figure shows the multiuser performance is dependent on the detection of signals at the user nodes, making it suitable for systems where the users are close to each other.

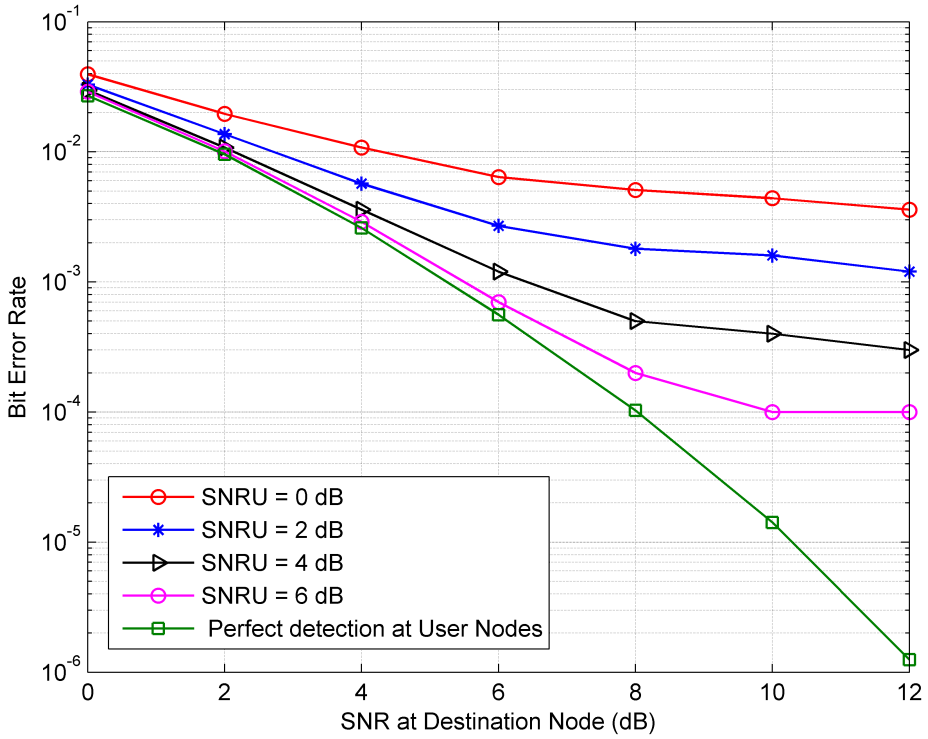

Figure 4.6: BER performance of the multiuser cooperation system with fixed SNR at the users with $N_r = 2$ receive antennas at destination.

Another imperfect user detection scenario is examined for the ZF cooperative scheme. In this case, the SNR at the user nodes is a constant amount

higher than the SNR at the destination meaning

$$SNR_{User}(dB) = SNR_{Destination}(dB) + Difference(dB). \tag{4.44}$$

Figure **??** shows a small coding gain is achieved by the $Nr = 2$ receive antenna cooperative system when perfect detection is assumed at the user nodes. Thus, this suggests a real system will not benefit greatly from cooperation. However, the system with $N_r = 4$ receive antennas is able to obtain significant coding gain. The simulation results for $N_r = 4$ is presented in Figure **??** for the imperfect scenario when the users have a constant SNR greater than the destination node. The results show the multiuser cooperative scheme is appropriate only when the users have sufficient SNR gain. Therefore, the performance of the multiuser scheme could be improved by using selective decode-and-forward, where user nodes only forward information if it is received without error. Furthermore, error detection codes can be used to bolster the performance of the multiuser system.

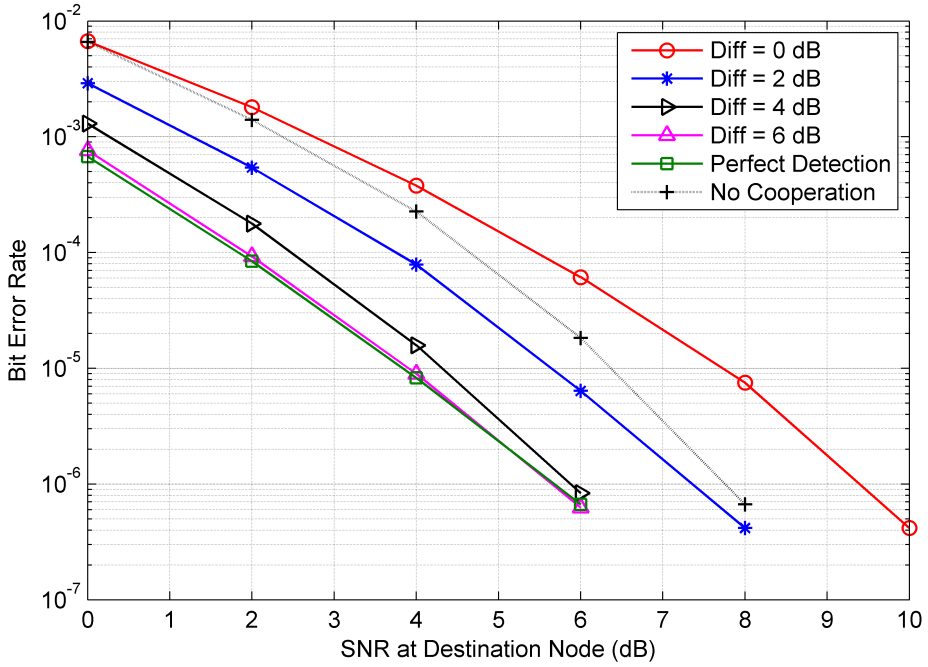

Figure 4.7: BER performance of the multiuser cooperation system with SNR(user) = SNR(destination) + difference (dB) with $N_r = 4$ receive antennas at destination.

4.4 Summary

In this chapter, a multiuser cooperative transmission scheme for two users in a frequency-selective environment is described. A transmission frame involves three transmit block intervals where a LDC is transmitted from a user in the first two blocks. During the first two block periods, the users exchange information which is also heard by the destination node and stores it in memory. In the last block interval, both users transmit a LDC to the destination. At the end of the transmission frame, the receiver at the destination combines all the stored data to detect the signals from both users. The LDC cooperative system is orthogonal and therefore both linear and zero forcing detection is possible at the receiver.

Linear detection is found to be an unsuitable detection scheme for the proposed multiuser cooperative system. In addition to increased detection complexity, linear detection and LDCs cannot incorporate time-reversal and therefore is not able to meet the performance of the uncooperative TR-STBC.

On the other hand, ZF is shown to be a good detection scheme, allowing the multiuser scheme to achieve greater performance improvement compared to the TR-STBCs. Like ZF detection for the V-BLAST and LDC, ZF detection for the multiuser system also needs to meet the dimensionality criterion required to prevent system overloading. Fortunately, transmitting over three intervals diminishes the loading problem and therefore a smaller number of receive antennas is required. The performance of ZF detection degrades with longer channels, however, it is more desirable than TR-STBCs because the complexity of the linear decoupling is prohibitive for longer dispersive chan-

nels.

The ZF multiuser cooperative system is investigated in imperfect scenarios where the user nodes may forward incorrect data to the destination. Simulation results show performance is degraded by incorrect detections at the users nodes. Therefore, selective decode and forward is suggested with the multiuser cooperative transmission scheme to achieve the best performance between cooperative coding gain and non-cooperative channel gain from time-reversal.

Chapter 5

Conclusions

"Storms make oaks take roots."

-Proverb

LDCs in frequency-selective channels have been proposed in this thesis that are capable of achieving high throughputs as dictated by the design of the dispersion codes. Mitigation of signal interference and ISI equalization are performed at the receiver to decode the LDC in frequency-selective channels. Mitigation of interfering signals can be achieved by both linear and zero-forcing detection schemes before the signals are equalized by a Viterbi maximum likelihood sequence estimator.

The combination of linear detection and time-reversal in the orthogonal STBC in frequency-selective channels has been developed in the literature and shown to achieve good performance. Linear detection mitigates signal interference by exploiting orthogonality in the STBC to decouple the transmit symbol streams. Therefore, orthogonality in the LDC is also exploited to decouple the transmit streams. The structure of the LDC, however, cannot incorporate

time-reversal without a significant increase in detection complexity. Thus, it cannot match the performance of the TR-STBC. Regrettably, the TR-STBC does not work for high-rate STBCs which lack orthogonality. In addition, detection complexity increases exponentially with the channel length for the TR-STBC.

ZF detection is also investigated which can be performed on orthogonal and non-orthogonal STBCs. Interference of unwanted signals is mitigated by nulling the interfering channels to zero which can only be accomplished when the system is not overloaded. The frequency-selective channel contributes to the system loading which is compensated by increasing the number of receive antennas in order to maintain high-rate in the STBC. Non-uniform channel profiles are examined for varying exponential delay taps. When low power taps are ignored by the Viterbi decoder, the system reduces in loading resulting in fewer receive antennas being required and better performance.

The LDC is adapted into a multiuser cooperative scheme in frequency-selective channels where user nodes in close proximity to each other have information to send to a common destination. The cooperative LDC is orthogonal and therefore both linear detection and ZF can be used to detect the signals from the users. The cooperative scheme is compared with the uncooperative scheme where each user transmits a TR-STBC in two separate block intervals. Linear detection is shown to be inadequate in meeting the performance of the TR-STBC. However, zero forcing, in the best case scenario is able to achieve better performance than the TR-STBC when sufficient receiver antennas are used. The multiuser cooperative scheme requires good detection of signals at the user nodes. Therefore, selective decode-and-forward is suggested for the

proposed multiuser cooperative scheme.

5.1 Future Work

STBCs in frequency-selective channels are shown to be limited by receiver computationalpower, with the Viterbi decoder as the predominant determinant. Future work to investigate a reduced state Viterbi decoder would benefit both detection schemes especially the higher complexity linear decoder for large channels. A reduced complexity Viterbi decoder would also assist in further investigations of other LDC structures, such as quasi-orthogonal STBCs requiring joint detection of two or more symbol streams.

Time-reversal is shown to have the best performance. Linear processing and time-reversal on the LDC structure does not support full channel decoupling. However, time-reversal on the LDC gives partial decoupling which could be exploited in an attempt to push the performance of orthogonal LDCs to match the performance of TR-STBCs. Additionally, LDCs have only been investigated where symbol streams have remained in the same sequential order before and after the streams have been dispersed into the LDC. Investigation of inter-dispersion of symbols within a symbol stream in addition to dispersion of signal streams in time and space could possibly give a performance gain for the LDC. Some form of error detection could also be adapted into the LDC. These suggestions can be applied to both the single user and multiuser LDC system in frequency-selective environments.

The multiuser cooperative system is shown to be suitable for communication systems where the user nodes are in the same vicinity and probability

of correct detection of the other signal is high. Selective-decode-and forward ensures the best performance is achieved between cooperative gain and channel diversity. However, further work could be investigated involving the use of relay nodes that are closer in distance to the destination. The relay nodes could be used interchangeably between the other cooperative user node, supporting the transmission when there are no nearby nodes to help with cooperation. Additionally, the multiuser cooperative transmission scheme could be extended to a bigger multiuser system involving more users.

References

[1] G. Falciasecca and B. Valotti. **Guglielmo Marconi: the pioneer of wireless communications**, in *Proc. EuMC*, Bologna, Italy, pp. 544-546, 2009. 1

[2] C. E. Shannon. **A mathematical theory of communication**. *Bell Syst. Tech. J.*, vol. 27, no. 3, pp. 379-423, 1948. 1

[3] V. Gautam and S. Sinha. **1946: First Mobile Telephone Call**. Internet: http://www.corp.att.com [Oct. 26,2011] 1

[4] E. Telatar. **Capacity of multi-antenna Gaussian channels**. *Europ. Trans. Telecommun., ETT*, vol. 10, no. 6, pp. 585-595, Nov. 1999. 2, 14

[5] V. Tarokh, H. Jafarkhani and A. R . Calderbank. **Space-time block codes from orthogonal designs**, *IEEE Trans. Inform. Theory*, vol. 45, no. 5, pp. 14561467, Mar, 1999. 2, 14, 15

[6] H. Mheidat and M. Uysal and N. Al-Dhahir. **Quasi-orthogonal time-reversal space-time block coding for frequency-selective fading channels**, *IEEE Trans. Signal Processing*, vol. 55, no.2, pp. 772-778, Jan. 2007. 15

[7] A. Ismail, J. Fiorina and H. Sari. **A new low-complexity decodable rate-1 full-diversity 4 × 4 STBC with nonvanishing determinants** *IEEE Trans. Wireless Commun.*, vol. 10, no.8, pp. 2456-2460, Aug. 2011. 15

[8] M. Jankiraman. **Space-Time Codes and MIMO Systems**. *Artech House Publishers*, Boston, London,July, 2004. 3

[9] J. G. Proakis. **Communications Systems Engineering**, *Prentice Hall*, 2nd Ed., Aug. 2001. 3

[10] A. Mammela, A. Kotelba, M. Hoyhiya and D. P. Taylor. **Relationship of Average Transmitted and Received Engergies in Adaptive Transmission**, *IEEE Trans. Vehi. Tech.*, vol. 5, no. 3, pp. 1257-1268, Mar. 2010. 4

[11] M. Patzold. **Mobile Fading Channels: Modelling, Analysis and Simulation**, *John Wiley and Sons*,2nd, Ed., United Kingdom, 2012. 3

[12] X. Chengshan and Y. R. Zheng. **A statistical simulation model for mobile radio fading channels**, in *IEEE WCNZ*, vol. 1, pp. 144-149, 2003. 4

[13] J. G. Proakis. **Digital Communications**, *McGraw-Hill Book Co*, 3rd Ed., 1995. 4

[14] T. S. Rappaport, **Wireless Communications: Principles and Practice**. *Prentice-Hall*, Upper Saddle River, NJ, 2nd Ed., 2002. 4, 5, 13, 20

[15] A. F. Naguib, N. Seshadri, and A. R. Calderbank. **Increasing data rate over wireless channels**, *IEEE Signal Processing Mag.*, vol. 17, no. 3, pp. 79-92, May, 2000. 7

[16] G. J. Foschini and M. J. Cans. **On limits of wireless communications in a fading environment when using multiple antennas**, *Wireless Personal Commun.*, vol. 6, pp. 311-335, 1998. 7

[17] D. Gesbert, M. Kountouris, R. W. Heath, C. -B. Chae and T. Salzer. **Shifting the MIMO paradigm**, *IEEE Signal Processing Mag.*, vol. 24, no.5 , pp. 36-46, Sept. 2007. 8

[18] S. Sandhu, R. Heath and A. Paulraj. **Space-time block codes versus space-time trellis codes**, in *IEEE ICC*, vol. 4, Helsinki, Finland, pp. 1132-1136, 2001. 8

[19] V. Tarokh, A. Naguib, N. Seshadri and A. R. Calderbank. **Spacetime codes for high data rate wireless communication: performance criteria in the presence of channel estimation errors, mobility, and multiple paths**, *IEEE Trans. Commun.*, vol. 47, no. 2, pp. 199207, Feb, 1999. 8

[20] V. Tarokh, N. Seshadri and A. R. Calderbank. **Space-time codes for high data rate wireless communication: performance criterion and code construction**, *IEEE Trans. Inform. Theory*, vol. 44, no. 2, pp. 774765, Mar, 1998. 8, 20

[21] S. M. Alamouti. **A simple transmit diversity technique for wireless communications**, *IEEE J. Sel. Areas. Commun.*,vol. 16, no. 8, pp. 1451-1458, 1998. 8, 14, 15, 98

[22] E. G. Larsson and P. Stoica, **Space-Time Block Coding for Wireless Communications**. *Cambridge*, 2nd Ed., 2003. 48

[23] H. Jafarkhani. **A quasi-orthogonal space-time block code**, *IEEE Trans. Commun.*, vol. 49, pp. 14, Ja., 2001. 9, 15

[24] P. W. Wolniansky, G. J. Foschini, G. D. Golden and R. A. Valenzuela. **V-BLAST: An architecture for realizing very high data rates over the rich-scattering wireless channel**., *URSI Int. Symp. Signals, Systems and Electronics, ISSSE 98*, pp. 295-300, Oct. 1998. 9, 14, 37

[25] B. Hassibi and B. Hochwald. **High rate codes that are linear in space and time**, *IEEE Trans. Inform. Theory*, vol. 48, no. 7, pp 1804-1824, Jul. 2002. 9, 15, 48, 49, 52, 58, 86

[26] D. Agrawal, V. Tarokh, A. Naguib, and N. Seshadri. **Space-time coded OFDM for high data-rate wireless communication over wideband channels**, in *Proc. Veh. Technol. Conf.*, vol. 3, Ottawa, ON, Canada, pp. 2232-2236, 1998. 9

[27] Z. Liu, G. B. Giannakis, A. Scaglione and S. Barbarossa. **Decoding and equalization of unknown multipath channels based on block precoding and transmit antenna diversity**, in *33rd Asilomar Conf. Signals, Syst., Comput.*, Pacific Grove, CA, , pp. 1557-1561, 1999. 9

[28] N. Al-Dhahir. **Single-carrier frequency-domain equalization for space-time block-coded transmissions over freuqnecy-selective fading channels**, *IEEE Commun. Lett.*, vol. 5, no. 7, pp. 304-306, July 2001. 9

[29] E. G. Larsson, P. Stoica, E. Lindskog and J. Li. **Space-time block coding for frequency-selective channels**, in *Proc. ICASSP*, vol. 3, pp. 2405-2408, 2002. 14, 15, 20

[30] G. H. Golub and C. F. Van Loan. **Matrix Computations**, *Johns Hopkins University Press*, Baltimore, Maryland, 3rd Ed., Nov. 1996. 22

[31] S. Zhou and G. B. Giannakis. **Single-carrier space-time block coded transmissions over frequency-selective fading channels**, *IEEE Trans. Inform. Theory*, vol. 49, no. 1, pp. 164-179, Jan. 2003 25

[32] J. Hicks, S. Bayram, W. H. Tranter, R. J. Boyle and J. H. Reed. **Overloads array processing with spatially reduced search joint detection**, *IEEE J. Select. Areas. Commun.*, vol. 19, no. 8, pp. 1584-1593, Aug. 2001. 30

[33] A. J. Viterbi. **Convolutional codes and their performance in communication systems** , *IEEE Commun. Tech.* , vol. 19, no. 5, pp 751-772, Oct. 1971. 30

[34] D. Forney, Jr.. **The Viterbi algorithm**, *Proc. of IEEE*, vol. 61, no. 3, pp. 268-279, May 1972. 31

[35] J. F. Hayes. **The Viterbi algorithm applied to digital data transmission**, *IEEE Commun. Mag.*, vo. 44, no. 2, pp. 26-32, May 2002. 31

[36] G. Forney, Jr.. **Maximum-likelihood sequence estimation of digital sequences in the presence of intersymbol interference**. *IEEE Trans. Inform. Theory*, vol. 18, no. 3, pp. 363-378, May 1972. 30, 31

[37] G. D. Golden, C. J. Foschini, R. A. Valenzuela and P. W. Wolniansky. **Detection algorithm and initial laboratory results using V-BAST space-time communication architecture**, *Electron. Lett.*, vol. 35, no. 1, pp. 14-16, Jan 1999. 38, 40

[38] D.K. C. So and R. S. Cheng. **Layered maximum likelihood detection for MIMO systems in frequency selective fading channels**, *IEEE Trans. Wireless Commun.*, vol. 5, no. 4, pp. 752-762, April 2006. 44, 72

[39] J. Wang, X. Wang and M. Madihian. **On the optimum design of space-time linear-dispersion codes**. *IEEE Trans. Wireless Communs*, vol. 4, no. 6, pp. 2928-2938, Nov. 2005. 48, 60

[40] R. W. Heath, Jr. and A. J. Paulraj. **Linear dispersion codes for MIMO systems based on frame theory**, *IEEE Trans. Signal Processing*, vol. 50, no. 10, pp. 2429-2441, Oct. 2002. 48

[41] H. Jafarkhani. **Space-Time Coding Theory and Practice**, *Cambridge University Press* , New York, 2005. 48

[42] Y. Li, J. C. Chuang, and N. R. Sollenberger. **Transmitter diversity for OFDM systems and its impact on high-rate data wireless networks**, *IEEE J. Select. Areas Commun.*, vol. 17, no.7, pp. 1233-1243, Jul. 1999. 57

[43] V. Erceg, D. G. Michelson, S. S. Ghassemzadeh. **A model for the multipath delay profile of fixed wireless channels**, *IEEE Journ. selec.areas in commun.* , vol. 17, no. 3, pp. 399-410, Mar. 1999. 57

[44] L. J. Cimini, Jr.,. **Analysis and simulation of a digital mobile channel using orthogonal frequency division multiplexing**, *IEEE Trans. Commun.*, vol. 33, no. 7, pp. 665-675, Jul. 1985. 58, 59

[45] J. Heiskala and J. Terry. **OFDM wireless LANS: a theoretical and practical guide**, *Sams Publishing*, 2002. 59

[46] D. Falconer. S. L. Ariyavisitakul, A. Benyamin-Seeyar, B. Eidson. **Frequency domain equalization for single-carrier broadband wireless systems**, *IEEE Commun. Mag.*, vol. 40, no. 4, pp. 58-66, Apr. 2002. viii, 59, 60

[47] H. Sari, G. Karam and I. Jeanclaud. **Frequency-domain equalization of mobile radio and terrestrial broadcast channels**, in *IEEE GLOBECOM*, vol. 1, pp. 1-5, 1994. 59

[48] J. Wu and S. D. Blostein. **Linear dispersion for single-carrier communications in frequency selective channels**, in *Vehicular Tech. Conf.*, pp. 1-5, Sept. 2006. 60

[49] A. R. Ghaderipoor, L. Beygi and S. H. Jamali. **Linear dispersion space-time codes for frequency selective fading channels**, in *ICSP Proc*, vol. 1, pp. 378-381, Aug. 2002. 60

[50] T. Kollo, D. von Rosen. **Advanced multivariate statistics with matrices**, *Springer*, Dordrecht, The Netherlands, 2005. 61

[51] A. Gutierrez and M. Cabrera. **Issues of the simulation of wireless channels with exponential-decay power-decay profiles**, in *IEEE Int. Symp. PIMRC*, pp. 507-511, Sept. 2005. 89

[52] T. Yang, J. Yuan and W. Zhang. **Recovering cooperative multiplexing gain in wireless relay networks**, *IEEE Trans. Commun.*, vol. 58, no. 12, pp. 3538-3549, Dec. 2010. 99

[53] J. Yuan, Y. Li and L. Chu. **Differential modulation and relay selection with detect-and-forward cooperative relaying**, *IEEE Trans. Vehi Tech.*, vol. 59, no. 1, Jan. 2010. 99

[54] A. Sendonaris, E. Erkip and B. Aazhang. **User cooperation diversity - Part I: System description**, *IEEE Trans. Commun.*, vol. 51, no. 11, pp. 1927-1938, Nov. 2003. 98

[55] A. Sendonaris, E. Erkip and B. Aazhang. **User cooperation diversity - Part II: Implementation aspects and performance analysis**, *IEEE Trans. Commun.*, vol. 51, no. 11, pp. 1939-1948, Nov. 2003. 98

[56] S. Chen, W. Wang and X. Zhang. **Performance analysis of multi-relay networks under rayleigh fading channels** . *IEEE Trans. Wireless Commun.*, vol. 8, no. 7, pp. 3415-3419, Jul. 2009.

[57] B. Schein and R. Gallager. **The Gaussian parallel relay network**, in *IEEE ISIT*, June 2000. 99

[58] J. N. Laneman, D. N. C. Tse and G. W. Wornell. **Cooperative diversity in wireless networks: efficient protocols and outage behaviour**, *IEEE Trans. Inform. Theory*, vol. 50, no. 12, pp. 3062-3080, Dec. 2004. 99

[59] T. Yang and J. Yuan. **Performance of iterative decoding for superposition modulation-based cooperative transmission**, *IEEE Trans. Wireless. Commun.*, vol. 9, no. 1, pp. 51-59, Jan. 2010. 99

[60] T.-W. Yune, J.-B. Lim and G.-H. Im. **Iterative multiuser detection with spectral efficient relaying protocols for single-carrier transmission** , *IEEE Trans. Wireless. Commun.*, vol. 8, no. 7, pp. 3787-3797, July 2009. 99

[61] H. Mheidat and M. Uysal. **Single-carrier frequency domain equalization for broadband cooperative communications**, in *WCNC*, vol. 3, pp. 1578-1584, Apr. 2006. 99

[62] Q-T View, L-N. Tran and E-K Hong. **Design of distributed space-time block code for two-relay system over frequency-selective channels**, in *GLOBCOM*, pp. 1-5, Dec. 2009. 99

[63] S. Xi and M. D. Zoltowski. **SINR-max cooperative beamforming for multiuser MIMO-OFDM systems**, *ICCASSP*, pp. 3237-3240, Apr. 2008. 99

[64] ST-W Yune, J- B. Lim and G-. H. Im. **Iterative multiuser detection with spectral efficient relaying protocols for single-carrier transmission**, *IEEE Trans. Wireless Commun.*, pp. 3787-3797, Jul. 2009. 99

[65] P. Tarasak and Y-. H. Lee. **Joint cooperative diversity and scheduling in OFDMA relay systems**, in *WCNC*, pp. 980-984, Mar. 2007. 99

[66] Z. Hong and W. Dao-Long. **Two-user cooperative diversity strategies and their performance analysis**,in *IEEE ICSP* pp. 1581-1584, Oct. 2010. 99

[67] E. C. van der Meulen. **Three-terminal communication channels**, in *Adv. in Appl. Probab.*, vol. 3, pp. 120-154, 1971. 98

[68] R. J. Barton, J. Chen, K. Huang and D. Wu. **Cooperative time-reversal communication in wireless sensor networks**, in *IEEE SP*, pp. 1146 - 1151, 2005. 99